

Selective Dispersion of Surface Modified Iron Oxide Nanoparticles
in Polymer Blends

by

Özlem Tekmek

A Thesis Submitted to the
Graduate School of Engineering
in Partial Fulfillment of the Requirements for
the Degree of

Master of Science
in
Material Science&Engineering

Koc University

July 2007

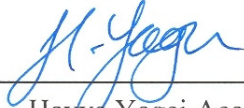
Koc University
Graduate School of Sciences and Engineering

This is to certify that I have examined this copy of a master's thesis by

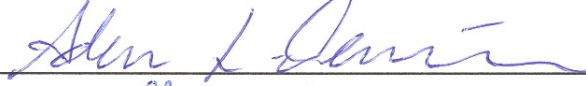
Özlem Tekmek

and have found that it is complete and satisfactory in all respects,
and that any and all revisions required by the final
examining committee have been made.

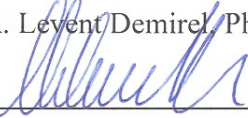
Committee Members:



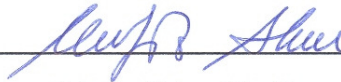
Havva Yagci Acar, Ph. D. (Advisor)



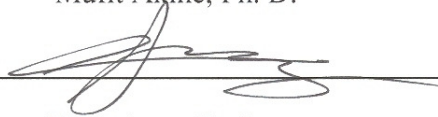
A. Levent Demirel, Ph. D. (co-Advisor)



Mehmet S. Somer, Ph. D.



Mufit Akinc, Ph. D.



Ersin Acar, Ph. D.

Date: 13.07.2007

ABSTRACT

Iron oxide nanoparticles display size dependent superparamagnetic behavior that is exploited in various areas of science and technology. Spatial positioning of these nanoparticles is of special interest to generate novel structures with tailored properties and for device fabrications. Phase separated morphology of immiscible polymer blends and block copolymers can create features from nanometer to micron scale.

In this study, selective dispersion of different surface modified iron oxide nanoparticles (SPIO) in the blends of PS and PEG were investigated by AFM. Surface of iron oxide nanoparticles were modified by two different methods in order to prevent agglomeration and to provide compatibility with the selected domain of the polymer blend.

In the first part, lauric acid (LA) and hexadecyltrimethoxysilane (HDMS) coated hydrophobic SPIOs dispersed well both in PS and PEG homopolymers but LA coated MNPs preferred PEG phase instead of PS in the blend. Ligand exchange mechanism was proved as a reason of this unexpected selectivity. HDMS coated MNPs mainly dispersed at the interface of the blend and formed larger clusters in the PEG domain of PS/PEG blend. Lastly, methoxy(polyethyleneoxy)propyltrimethoxysilane PEG-Si coated hydrophilic SPIOs dispersed in the PEG phase, as expected.

In the second part, synthesis of PS and PMMA by ATRP from surface of SPIOs was achieved and their blends with immiscible homopolymers were investigated by AFM. In all combinations, phase-separation of polymers occurred and selective dispersion was achieved. In addition, PMMA-b-PS was also grafted from the surface of iron oxide and preliminary studies about phase separation were performed by AFM.

ÖZET

Süperparamanyetik demir oksit nanoparçacıkları, büyüklüklerine göre değişen ve bundan dolayı sensör, manyetik ayırıştırma, terapi, hoparlör gibi birçok bilim ve teknoloji alanında kullanılan süperparamanyetik davranış gösterirler. Bu parçacıkların uzamsal düzenlenmeleri yeni yapıların oluşturulması ve yeni cihaz uygulamaları için özel bir ilgi alanıdır. Faz ayrışımı yapan, birbiri ile karışmayan polimer karışımları nanometreden mikron ölçeğe kadar değişik yapılar oluştururlar. Nanoparçacıkların bu fazların birine seçici dağılımı, mikro-faz ayrışımı yapan blok kopolimerler için benzersiz yapılar ve özellikler yaratır.

Dolayısıyla, bu çalışmada, değişik kaplamalı demir oksit nanoparçacıklarının polisitiren ve polietilenglikol karışımlarında seçici dağılımı atom kuvvet mikroskopuyla incelendi. Demir oksit nanoparçacıklarının yüzeyleri, çökmeyi engellemek ve polimer karışımının seçilmiş fazıyla uyumluluğunu sağlamak için iki farklı yöntemle değiştirildi.

Birinci kısımda, LA kaplanmış hidrofobik nanoparçacıklar PS ve PEG de düzgün bir dağılım gösterirken, bu polimerlerin faz ayrışımı yapan karışımlarında beklenmeyen bir şekilde PS yerine PEG içinde dağıldılar. Bu umulmayan değişimin nedeni 'ligand değişimi' olarak ispatlandı. Bunun üzerine, parçacık yüzeyi, yüzeyle kovalent bağ yapan HDMS ile kaplandı. Hidrofobik olan bu parçacıklar da, genel olarak PS/PEG karışımında, polimerlerin ara fazında dağıldılar ya da PEG içinde büyük kümeler oluşturdular. Hidrofilik, kovalent bağlı PEG-Si ile kaplanmış nanoparçacıklar beklenildiği üzere PEG in içinde seçici dağılım gösterdiler.

İkinci kısımda, nanoparçacık yüzeyinden ATRP metodu ile PS ve PMMA polimerleri başarı ile sentezlendi ve bunların faz ayrışımı yapan polimerlerle karışımı AFM ile incelendi. Bütün kombinasyonlarda, faz ayrışımı ve dolayısıyla seçici dağılım gözlemlendi. Ayrıca, parçacık yüzeyinden gene ATRP ile PMMA-b-PS blok kopolimeri sentezlendi ve faz ayrışmaları için ilk çalışmalar yapıldı.

ACKNOWLEDGEMENTS

I would like to express my gratitude to my advisor Assistant Prof. Havva Funda Yagci Acar for all her support, sensible patience, and motivation during my research. It was a great opportunity for me to work with such a friendly and insightful advisor. I would also like to acknowledge my co-advisor Associate Prof. A. Levent Demirel for his scientific guidance and kind friendship. Unfortunately, I had the chance to work with him closely only for one year. I would also like to thank Assist. Prof. Ersin Acar and his PhD student Engin Dođan for their invaluable help on the ATRP. The trips to Bođaziđi University were quite nice. In addition, I would like to thank sincerely to Prof. Mehmet Somer for his kind attitude throughout the two years that I have spend at KU and Prof. Mufit Akınç for his kindness and the time that he spent during the evaluation of my thesis.

I also want to thank my lab mates: Miray Demirer for teaching me everything about the lab with endless patience and for her friendship; Feyza Selçuk for listening me and broadening my perspective at the time of critical decisions; Eda Kutluözen for her help on the experimental part; Selçuk Acar for XRD and TGA measurements and being my friend for two years; Đlkin Kokal for teaching how to use FT-IR Spectrophotometer; Sinan Öztürk for his patience in the lab and Serdar Çelebi for his support in ICP and sharing a lab for two years in a friendly manner. Moreover, I have to thank Muharrem Guler for his help with the lab equipments.

Additionally, I want to thank my friends; Mustafa Kaymakci for his endless love, sensible understanding and kind support in the last two years; Murat Senan, Tarkan Güçlü and Buđra Toga for enjoyable lunches and for all the fun.

Finally, I want to thank my parents Reşit and Teslime Tekmek, my brother Can Tekmek and my cute sister Özge Tekmek for everlasting patience, support and love. I want to dedicate this thesis to my family.

TABLE OF CONTENTS

List of Tables	viii
List of Figures	ix
Chapter 1: Introduction	1
1.1 Nanoparticles	1
1.2 Self-assembling polymers	3
1.3 Nanoparticles in Self-assembling Polymers	5
1.4 Surface Initiated Polymerization from Nanoparticles	8
1.5 The aim of this study	14
Chapter 2: Experimental	16
2.1 Materials	16
2.2 Synthesis of surface modified iron oxide magnetic nanoparticles (MNPs)	16
2.3 ATRP from the surface of MNPs	21
2.4 Nanoparticle containing film preparation	23
2.5 Characterization methods	24
Chapter 3: Characterization of Surface Modified Nanoparticles	25
3.1 Characterization of LA coated MNPs	25
3.2 HDMS coated MNPs	35
3.3 PEG-Si coated MNPs	41
3.4 CMS coated MNPs	47

Chapter 4: Characterization of Polymer Coated Nanoparticles	53
4.1 PS coated MNPs	54
4.2 PMMA coated MNPs	67
4.3 PMMA-b-PS coated particles	70
Chapter 5: Selective Dispersion of Nanoparticles in Polymer Blends	74
5.1 Films containing surfactant coated MNPs	74
5.2 Films containing polymer coated MNP	87
Chapter 6: Conclusions	93
Appendix	97
Bibliography	104

LIST OF TABLES

Table 2.1	Reaction variables	17
Table 2.2	Design space obtained from Design Expert 7.0	18
Table 2.3	Polymerization conditions for PS growth from MNP surface	22
Table 2.4	Polymerization conditions for MMA growth from the MNP surface	22
Table 3.1	Characterization Table of Different Surfactant Coated MNPs	52
Table 4.1	Polymerization conditions (ATRP) for PS coated MNPs	55
Table 4.2	Polymerization conditions (ATRP) for PMMA coated MNPs	67
Table 4.3	Characteristics of Polymer coated MNPs	73
Table A.1	Reaction parameters and the results	98
Table A.2	Hydrodynamic size based on intensity and number average distribution by DLS	101
Table A.3	Comparison between theory and the experimental sizes	103

LIST OF FIGURES

Figure 1.1	Self-assembly of block copolymers	4
Figure 1.2	Self-assembly of block copolymers on the substrate surface	4
Figure 1.3	General mechanism for ATRP (RX: alkyl halide, initiator; Ln: ligand; Mt: transition metal)	10
Figure 3.1	(a) LA bilayer coated (b) LA monolayer coated iron oxide nanoparticles	25
Figure 3.2	DLS size distribution of LA monolayer coated iron oxide Nanoparticles in toluene prepared by precipitation method. Peak maximum: 120 nm	26
Figure 3.3	DLS size distribution of LA monolayer coated iron oxide nanoparticles in CHCl_3 prepared by extraction method. Peak maximum: 25 nm	27
Figure 3.4	Hydrodynamic sizes of LA coated MNPs prepared by extraction method with different amounts of IPA addition	28
Figure 3.5	XRD analysis of a) bare and b) bilayer coated particles	29
Figure 3.6	XRD analysis of particles synthesized in the presence of NaNO_3 (red), absence of NaNO_3 (black)	30
Figure 3.7	FT-IR spectrum of a) monolayer coated b) bare c) bilayer coated particles	31
Figure 3.8	Bidentate binding of carboxylate on the iron oxide surface	31
Figure 3.9	FT-IR spectrum of particles synthesized in the presence of NaNO_3 (red), absence of NaNO_3 (black)	32

Figure 3.10	TGA data of a) bare b) monolayer coated c) bilayer coated iron oxide nanoparticles	33
Figure 3.11	AFM images of LA coated iron oxide NPs (height, amplitude and phase, respectively)	34
Figure 3.12	Binding of HDMS from the methoxysilane onto the MNP	35
Figure 3.13	Hydrodynamic sizes of HDMS coated particles prepared from bare particles	36
Figure 3.14	Hydrodynamic sizes of HDMS coated particles prepared by ligand exchange	37
Figure 3.15	XRD diagram of HDMS coated particles prepared from the bare particles	38
Figure 3.16	XRD diagram of HDMS coated particles prepared by the ligand exchange	38
Figure 3.17	FT-IR spectrum of HDMS (red) and HDMS coated MNPs (black)	39
Figure 3.18	TGA data of HDMS coated MNPs	40
Figure 3.19	AFM image (height, amplitude, phase) of HDMS coated MNPs	41
Figure 3.20	Binding of PEG-Si from the methoxysilane onto the MNP	41
Figure 3.21	Hydrodynamic sizes of PEG-Si coated MNPs in water: washed (green) and unwashed (red)	42
Figure 3.22	Hydrodynamic sizes of washed PEG-Si coated particles (red), 1/10 (green), 1/100 (blue) dilution	43
Figure 3.23	Hydrodynamic sizes of PEG-Si coated MNPs in toluene (red) and in water (green)	44
Figure 3.24	XRD analysis of PEG-Si coated MNPs	44
Figure 3.25	FT-IR spectrum of PEG-Si (black) and PEG-Si coated MNPs (red)	45
Figure 3.26	TGA data of PEG-Si coated MNPs	46

Figure 3.27	AFM images of PEG-Si coated MNPs	46
Figure 3.28	Binding of CMS from the methoxysilane onto the MNP	47
Figure 3.29	Hydrodynamic sizes of CMS coated MNPs in toluene	48
Figure 3.30	Hydrodynamic sizes of CMS coated MNPs in xylene	48
Figure 3.31	Hydrodynamic sizes of CMS coated MNPs in DMF: stock (red), diluted (green)	49
Figure 3.32	XRD diagram of CMS (red) and LA (black) coated MNPs	50
Figure 3.33	FT-IR spectra of CMS (red) and CMS coated MNP (black)	51
Figure 3.34	TGA data of CMS coated MNPs	52
Figure 4.1	Typical scheme of polymerization from CMS coated MNPs	53
Figure 4.2	Hydrodynamic sizes of CMS coated MNPs in DMF (red); PS coated MNPs after 2 hr (OT2St) (green) and 3.5 hr (OT3St) (blue) polymerization measured in CHCl ₃ and THF, respectively	56
Figure 4.3	Hydrodynamic sizes of CMS coated MNP in DMF (red), 4.5 hr-PS coated MNP (OT5St) (green), 7.5 hr-PS coated MNP (OT4St) (blue)	57
Figure 4.4	Hydrodynamic size of PS coated MNPs after 3-day polymerization: washed and suspended in toluene	58
Figure 4.5	FT-IR spectrum of CMS (black) and PS synthesized from CMS (red)	59
Figure 4.6	FT-IR spectrum of CMS coated (red) and PS coated (black) MNPs	60
Figure 4.7	TGA of CMS-coated MNP, unwashed OT2St and unwashed OT3St	61

Figure 4.8	TGA of CMS-coated MNP, unwashed OT4St and unwashed OT5St	62
Figure 4.9	TGA curves of CMS-coated (blue), washed (black) and unwashed (red) PS coated MNPs	63
Figure 4.10	TGA curves of CMS coated MNP (blue), OT6St washed (black) and unwashed (red)	63
Figure 4.11	GPC traces of unwashed OT4St (blue), cleaved PS from MNPs (black) and free PS (red)	64
Figure 4.12	GPC traces of OT5St as prepared (red) and PS cleaved from the MNP surface (black)	65
Figure 4.13	GPC traces of cleaved OT6St (black) and OT6St with nanoparticles (red)	66
Figure 4.14	AFM (height, amplitude and phase) images of PS coated MNPs	66
Figure 4.15	Hydrodynamic size of PMMA coated washed MNPs (OT1PMMA) in toluene	68
Figure 4.16	FT- IR spectrum of CMS (black) and PMMA (red) coated MNPs	68
Figure 4.17	TGA of CMS coated (blue), washed (red) and unwashed (black) PMMA coated MNPs (OT2PMMA)	69
Figure 4.18	GPC trace of cleaved PMMA coated MNPs	70
Figure 4.19	Typical scheme of block-copolymerization from PMMA coated MNPs	70
Figure 4.20	Hydrodynamic sizes of washed-PMMA (red) and PMMA-b-PS (green) coated MNPs in toluene	71
Figure 4.21	FT-IR spectrum of PMMA (black) and PMMA-b-PS (red) coated MNP	71

Figure 4.22	TGA of CMS (blue), PMMA (red) and PMMA-b-PS (black) coated MNPs	72
Figure 4.23	GPC traces of cleaved PMMA-b-PS (black) and PMMA-b-PS-MNP (red)	72
Figure 5.1	AFM phase images of PS/PEG blend (30/70 weight ratio) cast from chloroform a) not annealed b) annealed	75
Figure 5.2	AFM images of PS/PEG blends cast from toluene at a) 30/70 (height)b) 5/95 (phase) weight ratio	76
Figure 5.3	AFM height image of PB-b-PEO	76
Figure 5.4	Dilution (red) and stock (green) sizes of LA coated MNPs, which were used for the preparation of thin films	77
Figure 5.5	Hydrodynamic sizes of the structures formed with the mixture of LA-MNPs and PS homopolymers in toluene	78
Figure 5.6	AFM height and phase image of LA-MNPs dispersed in PS	79
Figure 5.7	AFM height and phase image of LA-MNPs dispersed in PEG	79
Figure 5.8	Hydrodynamic sizes of the structures formed with the mixture of LA-MNPs and PEG homopolymers in toluene	80
Figure 5.9	AFM phase images of LA MNPs dispersed in blends of a) 30/70 b) 5/95 PS/PEG	81
Figure 5.10	Hydrodynamic size of the structures formed with the mixture of LA-MNPs and PS-PEG blend in toluene	81
Figure 5.11	Extraction of LA coated particles into PEG phase. On the left, LA- NP s are in toluene at the top of the aqueous phase containing PEG. On the right, all NP s are in the aqueous phase containing PEG	82

Figure 5.12	FT-IR spectra of the a) precipitated MNPs after ligand exchange b) colorless toluene phase and c) LA	83
Figure 5.13	AFM phase images of HDMS coated MNPs in a) PEG, b) PS and c) PS-PEG blend	84
Figure 5.14	AFM phase image of HDMS coated MNPs in PS-PEG blend	85
Figure 5.15	AFM phase image of HDMS coated MNPs in PS-PEG blend	86
Figure 5.16	AFM height and phase images of PEG-Si coated MNPs dispersed in PS- PEG blend	87
Figure 5.17	AFM height, amplitude and phase images of PS coated unwashed MNP in PEG	88
Figure 5.18	AFM height, amplitude and phase images of PS coated washed MNPs in PEG	89
Figure 5.19	Hydrodynamic size of PS coated washed MNPs mixed with PEG in toluene	89
Figure 5.20	AFM height, amplitude and phase images of PS coated washed MNPs in PMMA	90
Figure 5.21	AFM height, amplitude and phase images of washed PMMA-MNPs in PS	91
Figure 5.22	Hydrodynamic size of washed PMMA- MNPs mixed with PS in Toluene	91
Figure 5.23	AFM height, amplitude and phase images of PMMA-b-PS coated MNP	92
Figure A.1	Typical scheme of bilayer coated iron oxide nanoparticles' synthesis	97
Figure A.2	Cube plot for the stability of nanoparticles (1) suspension, (0) Precipitate	99

Figure A.3	Main effects chart for hydrodynamic size after synthesis. Large slope means strong effect	100
Figure A.4	a) Interaction plot of the variables b) Main effects chart for hydrodynamic size after synthesis	102

Chapter 1

Introduction

1.1 Nanoparticles

Nanoparticles are one of the most studied materials in the materials science area since they have unique size-dependent magnetic, photonic, chemical and electrical properties. These properties are dramatically different from the corresponding bulk materials [1]. Quantum dots, silica nanoparticles, gold, and iron oxides are probably the most widely studied nanoparticles. Quantum dots exhibit size-tunable optical properties arising from quantum confinement and surface effects. They are widely used as fluorescent tags in biology and in photonic applications [2].

Iron oxide nanoparticles, on the other hand, display size dependent superparamagnetic behavior that is exploited in various areas of science and technology including sensors, separation, therapy, medical imaging, audio speakers, seals etc [3]. Paramagnetic materials are attracted when subjected to an applied magnetic field and do not retain any magnetization in the absence of an externally applied field. On the other hand, superparamagnetism is a phenomenon by which magnetic materials may exhibit a behavior similar to paramagnetism even below Curie temperature. Generally, these are single domain, single crystal nanoparticles of 10 nm or less. In paramagnetic materials where spin alignment happens in domains, in superparamagnetic materials, the magnetic moment of the entire crystallite tends to align with the magnetic field creating a higher saturation value. Iron oxide nanoparticles, magnetite (Fe_3O_4) and maghemite ($\gamma\text{-Fe}_2\text{O}_3$), show superparamagnetic behavior at room temperature, are biocompatible and biodegradable, so

are widely studied. Magnetite, which is black, has a magnetic saturation of 92-100 J/T.kg at 300 K. Maghemite, on the other hand, has a bit lower magnetic saturation (60-80 J/T.kg) and is dark brown [4].

Certain applications of the nanoparticles require either stable dispersions in a suitable carrier solvent or deposition on surfaces. Much effort has been made to define strategies for surface functionalization of superparamagnetic iron oxide nanoparticles (SPIONs) to achieve such applicability. These nanoparticles are generally formed in a core-shell structure where the magnetic core is surrounded by a coating that adsorbs on the crystal surface and is suitable for the desired application. A variety of small molecules with silane, thiol, carboxylic acid and alcohol functional groups has been successfully adopted as coatings for iron oxide nanoparticles [5,6]. These coating materials not only determine the solubility or miscibility but also used to prevent aggregation and provide colloidal stability by altering the interparticle interactions. Particles experience repulsive and attractive forces as they approach one another in the solution. Stability of a colloidal system is the sum of these forces. Repulsive forces consist of electrostatic repulsion, which is a result of charged species in the system and steric repulsion caused by the coatings added to the system and adsorbed onto the particle. These forces cause an energy barrier, which prevents two particles to come close to one another and stick together. If the particles come together and be able to pass this energy barrier, then attractive force, which is a result of Van der Waals interaction, causes the particles to adhere each other.

Adsorption of the surfactants on growing crystal is effective in controlling the particle size, as well. Yet, the binding strength is a key issue when stability is a concern for the application. Carboxylic acid containing species are proven as effective coatings for iron oxide through chemical adsorption of the carboxylate on the iron oxide surface [1, 3]. Alkoxysilanes are also successful coatings forming Fe-O-Si covalent bond, which again serves to prevent aggregation [1, 3].

Polymers can also be used for the coating of magnetic cores. Dextran, polyvinyl alcohol and polyacrylic acid are some of the major polymeric materials used with iron oxides. There are two techniques for coating the nanoparticles with polymers. One of them is 'grafting-to' technique in which the functionalized polymers are preformed and then grafted onto the nanoparticle through physisorption or chemisorption [7]. This technique has the disadvantage of low degrees of grafting because of steric hindrance. The other and more controlled technique is called 'grafting-from' in which well-defined polymers can functionalize the surfaces of nanoparticles by surface initiated polymerization (SIP) [7]. As a result, polymer brushes or hairy nanoparticles are formed. This does not only provide steric stabilization but also enhanced compatibility to similar polymer matrices if desired. Atom Transfer Radical Polymerization (ATRP) gives satisfactory results in terms of degree of grafting and control in the polymerization processes.

1.2 Self-assembling Polymers

Block copolymers consist of two or more homopolymers, which are linked by covalent bonds. If these homopolymers are chemically incompatible, the block copolymer undergoes 'microphase separation' with a length scale of tens of nanometers depending on the length of each block. This separation causes different morphologies ranging from spherical to lamella and results in size-controllable regular arrays of domains in the solution (Figure 1.1). For example, polystyrene-*b*-poly(methyl methacrylate) (PS-*b*-PMMA) can be synthesized by first polymerizing styrene, and then consequently polymerizing MMA from the reactive ends of the polystyrene chains. This polymer is a "diblock copolymer" because it contains two different chemical blocks. Triblocks, tetrablocks, multiblocks can also be similarly synthesized using ATRP, RAFT (Reversible addition-fragmentation chain transfer), ring-opening metathesis polymerization (ROMP), and living cationic or living anionic polymerizations [8].

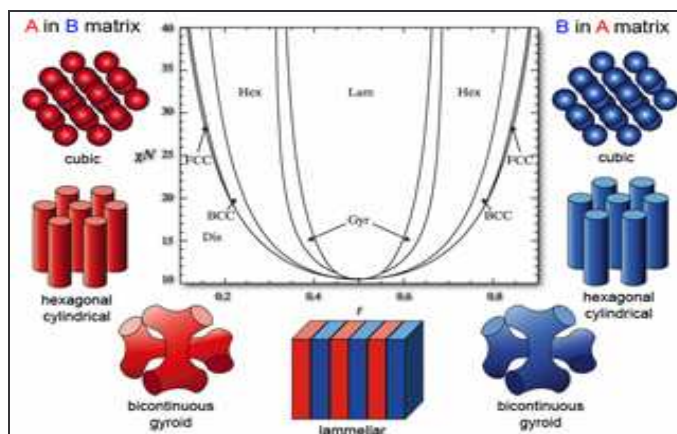


Figure 1.1 Self-assembly of block copolymers [9]

The orientation of block copolymer domains in thin films with respect to the substrate surface is important for many applications such as fuel cells, batteries and optoelectronic devices. For example, the uniformly sized and shaped nanodomains formed in the films have been used for nanolithography, nanoparticle synthesis, and high-density information storage media (Figure 1.2) [10].

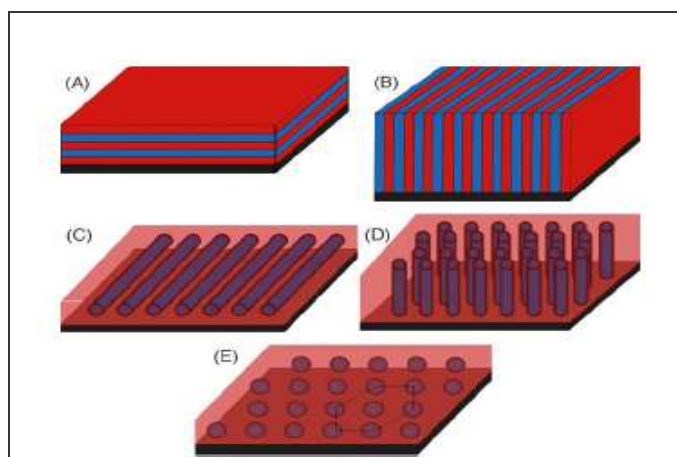


Figure 1.2 Self-assembly of block copolymers on the substrate surface [10]

These self-assembled structures can also be used as templates for the spatial positioning of nanomaterials since target properties of nanoparticle-polymer composites largely depend on the arrangement of nanoparticles in the matrix used. For example, gold nanoparticles were distributed selectively into the P4VP (polyvinyl pyridine) lamellae of a PS–P4VP diblock copolymer thin film by making use of the strong interfacial segregation of the blocks for electronic and optical applications [11].

Blends of immiscible homopolymers phase-separate at micron length scales and act as model systems for quick and easy investigation of selective dispersion of nanoparticles in various matrices. Once the selective dispersion is observed, suitable block copolymers of the blend components could then be used to position the nanoparticles in the self-assembled structures with finer dimensions. Thin films of phase separated polymer blends are studied not only for various coating products such as dielectric layers, photographic materials, and paints but also for technological applications [12].

1.3 Nanoparticles in Self-assembling Polymers

Nanoparticles embedded in phase separated polymer films provide a broad and realistic platform to achieve new materials and devices with unique magnetic, electronic and optical properties. Spatial positioning of nanoparticles (NPs) into ordered structures is of special interest in obtaining tailored structures for device applications [13,14,15].

The key mechanism in spatial positioning involves the selective dispersion of surface functionalized nanoparticles in a multi-component matrix (a block copolymer or a polymer blend) or on a surface. The ordered structures of NPs are achieved either through self-assembly of block copolymers or on previously patterned surfaces [16]. The use of polymeric systems is advantageous over patterned surfaces both in terms of better selectivity and in terms of simplicity.

There are three approaches that combine the nanoparticles and self assembled polymeric environments for the design of miniature devices in fields ranging from optoelectronics to sensing.

Self-organization of block copolymers in micellar forms is one of the successful methods. This approach may involve formation of the nanoparticles in organized micelles or loading micelles with pre-synthesized NPs. For example, iron and platinum salts were located in PVP cores of PS-*b*-PVP micelles in solution and dip coating of solid substrates provided a monolayer of micelles as a film [17]. In another example, PS coated quantum dots (QDs) were organized into aqueous QD compound micelles in the presence of PS-*b*-PAA copolymer. This was achieved in two steps. First, PS coated QDs were prepared by self-assembly of PS-*b*-PAA copolymer in a selective solvent. Then, upon dropwise addition of water and PS-*b*-PAA to these nanoparticles, PS chains of the block copolymer segregated onto the nanoparticles forming a micelle with a PAA shell and PS coated QD core [18].

As a second approach, micro-phase separated block copolymers are used as templates for the positioning of the nanoparticles to develop functional hybrid materials [19,20]. TOPO covered CdSe nanoparticles were mixed with phase separated PS-*b*-P2VP copolymer resulting in the selective organization of nanoparticles in the P2VP phase, changing the morphology. With the same manner, PEG-tagged ferritin particles were incorporated into the PEO phase of the P2VP-*b*-PEO copolymer suppressing the crystallization of PEO phase [21]. TiO₂ nanoparticles either dispersed well in the PMMA domain or form aggregates in PS domains of the PS-*b*-PMMA copolymer depending on the hydrophilicity of the surfactant coating on the TiO₂ [22]. In addition, a change of the ordered morphology of PS-*b*-PI block copolymers due to the concentration and particle interactions of Fe₂O₃ and Ag nanoparticles was also observed [23].

Lastly, simple and cost efficient approach about nanoparticle positioning into polymers is nanoparticle-polymer blend matrices. Immiscibility of homopolymers causes micrometer sized domains of polymer components. These domains are not ordered but provide a model system to investigate the selective dispersion of nanoparticles as a function of their surface coatings. Selective deposition of nanoparticles in one of these phases would indicate the potential of block copolymers formed by the blend components to position nanoparticles into ordered structures, which is important for device applications. There are various studies in the literature investigating the polymer blend/nanoparticle composites. TOPO covered CdSe nanoparticles were demonstrated forming lateral organization in PS/PMMA thin films [24]. An extension of this study investigated the influence of CoPt:Cu nanoparticles on the morphology of PS/PMMA thin film polymer blend. In this study, it was shown that particle concentration affects roughness and thickness of the polymer film [25]. However, concentration of quantum dot coated with PAA-b-PS copolymer has no effect on the film morphology when the particles are dispersed in PS domains of a PS/PMMA blend [26]. Silica particles having various surface functionalities have been shown to disperse selectively in the PMMA domains or concentrate at the interface of PMMA/SAN blend [27]. Phase separated films of poly (DL-lactide)/poly (caprolactone) blends were exposed to dendrimer coated quantum dot (QD) solutions [28]. In all these studies, the selective dispersion of the nanoparticles was achieved by suitable surface functionalities. Most of the blend/NP composites involved quantum dots and silica nanoparticles.

1.4 Surface Initiated Polymerization from Nanoparticles

As said before, to attain solubility and stability, polymers can be grafted from the surface of nanoparticles, as well [7]. Polymerization from the nanoparticle surface provides the control of the polymer grafting density, composition and molar mass. It is also a way of attaining materials with hierarchical self-organization. There are many types of mechanisms for surface initiated polymerization (SIP), which are ring opening metathesis polymerization, atom-transfer radical polymerization, TEMPO based polymerization and anionic polymerization. These are suitable for the polymerization of different types of monomers from various surfaces. Among these, ATRP has the most promising characteristics for controlled polymerization of the monomers such as styrene and methyl(methacrylate) at relatively low temperatures with relatively easy procedures [7].

1.4.1 Controlled Polymerization Techniques

The living polymerization technique encompasses all chain-growth polymerization methods: cationic, anionic, transition metal-catalyzed over the past decades, and recently, free radical polymerization. The difference of a living polymerization from others is the absence of irreversible chain termination and chain transfer. Therefore, if one chain is initiated at the beginning, ideally it will grow until no monomer is left. If a terminating agent is not introduced, the living chain will stay active, and therefore block copolymers can be synthesized by the addition of different monomers. The most important advantages of living polymerizations are that, the average molecular weight of the final polymer can be determined by the initial monomer/initiator ratio and the molecular weight distribution will be narrow if the initiation is complete (efficiency of 100 %) and fast. However, in practice, complete elimination of chain transfer and chain termination reactions is impossible. Nevertheless, well-defined polymers can be prepared if the rates of these side reactions are

kept sufficiently slow. In such cases, the polymerization reactions are called “controlled/‘living’ polymerizations” [7,29].

In ionic polymerizations, the number of monomers, employed, is limited, and the presence of functional groups causes undesirable side reactions. In addition, complete elimination of moisture and very low temperature are required to carry out these reactions. On the other hand, radical polymerizations have many advantages over the ionic polymerizations including: suitable to a large variety of monomers, tolerant to functional groups and impurities, mild reaction conditions etc. Therefore, radical polymerization has become the most popular industrial method to produce materials. However, the main disadvantage of conventional radical polymerization is the lack of control over the polymer structure meaning polymers with high molecular weights and high polydispersities are generally produced, due to the slow initiation, fast propagation and subsequent chain transfer or termination [30, 31].

Therefore, controlled radical polymerizations (CRP) have been developed to control the polymerization process with respect to molecular weight and polydispersity. The lifetime of a growing radical can be extended to several hours in a CRP, therefore polymers with predefined molecular weight, low polydispersity, controlled composition, and functionality can be prepared.

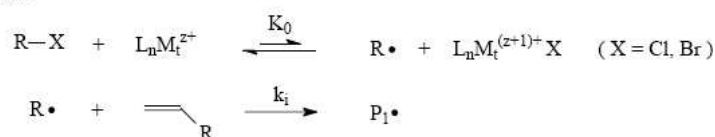
The three main CRP techniques are nitroxide-mediated polymerization (NMP), atom transfer radical polymerization (ATRP) and reversible addition/fragmentation chain transfer (RAFT) polymerization [30]. Use of initiators, radical mediators (i.e., persistent radicals or transfer agents), and in some cases catalysts are the general similarities in the CRP processes.

Transition-metal-mediated ATRP is considered as the most successful method among CRP techniques. So far, copper (I)-catalyzed ATRP is the most popular and successful one [30].

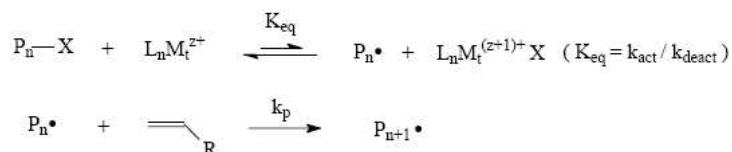
1.4.2 Mechanism of ATRP

In ATRP, propagating radicals are produced via reversible metal-catalyzed atom transfer, as shown in Figure 1.3. There are two necessities in order to get good control on a radical polymerization: (i) the equilibrium between radicals and dormant species must lie strongly to the side of the dormant species to guarantee that the overall radical concentration remains very low and the rate of the irreversible termination is negligible compared to the propagation rate; (ii) the exchange rate between radicals and dormant species must be faster than the rate of propagation so that all polymer chains have equal probability of growing [29].

Initiation



Propagation



Termination

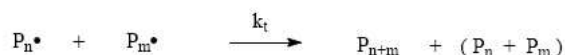


Figure 1.3 General mechanism for ATRP (RX: alkyl halide, initiator; Ln: ligand; Mt: transition metal) [30].

A typical mixture of initiator, metal, ligand, deactivator, solvent, temperature, and reaction time must be employed for the ATRP of each particular monomer. Therefore, understanding the role of each constituent of ATRP is important for achieving well-defined polymers and to apply the technique to other monomers[31].

Monomers: Typical monomers polymerized with the ATRP technique are vinyl monomers such as styrenes, acrylates, methacrylates, acrylonitrile (meth)acrylamides, dienes and other monomers which contain substituents capable of stabilizing the propagation radical [7, 29].

Initiators: Alkyl halides (RX) are the most common initiators for ATRP. Bromides and chlorides are the halogens affording the best molecular weight control [29].

Catalyst system: transition metals and ligands: Copper halides are used successfully with bipyridyl ligands. Most effective ligands for ATRP are derivatives of 2,2'-bipyridine. Bipyridyl ligands with long alkyl chains at the 4,4'-positions (such as dNbipy, 4,4'-di(5-nonyl)-2,2'-bipyridine) can completely solubilize the copper halide [29].

Deactivator: The deactivator in ATRP is the higher oxidation state metal complex formed after atom transfer, and it plays an important role in ATRP in reducing the polymerization rate and the polydispersity of the final polymer. An example is CuCl_2 [29].

1.4.3 Literature Review on Surface Initiated ATRP

Polymers from surface initiated ATRP can be grafted both from the flat surfaces and the surfaces of spherical nanoparticles by surface initiated ATRP. Brittain et al reported the synthesis of different diblock and triblock copolymers from Si/SiO₂ flat surfaces [32]. In that study, their systems displayed reversible rearrangement of block segments upon treatment with selective solvents and in some of the rearranged systems; they observed unusual nano-morphologies, which are pin micelles of folded structures. In another study of Brittain and coworkers, the responsive nature of the polyacrylic acid brushes, which were grafted from silica surfaces to stimuli such as pH and electrolyte concentration, was shown [33].

Numerous combinations of nanoparticle/polymer coatings were demonstrated with ATRP. For example, pH responsive nanocomposites consisting of gold / PVP for potential applications such as drug carriers were reported [34]. Core-shell CdS/SiO₂ nanoparticles

were modified with PMMA and used for the preparation of photoluminescent films in which the nanoparticles were regularly dispersed in the microscopic level [35].

Besides these, most of the studies about surface initiated ATRP are on silica nanoparticles. Zhao et al reported the synthesis of thermoresponsive and thermosensitive silica nanoparticles coated with PNIPAM, DEGMA or TEGMA [36,37]. Also, Matyjaszewski et al synthesized Si-graft PS hybrid nanoparticles and showed that glass transitions of PS in the films of that nanocomposites were elevated relative to those of free bulk PS because of the chain grafting and the chain extension due to the steric confinement [38]. Boue et al again synthesized Si-graft PS by ATRP and investigated the solutions by SANS to improve the synthetic conditions to get a better dispersion of particles and better control of the polymerization process [39]. Patten et al studied different sizes of Si nanoparticles and grafted PS and PMMA from them [40]. They demonstrated that polymerization of styrene exhibited a good molecular weight control (MW) while polymerization of MMA exhibited good MW control only with the addition of small amount of free initiator for the smaller particles. For the large particles, polymerization did not show molecular weight control. Fukuda et al benefiting from those results synthesized Si-graft PMMA in the presence of free initiator succeeded in controlling the molecular weight up to 480K and showed these particles have good dispersibility in 2D ordered arrays [41]. Besides these, Matyjaszewski et al synthesized block copolymers of PS, PMMA and n-BA from silica nanoparticles and studied the phase separation in ultrathin films of those nanocomposites [42]. Neoh et al and Hult et al prepared hollow nano or microspheres by synthesizing PS-b-PMMA from silica nanoparticles [43,44]. Fukuda et al synthesized PEO-b-PMMA and formed hollow spheres by etching the Si nanoparticle with HF [45].

Examples of surface initiated polymerization from iron oxide are relatively scarce and new. Fukuda et al synthesized PMMA coated iron oxide nanoparticles and reported

changes in the coercivity and the blocking temperature owing to the surface effects [46]. Mondragon et al also prepared PMMA modified iron oxide nanoparticles very recently, showing the polymerization had first order kinetics until the first four hours of the reaction and then gelation has occurred [47]. He also saw a corona of PMMA brushes on the particles in AFM studies. In another research, Schmidt et al synthesized thermoreversible magnetic fluids based on magnetite coated with PMEMA, which contribute to the development of easily recoverable polymer supported magnetic separation kits and catalytic systems [48]. In this study, the initiator was attached to the iron oxide surface by COOH group, which was not a permanent linkage for hydrophilic polymers. However, Neoh et al used trichlorosilane for the stability and grafted PEGMA from nanoparticles in order to study the response of macrophage cells to these particles [49]. On the PS side, Zhang et al formed PS shell on MnFe_2O_4 nanoparticles and exhibited a decrease in magnetic coercivity, which is consistent with the reduction of magnetic surface anisotropy upon polymer coating for specific applications in data storage and MRI contrast enhancement [50]. Peng et al enhanced a method for the preparation of magnetic nanoparticles covalently bonded with PS shell having up to 45K molecular weight by ATRP [51]. As far as we know, there is only one study in the open literature on the synthesis of block copolymer coated magnetic nanoparticles with ATRP method. Li et al prepared magnetic nanoparticles coated with amphiphilic block copolymers of PEMA-b-PHEMA as a potential drug delivery vehicle and demonstrated that the presence of hydrophobic segment can effectively control the release of a hydrophobic drug [52]. In most of these studies, linear kinetic plots (linear plots of MW vs. conversion), increases in hydrodynamic diameter with increasing conversion and narrow MW distributions for the grafted polymer samples were observed. The size of the nanoparticle, presence of free initiator and the type of monomer affected polymer MW control for these systems. In all of these studies, colloidal particles were suspended in a liquid for magnetic separation or for

drug encapsulation. As far as we know, there is no study investigating the distribution of these polymer coated iron oxide nanoparticles in an immiscible homopolymer forming phase-separation on a substrate. The only one study that investigated the synthesis of well-defined block copolymer of PS-*b*-PBzA tethered to polysilsesquioxane nanoparticles show that the PS-*b*-PBzA hybrid particles appeared as core-shell spots with distinctly different shells embedded in a continuous phase [53].

1.5 The aim of this study

The aim of this work is to synthesize iron oxide nanoparticles with various surface coatings and to investigate the selective dispersion of these surface coated nanoparticles in model polymer blends. The results are expected to lead to simple and cost effective routes to the development of polymer/nanoparticle composites that would aid to the development of practical devices, which utilizes the processability, and flexibility of polymeric matrices and unique size dependent properties of nanoparticles. One of the initial goals to achieve such end product is to develop surface functionalized nanoparticles with hydrophilic and hydrophobic surfaces that would have a favorable interaction with the polymeric matrices.

We can achieve this through two different approaches: (i) use of small surfactants that binds to surfaces of nanoparticle, (ii) grow the desired polymer from the nanoparticle surface. We are mostly interested in magnetic nanoparticles that found applications in a variety of fields from medicine to data storage. There is a growing interest to arrange nanoparticles into arrays for the applications such as sensors and data storage. Such arrays can be achieved with polymers. A relatively simple method of forming features with a polymeric film is the exploitation of micro-phase separation of immiscible blocks of copolymers. In this thesis, we attempted to show the potential of macro phase separation in model polymer blends as a simple and quick method for investigation of selective dispersion of nanoparticles. For this purpose, we have investigated three different systems:

(i) nanoparticles were mixed with immiscible polymer blends, (ii) a polymer was grown on the surface of nanoparticles and the nanoparticles were blended with an immiscible homopolymer, (iii) block copolymers were grown on the surface of the nanoparticles. These different approaches would be instrumental in providing micro and nano features to polymer/nanoparticles composite structures. Thin films of particle/polymer composites can be easily formed through spin coating and features as well as selectivity of nanoparticles in the phase-separated films can be observed with AFM.

Consequently, to achieve these goals, iron oxide nanoparticles were functionalized first with three kinds of low molecular weight surfactants, lauric acid (LA), hexadecyltrimethoxysilane (HDMS) and methoxypoly(ethyleneoxy)trimethoxysilane (PEG-Si) which were grafted onto the nanoparticles by physical or chemical adsorption. Selective dispersion of iron oxide NPs as a function of the surface functionalization was investigated in a model polymer blend containing PS and PEG. PS and PEG were chosen because of their well-known hydrophilic/hydrophobic contrast and the ease to observe the micron sized domains of the minor component in the matrix of the major component.

In the second method, PS, PMMA or PMMA-b-PS were grafted from the surface of iron oxide nanoparticles with ATRP polymerization technique and their dispersion in PEG, PS or PMMA was investigated by AFM.

Chapter 2

EXPERIMENTAL

2.1 Materials

All reagents were used as received unless indicated otherwise. $\text{FeCl}_3 \cdot 6\text{H}_2\text{O}$, $\text{FeCl}_2 \cdot 4\text{H}_2\text{O}$ and lauric acid (LA) were purchased from Fluka. Ammonium hydroxide (26% NH_3 in water, w/w) was purchased from Riedel-de Haen. Hexadecyltrimethoxysilane (HDMS), p-chloromethylphenyl trimethoxysilane (CMS), methoxy polyethyleneoxy propyl trimethoxysilane (PEG-Si) were purchased from Gelest. NaNO_3 , reagent grade chloroform, toluene and dimethylformamide (DMF) were purchased from Merck. Milli-Q water was used for all preparations and work-up. Polystyrene (300,000 g/mol) was kindly provided by Prof. Yusuf Yagci of Istanbul Technical University, Chemistry Department. Polyethylene glycol (10,000 g/mol), CuCl , pentamethyl diethylenetriamine (PMDETA), styrene, xylene, CuBr , CuBr_2 , methyl methacrylate (MMA) were purchased from Acros Organics.

2.2 Synthesis of surface modified iron oxide magnetic nanoparticles (MNPs)

2.2.1 Lauric acid coated iron oxide MNPs

The following procedure was performed for all experiments of the LA coated nanoparticles:

2.2.1.1 Preparation of LA bilayer coated MNPs: 45 mL of distilled water was put into a 100 mL three-necked round bottom flask fitted with a mechanical stirrer and a condenser

and deoxygenated for 30 minutes. Iron salts ($\text{Fe}^{3+} / \text{Fe}^{2+}$ mole ratio of 2), lauric acid and NaNO_3 were added to the flask and stirred at 400 rpm under nitrogen for about 15 min. Reaction flask placed into an oil bath at 85°C . After 10 min of mixing, ammonium hydroxide was injected to the flask with vigorous stirring at 600rpm. Reaction was allowed to continue for 30 minutes to produce a stable colloidal solution, then cooled to room temperature and placed atop a magnet (0.3 Tesla) for few hours. Any precipitate was removed with magnetic decantation.

A two factorial, three variable Design of Experiments (DOE) was created to investigate the effect of reaction variables on particle size in LA coated MNPs. Total iron ion concentration, LA/iron mole ratio and NaNO_3 were the reaction variables and the upper and lower limits for each are given in Table 2.1. These limits were chosen based on our previous experiments and literature values.

Table 2.1 Reaction variables

Variables	Low	High
$[\text{Fe}]^a$	0.03	0.5
$[\text{LA}]/[\text{Fe}]^b$	0.1	1
NaNO_3^c	No	Yes

^a Total iron concentration (M): (mole Fe (II) + mole Fe (III))/Volume

^b LA/Fe: mole ratio

^c Presence of NaNO_3

Sixteen experiments were created by the statistical programs (Design Expert 7.0 and MiniTab) based on three factor two-level full factorial design with two center points per block within the given limits of each variable (Table 2.2).

Table 2.2 Design space obtained from Design Expert 7.0.

Sample ID	[Fe]	LA/Fe	NaNO ₃
OT5LA	0.030	0.1000	YES
OT9LA	0.030	0.1000	NO
OT16LA	0.500	0.1000	YES
OT23LA	0.265	0.5500	YES
OT19LA	0.265	0.5500	NO
OT7LA	0.265	0.5500	YES
OT8LA	0.500	1.0000	YES
OT18LA	0.265	0.5500	YES
OT25LA	0.265	0.5500	NO
OT22LA	0.265	0.5500	YES
OT24LA	0.265	0.5500	NO
OT15LA	0.030	1.0000	NO
OT21LA	0.030	1.0000	YES
OT11LA	0.265	0.5500	NO
OT20LA	0.03	1.0000	NO
OT10LA	0.500	1.0000	NO

2.2.1.2 Preparation of LA monolayer coated MNPs by extraction method: 10 ml of dark brown colloidal suspension (LA bilayer coated iron oxide) was mixed with 20 ml of chloroform and shaken well. After the equilibrium was reached, the dark brown chloroform layer with the monolayer coated particles was separated. In order to speed up the extraction, a small amount of isopropanol can be added into the solution. The chloroform layer was dried with molecular sieves.

2.2.1.3 Preparation of LA monolayer coated MNPs by precipitation method: 10 ml of colloidal suspension (LA bilayer coated iron oxide) was mixed with 10 ml of isopropanol. LA monolayer coated nanoparticles were precipitated and removed out by magnetic decantation. Particles were dried by rotary evaporator and resuspended in toluene with ultrasonication.

2.2.2 HDMS coated iron oxide MNPs

2.2.2.1 Preparation of bare MNPs: Bare MNPs were synthesized with the same procedure explained in section 2.2.1.1 (preparation of LA bilayer MNPs) except LA was not added to the reaction pot. After the reaction was cooled to room temperature and placed atop a magnet (0.3 Tesla) for few hours, the precipitated particles were removed with magnetic decantation and dried with rotaryevaporator.

2.2.2.2 Preparation from bare MNPs: 20 mg of previously synthesized bare iron oxide nanoparticles were sonicated for 30 minutes in toluene. Few drops of acetic acid and 0.5 ml HDMS was added and sonicated for another 2 hours. The reaction mixture was stirred with a magnet overnight and then placed atop a magnet (0.3 Tesla) for few hours to isolate any precipitate with magnetic decantation.

2.2.2.3 Preparation by ligand exchange: 0.20 g of LA monolayer coated nanoparticles was stirred vigorously with 0.34 ml of HDMS in 40 ml toluene mechanically under nitrogen at 60 °C. After 1 hour stirring, 0.15 ml of NH₄OH was injected. Reaction was allowed to continue for 30 minutes to produce a stable colloidal solution, then cooled to room temperature and placed atop a magnet (0.3 Tesla) for few hours. Any precipitate was removed with magnetic decantation. Then, the particles were precipitated into acetone and isolated by an external magnet. Fresh toluene were added to the precipitated nanoparticles, sonicated briefly and precipitated by 1h centrifugation at 50,000 rpm at room temperature. This procedure was applied twice.

2.2.3 PEG-Si coated iron oxide MNPs

45 ml of MilliQ water was deoxygenated for 30 minutes in a 100 ml three necked round bottom flask fitted with a mechanical stirrer and a condenser. Iron salts (Fe³⁺ / Fe²⁺ mole ratio= 2) were added to the flask and stirred at 400 rpm under nitrogen for about 15 min. Reaction flask placed into an oil bath at 85 °C. After 10 min of mixing, PEG-Si containing ammonium hydroxide solution was injected to the flask with vigorous stirring at 600 rpm. Reaction was allowed to continue for 30 minutes to produce a stable colloidal solution, then cooled to room temperature and placed atop a magnet (0.3 Tesla) for few hours. Any precipitate was removed with magnetic decantation. Colloidal solution was added to an ultrafiltration tube (AMICON ULTRA 50.000 cut off) and washed with fresh water in centrifuge three times which is almost equivalent to changing the whole volume three times with the fresh water.

2.3 ATRP from the surface of MNPs

2.3.1 Preparation of initiator coated MNPs

0.20 g of LA monolayer coated nanoparticles was stirred vigorously with 0.5 ml of CMS in 40 ml toluene mechanically under nitrogen at room temperature. After 1 hour stirring, 0.5 ml of NH_4OH was injected. Reaction was allowed to continue for 30 minutes to produce a stable colloidal solution, then placed atop a magnet (0.3 Tesla) for few hours. Any precipitate was removed with magnetic decantation. Then, the particles were precipitated into hexane and washed with toluene twice by 1h centrifugation at 50,000 rpm at room temperature. Particles were resuspended in DMF by sonication.

2.3.2 Surface initiated polymerization

Initiator coated nanoparticles were either used as dried powder or as a colloidal solution in DMF or xylene. In a typical preparation, initiator coated particles; CuCl for styrene, CuBr and CuBr₂ for methyl methacrylate and the monomer were first deoxygenated for 30 minutes in a Schlenk flask. Then, deoxygenated PMDETA was injected to the reaction and polymerization was carried out at the desired temperature. The viscosity of the solution increased with time. At the desired polymerization time, polymerization solution was diluted with dichloromethane and precipitated into methanol. The precipitated brown powder was dried in vacuum oven at 40°C overnight. Fresh toluene or CHCl_3 were added to the dry polymer coated nanoparticles, sonicated briefly and precipitated by 1h centrifugation at 50,000 rpm at room temperature with the addition of few drops of methanol. This procedure was repeated twice. Details of the polymerization conditions are given in Table 2.3 for PS and Table 2.4 for PMMA.

Table 2.3 Polymerization conditions for PS growth from MNP surface

Sample ID	Initiator/CuCl/PMDETA/ styrene (mol ratio)	Xylene/styrene (V/V)	Temperature (°C)	Time (h)
OT2St ^a	1/1/100 ^a	1/1	70	2
OT3St ^a	1/1/100 ^a	1/1	80	3,5
OT4St ^b	1/10/10/3000	1/1	110	7,5
OT5St ^b	1/10/10/3000	0	110	4,5
OT6St ^c	1/10/10/3600	2/1	110	72

^a dilute colloidal suspension of CMS coated MNPs used as an initiator & unknown amount of initiator

^b dried powder of CMS coated MNPs used as an initiator

^c concentrated colloidal suspension of CMS coated MNPs used as an initiator

Table 2.4 Polymerization conditions for MMA growth from MNP surface

Sample ID	Initiator/CuBr/CuBr ₂ / PMDETA/MMA	Solvent/MMA (V/V)	Temperature (°C)	Time (h)
OT1PMMA ^a	1/10/0.5/10/2500	2/1	70	24
OT2PMMA ^a	1/10/0.5/10/2500	2/1	70	24

^a concentrated colloidal suspension of CMS coated MNPs used as an initiator

2.3.3 Growth of PMMA-b-PS polymer from the surface of MNPs

30 mg of PMMA coated washed particles (macroinitiators) in 4 ml xylene, 5.3 mg CuCl and 2 ml styrene were first deoxygenated for 30 minutes. Then, deoxygenated 11.3 μ l PMDETA was injected to the reaction. The reaction was allowed to continue at 110 °C for one day. The viscosity of the solution increased with time. After the polymerization was complete, the remaining solution was diluted with dichloromethane and precipitated to methanol. The precipitated powder was dried in vacuum oven. PMMA-b-PS chains were cleaved from the MNPs as described below.

2.3.4 Cleavage of polymers from the MNPs

Typically, 20 mg of the polymer-grafted MNPs were treated with 3 ml 10 % HF aqueous solution for 4 hours. The brown color of the MNP cannot be seen after the HF treatment. After being neutralized by dilute 3 ml of NaOH, cleaved polymer chains were extracted with chloroform. The chloroform was removed by rotaryevaporator and the remaining polymer was redissolved in THF for molecular weight analysis with GPC.

2.4 Nanoparticle containing film preparation

2.4.1 Films containing surfactant coated MNPs

Polymer solutions were prepared at a total polymer concentration of 10-20 mg/ml and at various mass fractions in toluene or chloroform. In the PS/PEG blends, PS was kept as the minor component with up to a maximum of 30% by mass. Nanoparticles were added into the polymer solutions from nanoparticle suspensions in the same solvent. Thin films were prepared by spin coating from solutions onto glass substrates at 2000 rpm for 1 min.

2.4.2 Films containing polymer coated MNPs

Blends of PEG with polymer coated nanoparticles were prepared at a total polymer concentration of 10 mg/ml and at various mass fractions in toluene. PS has been kept as the minor component in the blend up to a maximum of 30% by mass. Thin films were prepared by spin coating from solutions onto glass substrates at 2000 rpm for 1 min.

2.5 Characterization methods

Hydrodynamic size of the particles were measured by Malvern ZetaS Dynamic Light Scattering unit and reported as the intensity based average. Optical microscopy (OM) images were taken using Leica DMLM Optical microscope at different magnifications to observe phase separation in the films. Atomic Force Microscopy (AFM) images were recorded using NT-MDT Solver P47 in the tapping mode using silicon cantilevers. AFM was used to image the distribution of nanoparticles in the polymer films. Chemical characterization of nanoparticles was done by FTIR. IR spectra of the nanoparticles were recorded on a Nicolet FTIR instruments using KBr pallet of the dried samples. Organic content of the nanoparticles and quantification of the initiators on the particles were determined by Thermogravimetric analyses (TGA). TGA was performed on a Seiko SSC 5200 TG/DTA under N₂ with 10°C/min heating rate. Crystal structure and the crystal size of the nanoparticles were determined by XRD. XRD data were collected on a Huber, Guinier System 642 X-ray Powder Diffractometer using monochromatic Cu-K α radiation ($\lambda=1.5418 \text{ \AA}$). Iron content was determined by Inductively Coupled Plasma analysis on a Spectro Genesis EOP ICP from the acid treated samples and reported as the average of three runs of three samples. Polymer molecular weights were determined by Gel Permeation Chromothography (GPC). GPC analysis was done on an Agilent GPC with Mixed-C column using THF as an eluent, refractive index detector and PS standards at flow rate of 1ml/min.

Chapter 3

Characterization of Surface Modified Nanoparticles

3.1 Characterization of LA coated MNPs

Lauric acid (LA) stabilized iron oxide nanoparticles were synthesized from aqueous solution of iron salts with NH_4OH in the presence of excess amount of LA. Aqueous suspension of nanoparticles is formed as the lauric acid organizes in an interdigitated bilayer around the nanocrystal surface [5,54]. Removal of the second surfactant layer by alcohols provide LA monolayer coated hydrophobic nanoparticles that can be dispersed in toluene and chloroform as reported by Yagci et al (Figure 3.1) [5].

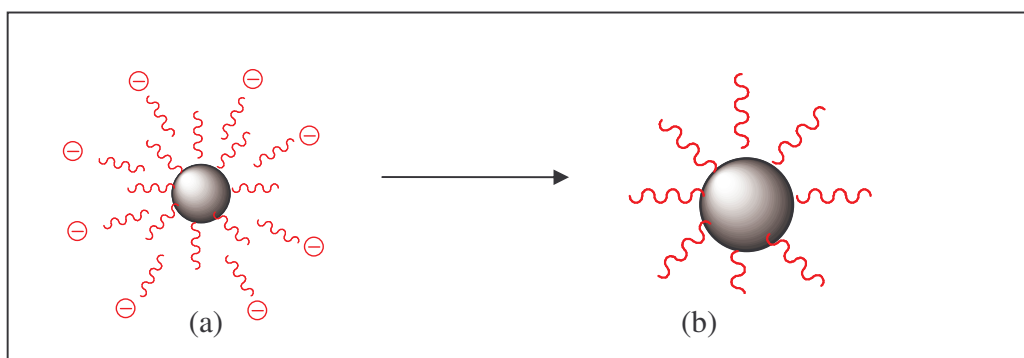


Figure 3.1 (a) LA bilayer coated (b) LA monolayer coated iron oxide nanoparticles

3.1.1 Dynamic Light Scattering (DLS)

Precipitation of LA monomer layer coated particles in isopropanol provided small aggregates of 120nm (Figure 3.2).

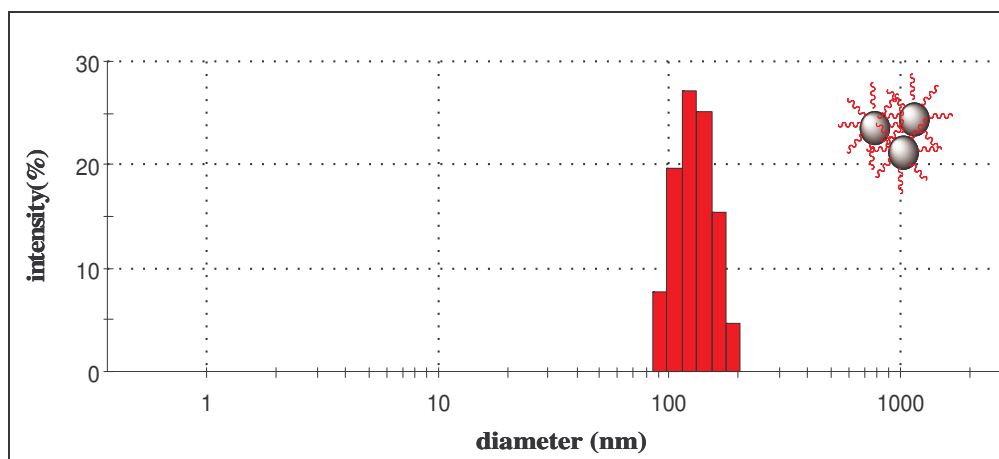


Figure 3.2 DLS size distribution of LA monolayer coated iron oxide nanoparticles in toluene prepared by precipitation method. Peak maximum: 120 nm

In order to obtain smaller particles, LA monolayer coated particles were extracted from the initial aqueous suspension supporting the bilayer-coated particles with chloroform. The extraction method provides small clusters (10-50 nm) (Figure 3.3).

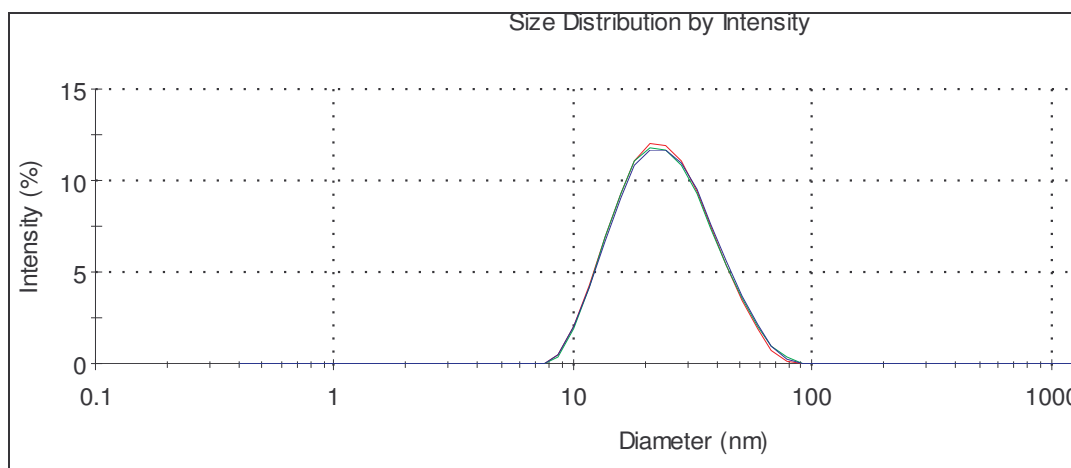


Figure 3.3 DLS size distribution of LA monolayer coated iron oxide nanoparticles in CHCl_3 prepared by extraction method. Peak maximum: 25 nm

In the extraction process, phase separation was quite slow. In order to decrease the equilibrium time of the extraction, we have added a small amount of isopropanol (IPA) to the chloroform/water mixture. IPA would remove the second layer of the lauric acid from the particles, which are in water, and the hydrophobic monolayer-coated particles would be captured by the chloroform. The ratio of isopropanol that should be added was an important factor in terms of size of the monolayer coated particles. As shown in Figure 3.4, as the IPA amount increased, the particle size increased. Optimization was achieved at 0.1 ml IPA for 5 ml stock solution.

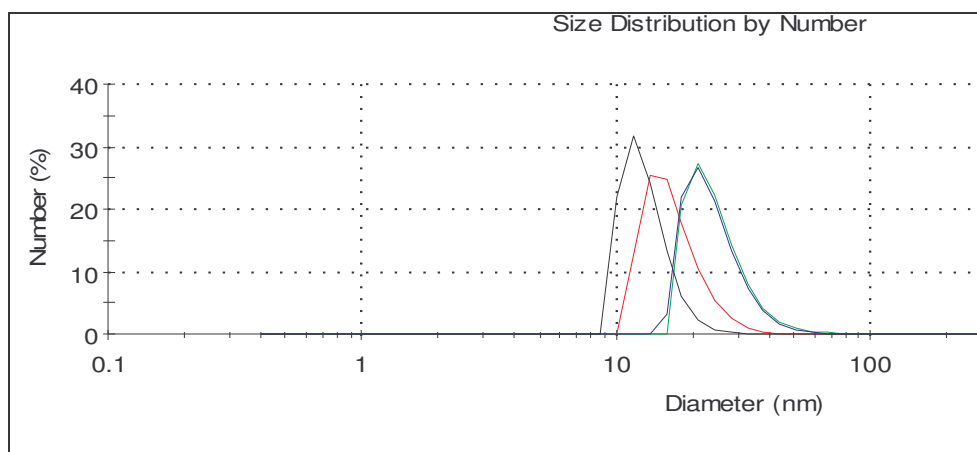


Figure 3.4 Hydrodynamic sizes of LA coated MNPs prepared by extraction method with different amounts of IPA addition

3.1.2 X-Ray Diffraction

X-Ray Diffraction (XRD) technique was used to determine the size and composition of crystalline magnetic cores of the LA-coated iron oxide nanoparticles.

Crystal size of magnetic cores were calculated based on the major diffraction peaks ($2\theta = 35.512^\circ$ and 35.559°) in XRD by using Debye–Scherrer equation;

$$D = 0.9\lambda / \beta \cos \theta$$

Where D is the average crystallite size (\AA), λ is the wavelength of X-rays ($\text{CuK}\alpha$: $\lambda = 1.5418 \text{ \AA}$), θ is the Bragg diffraction angle, and β is the full width at half maximum (FWHM) (in radians). Magnetic iron oxide crystals that are coated with a LA bilayer are about 7.25 nm whereas those prepared without a surfactant (bare particles) are about 11 nm (Figure 3.5). Sharp peak at $2\theta = 32.714^\circ$ is due to the complex of excess LA with

ammonium. The difference in crystal size indicates effective surface passivization through adsorption of LA on the surface of the growing crystal preventing further growth. Both the bare particles and the coated particles are γ -Fe₂O₃, maghemite crystals.

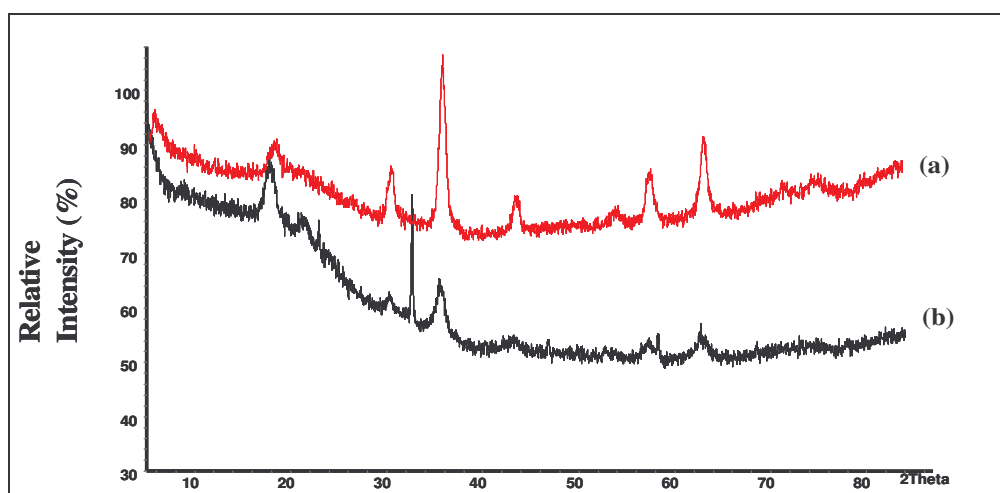


Figure 3.5 XRD analysis of a) bare and b) bilayer coated particles.

However, it was thought that these particles should be magnetite, because $\text{Fe}^{+3} / \text{Fe}^{+2}$ was chosen as 2 for Fe₃O₄ synthesis. Therefore, in order to observe if NaNO₃ is the reason for this unexpected crystal, the XRD analyses of the particles with and without NaNO₃ were carried out (Figure 3.6). Two different sharp peaks were observed between them. They are $2\theta=22$ and $2\theta=58$. Nevertheless, this XRD data did not give an exact idea about NaNO₃ effect on the crystal structure. Because these peaks belong to NaNO₃ crystal itself. In order to identify the crystals, FT-IR spectra of both were observed. Crystal sizes of the particles with NaNO₃ were calculated as 7.25 nm, without NaNO₃ was 8 nm.

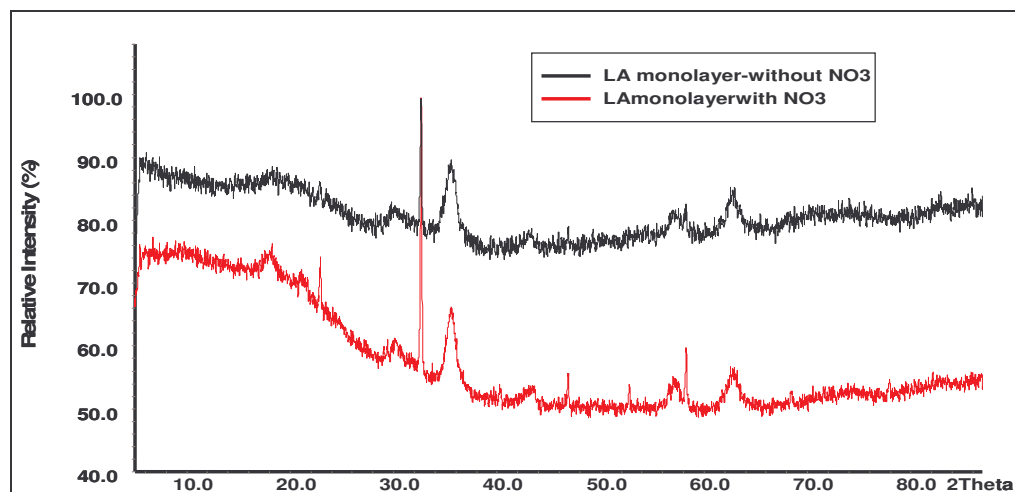


Figure 3.6 XRD analysis of particles synthesized in the presence of NaNO_3 (red), absence of NaNO_3 (black)

3.1.3 Infrared Spectra

LA is an effective stabilizer for the iron oxide nanocrystal. IR spectrum of all samples showed signals at $635\text{--}592\text{ cm}^{-1}$ for Fe-O bonds of maghemite ($\gamma\text{-Fe}_2\text{O}_3$) (Figure 3.7) [4]. LA bilayer coated iron oxide showed peaks at 1715 , 1524 and 1400 cm^{-1} corresponding to carbonyl (C=O), asymmetric and symmetric carboxylate (COO^-) stretching modes (Figure 3.7c). The dramatic decrease of the first two peaks in LA monolayer coated particles proves that the second layer of the particles are completely removed after precipitation in alcohol and actually carboxylate groups attached on the particle surface in bidentate form (Figure 3.8) [55].

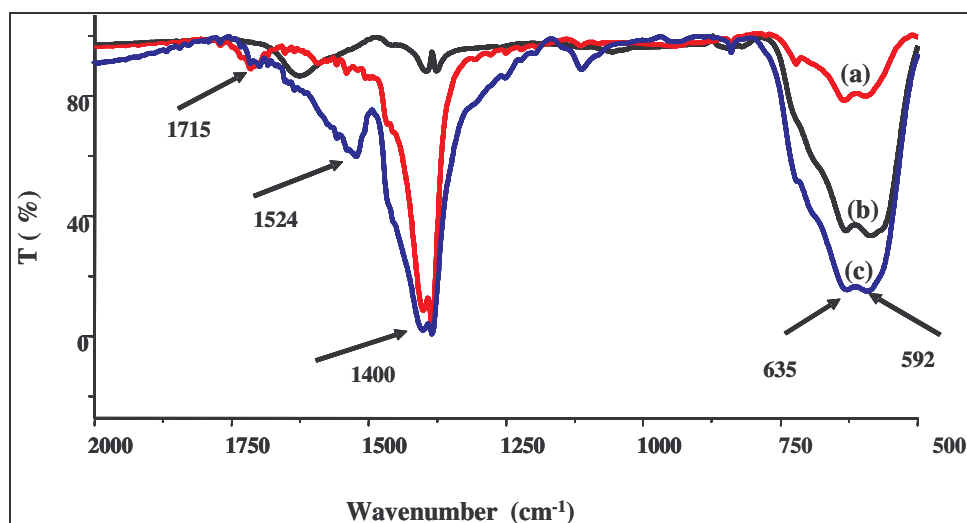


Figure 3.7 FT-IR spectrum of a) monolayer coated b) bare c) bilayer coated particles.

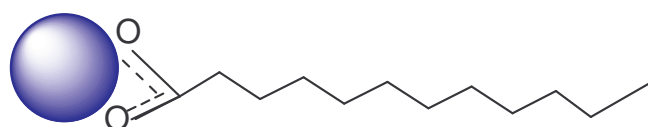


Figure 3.8 Bidentate binding of carboxylate on the iron oxide surface

IR spectrums of LA coated MNPs with and without NaNO_3 were also investigated to see the effect of NaNO_3 on the crystal. The signals belong to the Fe-O bond were different for each particles. For the particles with NaNO_3 , 635-592 cm^{-1} signals were observed belonging to the $\gamma\text{-Fe}_2\text{O}_3$ (maghemite), and particles without NaNO_3 have the Fe-O bond signal at 590 cm^{-1} which belongs to the magnetite Fe_3O_4 (Figure 3.9) [4]. NaNO_3 oxidizes Fe^{+2} to Fe^{+3} resulting in formation of maghemite.

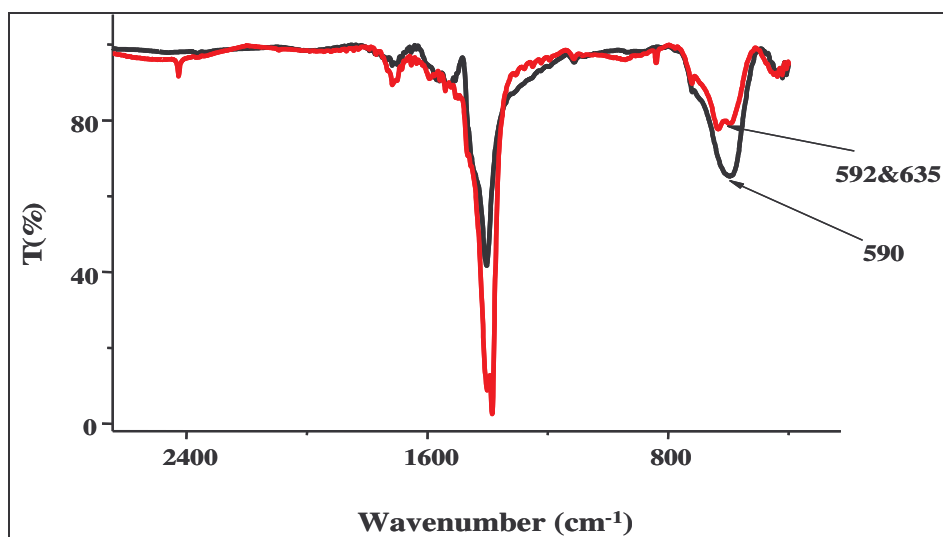


Figure 3.9 FT-IR spectrum of particles synthesized in the presence of NaNO₃ (red), absence of NaNO₃ (black)

3.1.4 Thermogravimetric Analysis

Thermogravimetric analysis provides information about the coating as well (Figure 3.10). Bare iron oxide nanoparticles showed a 4% weight loss, which is most probably surface adsorbed water, or loss of water from surface hydroxyls. The monolayer coated particles had a 28% weight loss starting at about 120 °C which is plausible for the decomposition of the LA. The bilayer coated particles showed two-step decomposition with 50% weight loss at 122 °C and 22% at 244 °C. First decomposition step is due to the free LA and physically adsorbed outer layer and the second step at higher temperature is for the chemically and more strongly adsorbed inner layer. Higher temperature weight loss amount is comparable to the weight loss obtained with the monolayer-coated particles. In addition, from the weight loss, the number of molecules per nm² was calculated according to the following equation[51]:

$$\text{Number of molecules / nm}^2 : \frac{W * d_{\text{Fe}_2\text{O}_3} * r * N_A}{M(1-W) * 3 * 10^{21}}$$

.....**Equation 1**

Where; W is weight loss of sample, $d_{\text{Fe}_2\text{O}_3}$ is the density of Fe_2O_3 , N_A is the Avagadros number, M is the molecule weight of the coating molecule and r is the radius of the MNPs. Application of this equation suggested that there are about 26 LA molecules per nm^2 of LA monolayer coated MNPs

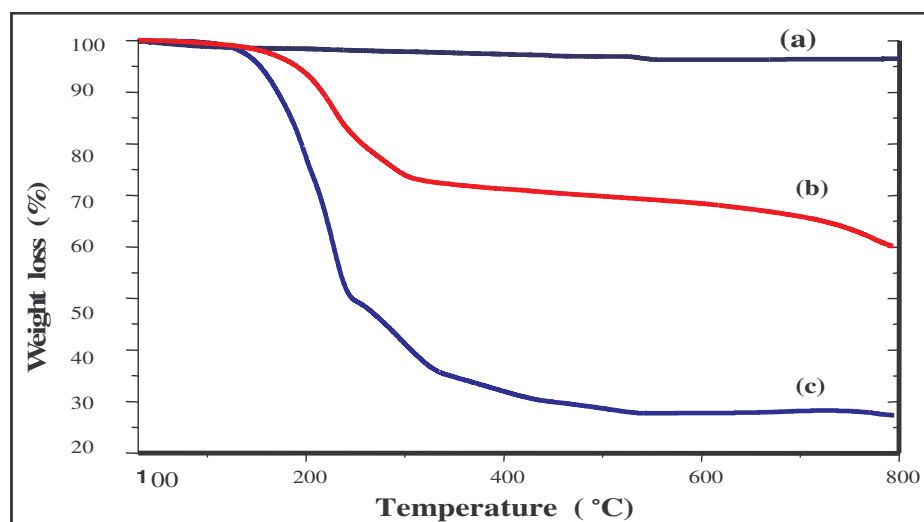


Figure 3.10 TGA data of a) bare b) monolayer coated c) bilayer coated iron oxide nanoparticles

3.1.5 Atomic Force Microscopy

Atomic force microscope (AFM) was used to observe particle size and size distribution. Hydrodynamic size of LA-coated iron oxide nanoparticles, which were prepared by the extraction method, was around 20 nm with a size distribution of 10-100 nm according to intensity-averaged results of DLS measurement (Figure 3.3). AFM images showed similar aggregate sizes confirming that the intensity based size measurement by DLS is a correct representation of these particles (Figure 3.11).

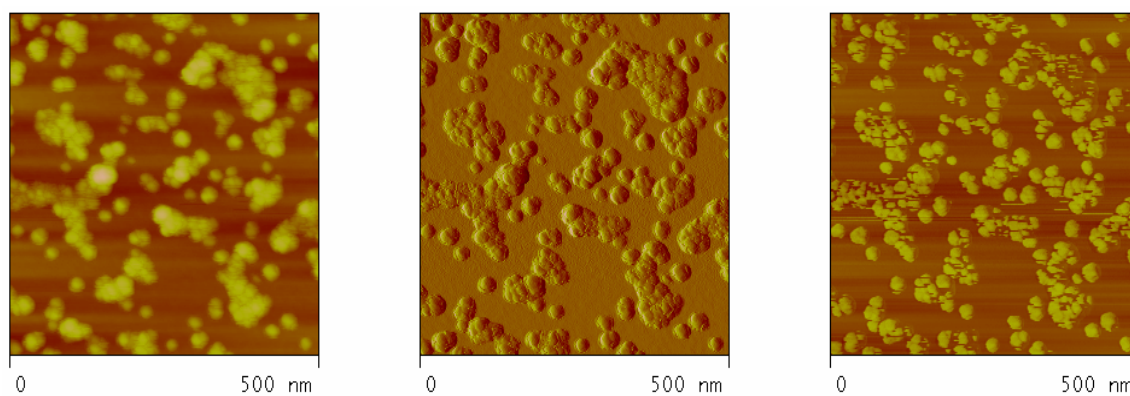


Figure 3.11 AFM images of LA coated iron oxide NPs (height, amplitude and phase, respectively)

3.2 HDMS coated MNPs

Silane coupling agents are versatile compounds invaluable in linking organic and inorganic materials together. A typical general structure is:



Where Y is a hydrolysable group, usually alkoxy or halogen groups, R is a hydrocarbon linker and X is an organofunctional group, such as amino, methacryloxy, epoxy, etc. Alkoxysilanes are effective in modifying metal oxide surfaces. One of the silane coupling agents that we have used is HDMS (hexadecyltrimethoxysilane) (Figure 3.12). Trialkoxysilanes easily bond onto the metal hydroxyl groups, especially if the metal contains silicon, aluminum or if it is a heavy metal. Therefore, in order to have hydrophobic MNPs, HDMS was used as a coating material.

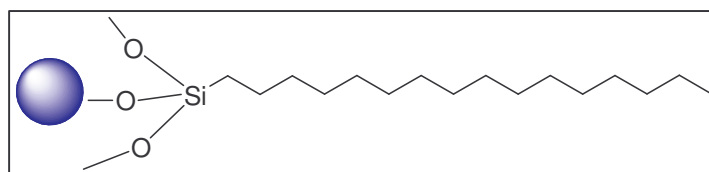


Figure 3.12 Binding of HDMS from the methoxysilane onto the MNP

It was observed that sol-gel method, which is often used for the surface modification of NPs, is difficult for the silane modification of NPs because of silica formation [56]. Therefore, HDMS coated particles were prepared from either pre-synthesized bare particles or by ligand exchange of LA with HDMS. Bare particles cannot form colloidal suspension in water since they don't have stabilizers (coatings) and form aggregated clusters. Interaction of magnetic dipoles does enhance this interaction. Therefore, stabilizing the bare particles with a surfactant (ex-situ synthesis) is a difficult and time consuming procedure.

On the other hand, ligand exchange is a well-known method for tuning the surface properties of nanoparticles. It consists of adding excess ligand to the nanoparticle suspension resulting in the displacement of the former ligand which is on the nanoparticle's surface. Moreover, ammonium hydroxide or acetic acid catalyzes the hydrolysis and condensation of alkoxy silane groups, facilitating the bonding. Therefore, ammonium hydroxide was used for the ligand exchange reaction and acetic acid was used for the coating process of the bare particles. As a result, HDMS can be grafted onto the iron oxide nanoparticle surface from the methoxy silane groups forming Fe-O-Si covalent bond forming a stable colloid of hydrophobic nanoparticles in organic solvents such as toluene and chloroform.

3.2.1 Dynamic Light Scattering

The hydrodynamic sizes of particles synthesized from the bare particles or by the ligand exchange were similar. They are about 30-50 nm with a range of 10-100 nm (Figure 3.13 & 3.14).

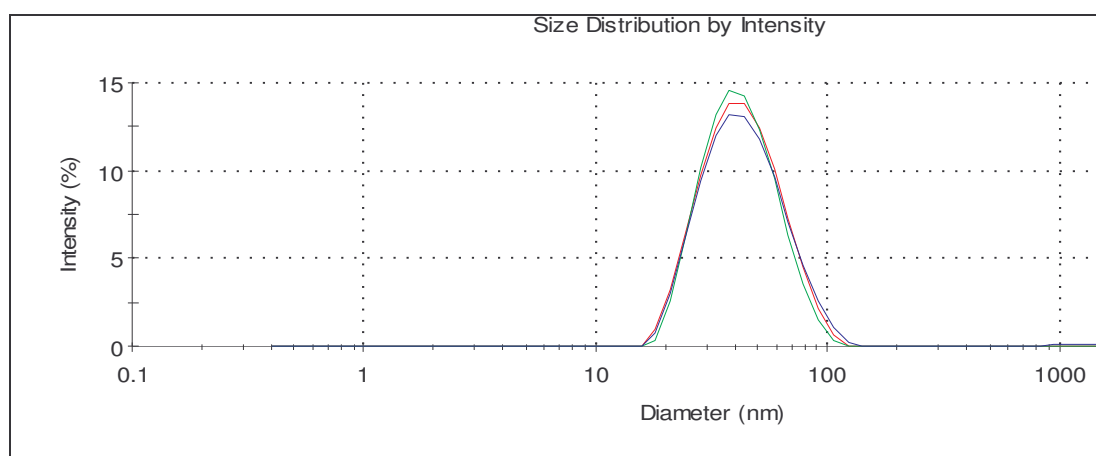


Figure 3.13 Hydrodynamic sizes of HDMS coated particles prepared from bare particles

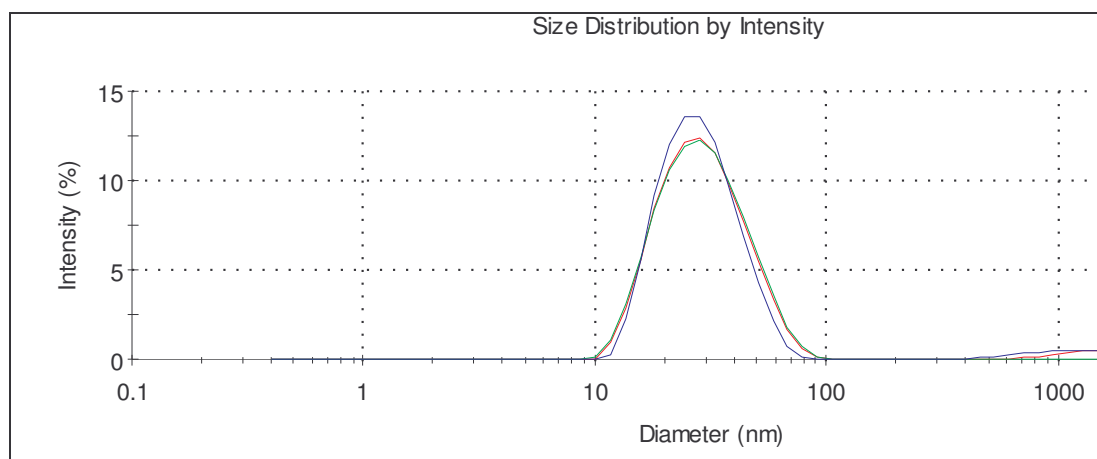


Figure 3.14 Hydrodynamic sizes of HDMS coated particles prepared by ligand exchange

3.2.2 X-Ray Diffraction

Figure 3.15 and 3.16 show the XRD analyses of the HDMS coated MNPs from the bare NP and by the ligand exchange, respectively. The sharp peak in Figure 3.15 which is at $2\theta=22^\circ$ corresponds to the SiO_2 crystal. Self-condensation of HDMS would form Si-O-Si network that would give rise to such observation. However, that sharp peak had disappeared for the particles prepared by ligand exchange. This shows that ligand exchange is more effective and cleaner coating method. In addition, the peak at $2\theta= 32.714^\circ$ which was seen in the XRD diagram of LA coated MNPs (Figure 3.12) had also disappeared after the ligand exchange. This shows the LA was removed during ligand exchange. The sizes of the HDMS coated MNPs synthesized by ligand exchange method were calculated as 7.3 nm, which is same with LA coated particles as expected since this process would not cause a crystal growth.

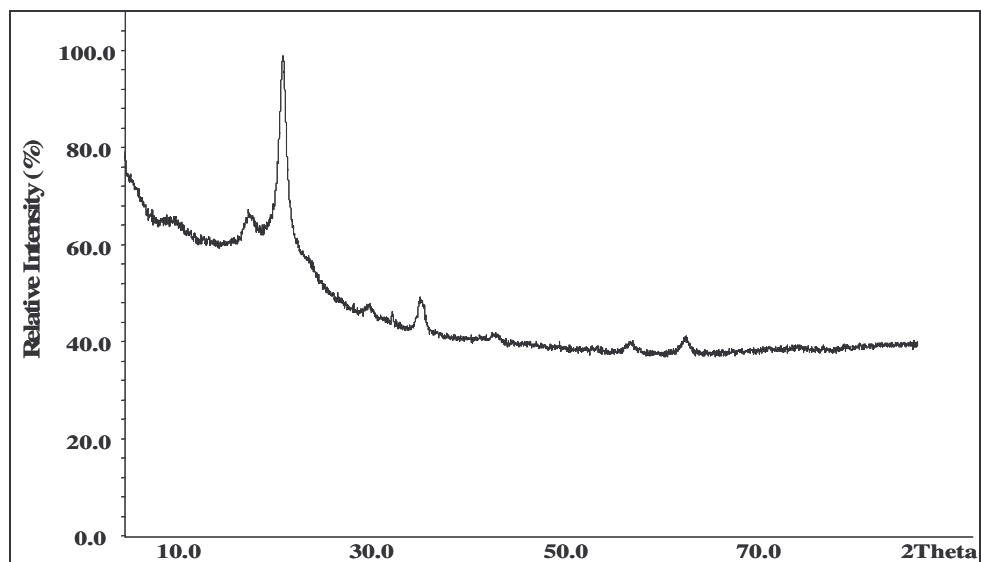


Figure 3.15 XRD diagram of HDMS coated particles prepared from the bare particles

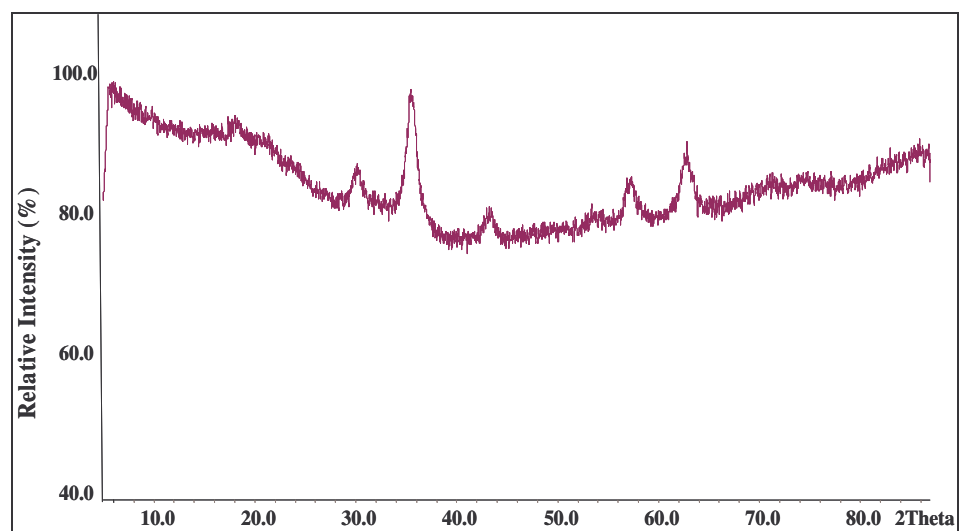


Figure 3.16 XRD diagram of HDMS coated particles prepared by the ligand exchange

3.2.3 Infrared Spectroscopy

To see if the ligand exchange of HDMS with LA is effective on the MNP surface, IR spectra of HDMS surfactant and HDMS coated particles were taken and shown in Figure 3.17. The signals at 622-593 cm^{-1} are for Fe-O bond of maghemite ($\gamma\text{-Fe}_2\text{O}_3$) [4]. The covalent bonding of HDMS to the particle forms Fe-O-Si bond, which has the absorption band at around 584 cm^{-1} but it overlaps with the Fe-O of maghemite [57]. Therefore, it cannot be seen. However, the adsorption of HDMS onto the particle can be verified by the peaks at 800, 996, 1053 cm^{-1} corresponding to OH vibrations, Si-OH and Si-O-Si groups [57].

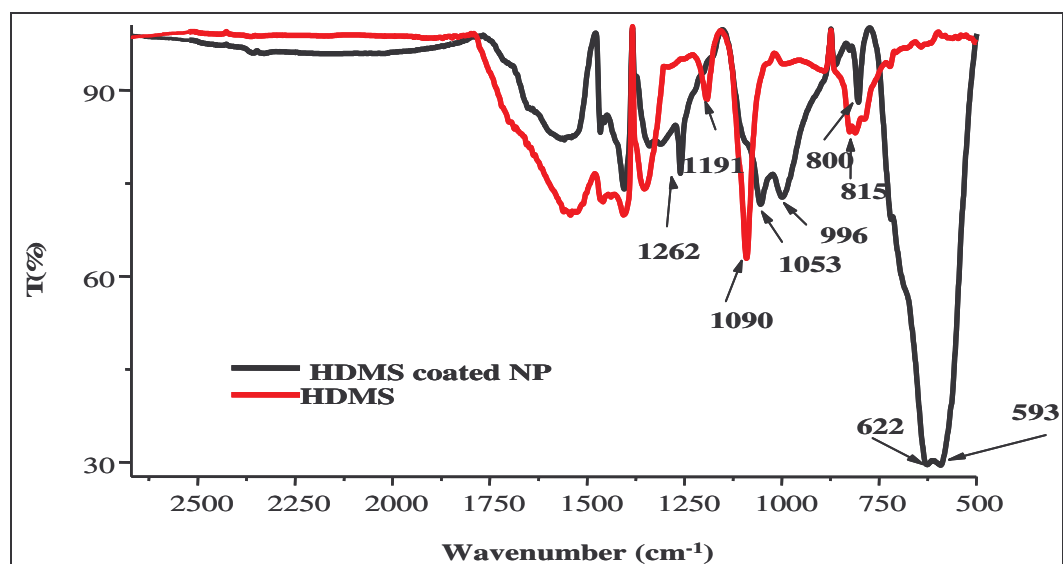


Figure 3.17 FT-IR spectrum of HDMS (red) and HDMS coated MNPs (black)

3.2.4 Thermogravimetric Analysis

Thermogravimetric analysis of HDMS coated MNPs provides information about the coating and the number of molecules grafted onto the surface of MNPs (Figure 3.18). The coated particles showed a 4% weight loss at 100 °C, which is most probably surface adsorbed water. They had a 14.5 % weight loss starting at about 220 °C, which is believed to be for the decomposition of the HDMS. From the weight loss, the number of molecules per nm² was calculated as 7.6 according to the equation 1.

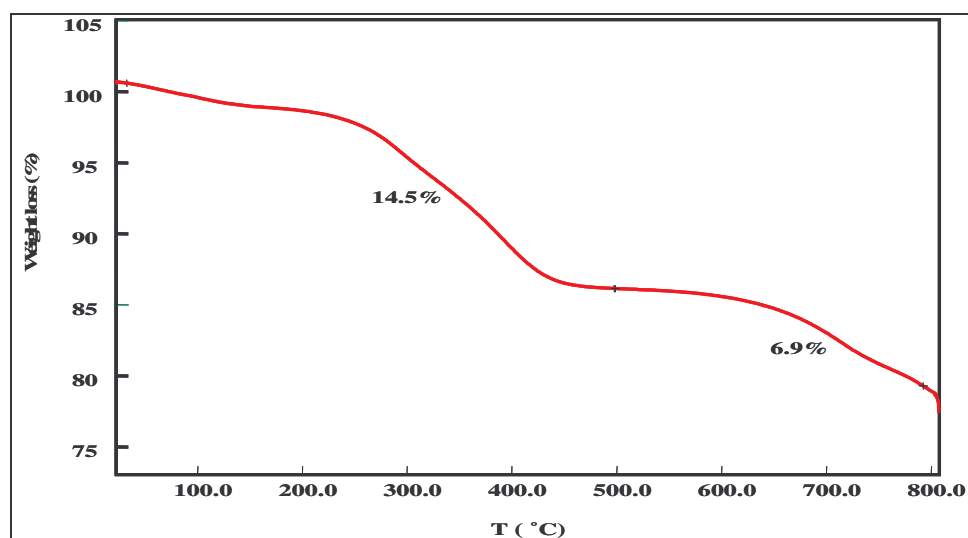


Figure 3.18 TGA data of HDMS coated MNPs

3.2.5 Atomic Force Microscopy

Figure 3.19 shows the AFM micrographs of the HDMS coated particles prepared by ligand exchange method. Nanoparticles are about 30 nm in these images, which are consistent with the hydrodynamic sizes.

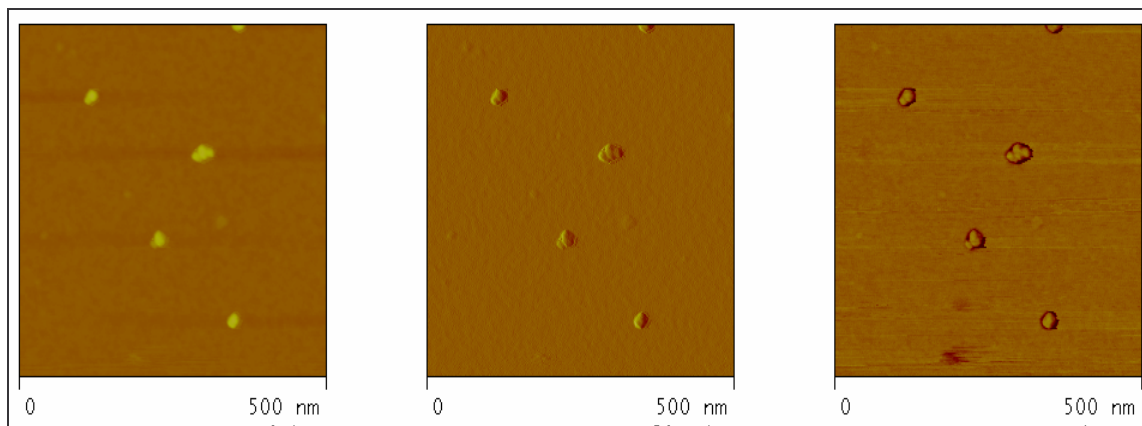


Figure 3.19 AFM image (height, amplitude, phase) of HDMS coated MNPs

3.3 PEG-Si coated MNPs

Another surfactant used to stabilize the iron oxide nanoparticles in this research is methoxy-polyethyleneoxy-propyl trimethoxysilane (PEG-Si) which is also a silane-coupling agent (Figure 3.20).

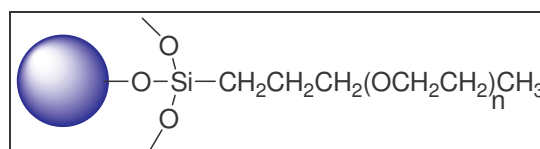


Figure 3.20 Binding of PEG-Si from the methoxysilane onto the MNP

As explained in Chapter 1, polymeric coatings are widely used for iron oxide stabilization. PEG-Si coated particles were synthesized via in-situ coating of the MNPs with PEG-Si. PEG-Si bound to the iron oxide surface through Fe-O-Si bonds and the PEG tail causes the stabilization and dispersion of the particles both in polar solvents such as water and in apolar solvents such as toluene.

3.3.1 Dynamic Light Scattering

Excess unbound polymer in stock solutions was removed via ultrafiltration with distilled water. This process allows us to test the stability of the nanoparticles in the absence of excess coating material indicating the stability of polymer adhesion to the crystal surface. Although size distribution of unwashed particles is narrower than washed particles, there is no dramatic difference in terms of size between the two (Figure 3.21). This indicates that the particles are stable.

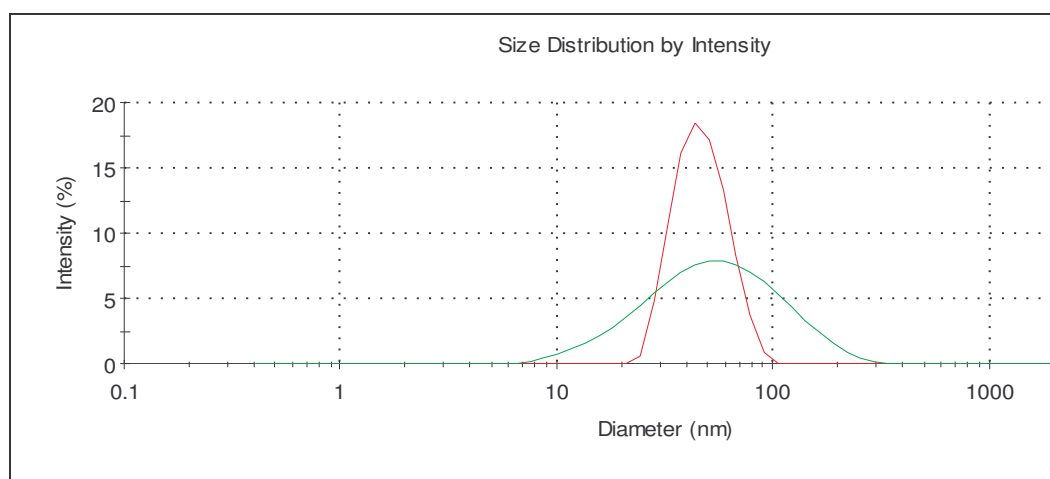


Figure 3.21 Hydrodynamic sizes of PEG-Si coated MNPs in water: washed (green) and unwashed (red)

Stability of washed particles was also tested with dilutions and it was seen that the particles were stable up to 1/100 dilution (Figure 3.22). This may confirm covalent/irreversible bonding of the coating.

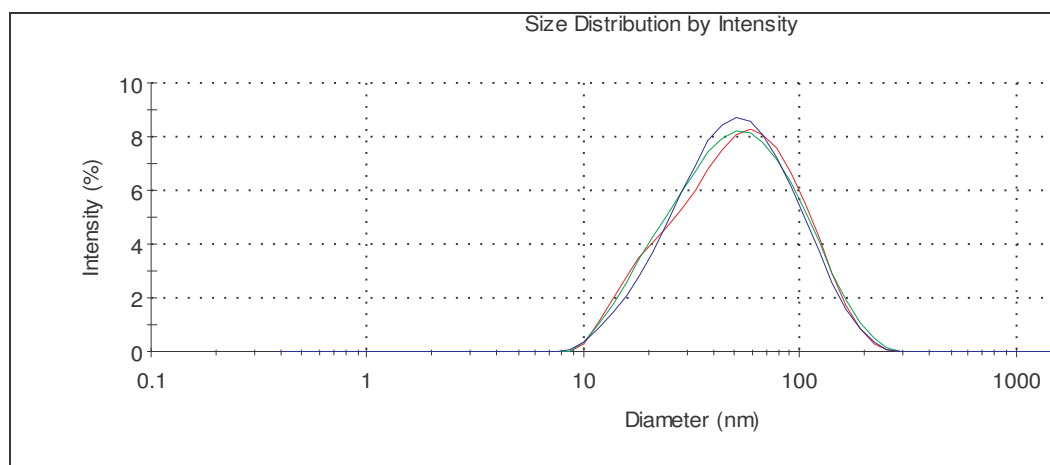


Figure 3.22 Hydrodynamic sizes of washed PEG-Si coated particles (red), 1/10 (green), 1/100 (blue) dilution

In order to disperse these particles in homopolymers and polymer blends, they were first taken into toluene or chloroform, which are good solvents for both particles and the polymers. PEG-Si coated MNPs, which were synthesized in water, were dried after washing and then redispersed in toluene. There seems to be slight increase in the hydrodynamic size (Figure 3.23) in toluene. There might be several reasons for this, but generally, when particles are suspended from dry powder, larger aggregates tend to form. In addition, interaction of PEG with toluene and water is different and therefore hydration is different as well. If the particles were sonicated for a longer time, they may have the same size with the stock solution.

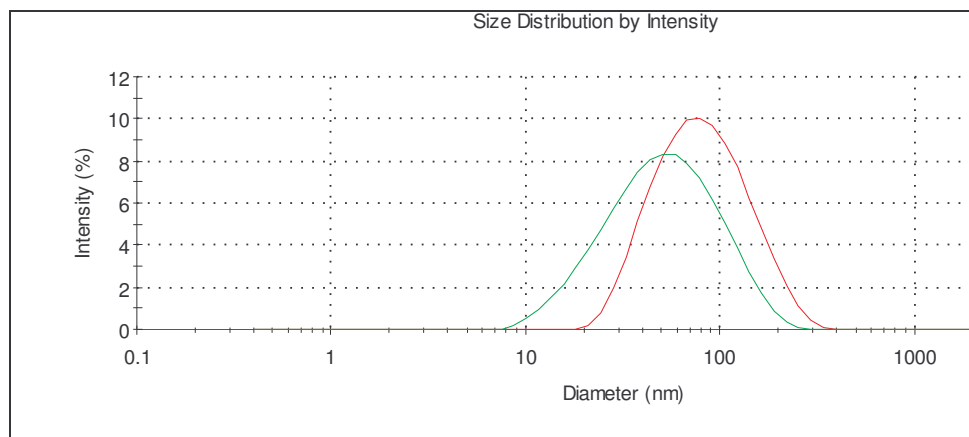


Figure 3.23 Hydrodynamic sizes of PEG-Si coated MNPs in toluene (red) and in water (green)

3.2 X-Ray Diffraction

Crystal structure and size was determined by XRD analysis of PEG-Si coated particles. The crystal structure is γ - Fe_2O_3 maghemite, and the size was calculated as 8.1 nm (Figure 3.24).

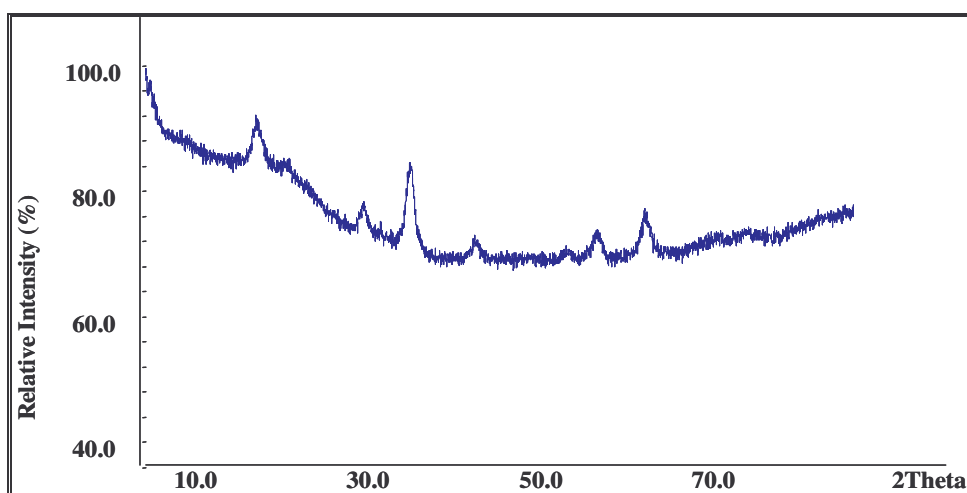


Figure 3.24 XRD analysis of PEG-Si coated MNPs

3.3.3 Infrared Spectra

IR spectra of PEG-Si coated MNPs show peaks at 588 and 631 cm^{-1} that belong to Fe-O of maghemite nanocrystals (Figure 3.25). Fe-O-Si bond (584 cm^{-1}) overlaps with the Fe-O peak. [57] However, the other peaks at 840, 1048, 1105 and 3127 corresponding to Si-O-CH₃, Si-O-Si and Si-OH verify the presence and adsorption of PEG-Si onto the iron oxide nanoparticles [57].

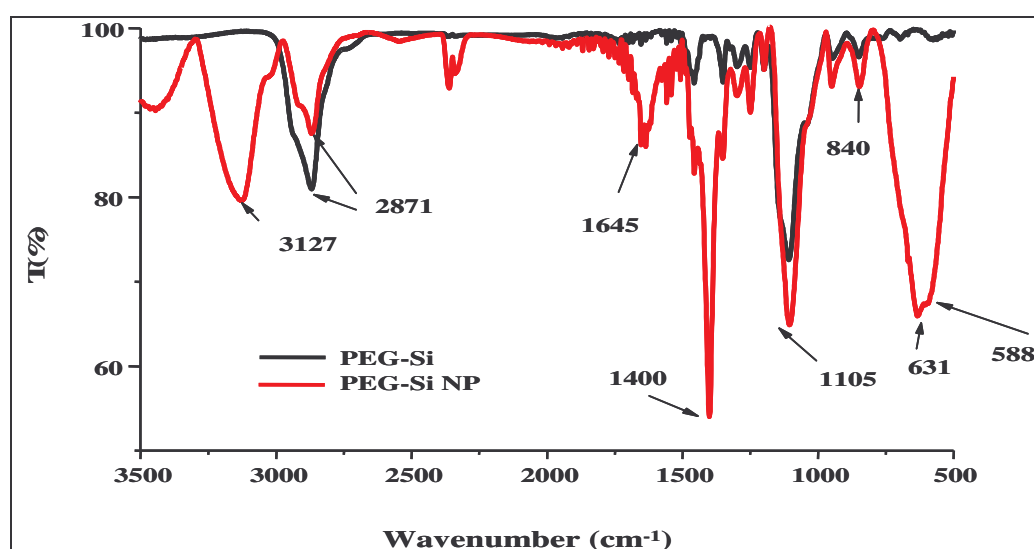


Figure 3.25 FT-IR spectrum of PEG-Si (black) and PEG-Si coated MNPs (red)

3.3.4 Thermogravimetric Analysis

TGA plot of PEG-Si coated MNPs is shown in Figure 3.26. There is a weight loss of 1.5% due to surface adsorbed water. Then, a weight loss of 14% starts at about 200 °C for the decomposition of PEG-Si [58]. According to the equation 1 and using the weight loss, the number of molecules per nm^2 was calculated as 3.07 [51].

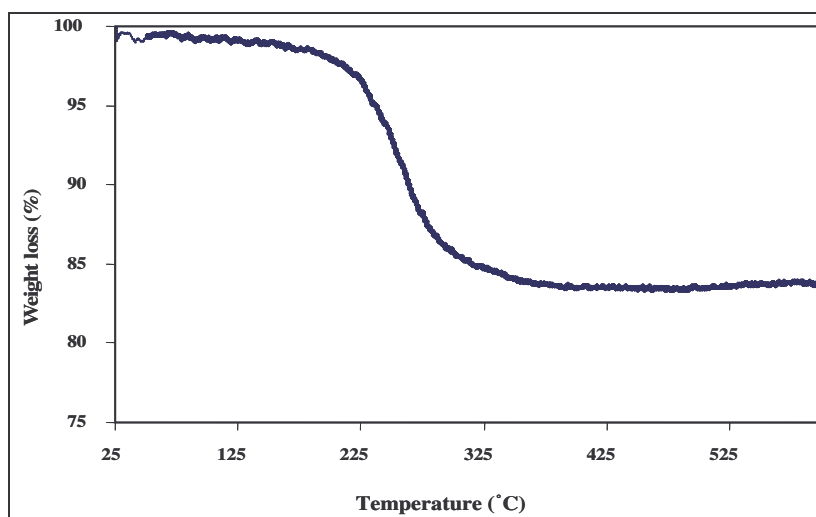


Figure 3.26 TGA data of PEG-Si coated MNPs

3.3.5 Atomic Force Microscopy

Figure 3.27 shows the AFM micrographs of the PEG-Si coated particles synthesized. The height of these particles are about 10-20 nm and the width is about 40 nm indicating that the particles are buried in the PEG coating.

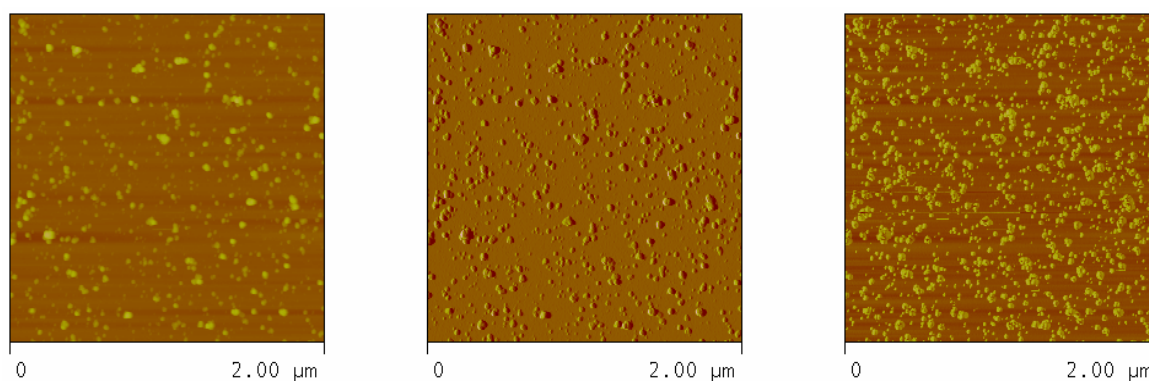


Figure 3.27 AFM images of PEG-Si coated MNPs

3.4 CMS coated MNPs

To initiate polymerization of styrene and methyl methacrylate from the surface of the iron oxide nanoparticles with ATRP method, first the particles should be coated by an initiator. CMS (p-chloro methylphenyl trimethoxysilane) was used for this purpose since it can bind to iron oxide surface with methoxy silane and it can initiate ATRP polymerization with the $-\text{CH}_2\text{Cl}$ group (Figure 3.28).

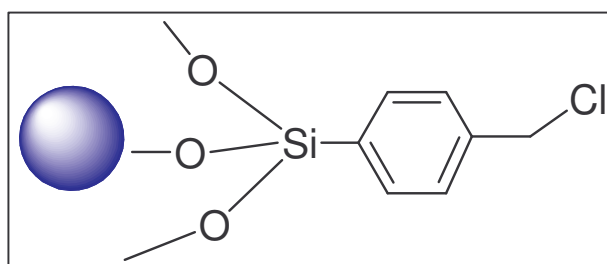


Figure 3.28 Binding of CMS from the methoxysilane onto the MNP

The stabilization of the particles with CMS was achieved by ligand exchange of LA with CMS in the presence of ammonium hydroxide as a catalyst. In order to prevent decomposition of the ligand, exchange was performed at room temperature. Since toluene and xylene are appropriate solvents for the styrene polymerization, ligand exchange was done in toluene. However, CMS coated MNPs were not very stable in toluene or xylene after ligand exchange, because Cl tail of the initiator causes the particles to be relatively polar.

3.4.1 Dynamic Light Scattering

Hydrodynamic sizes of the CMS coated particles are about 200 nm in toluene, about 100 nm in xylene as shown in Figures 3.29 and 3.30.

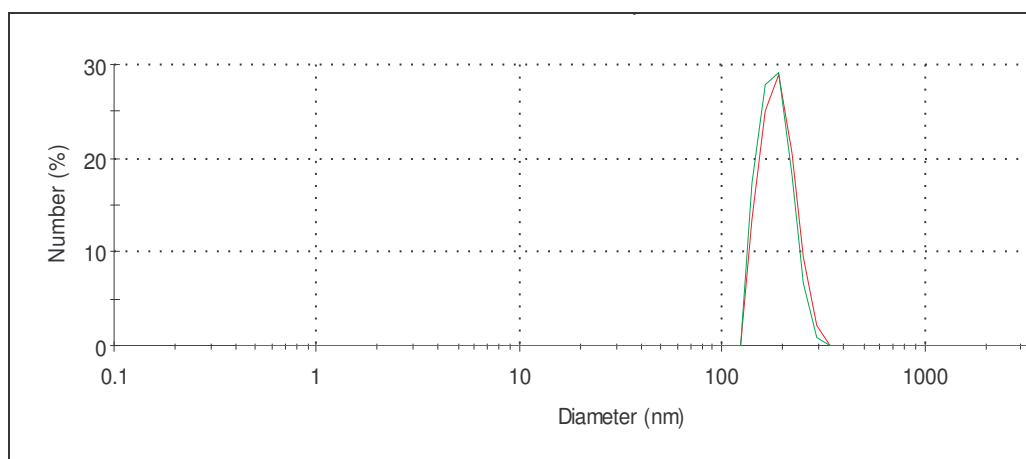


Figure 3.29 Hydrodynamic sizes of CMS coated MNPs in toluene

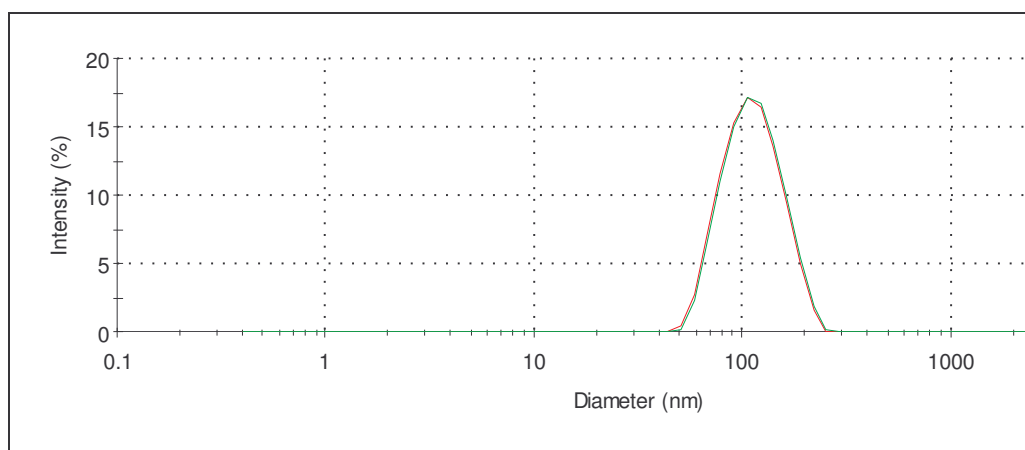


Figure 3.30 Hydrodynamic sizes of CMS coated MNPs in xylene

Due to the lack of long-term stability in these solvents, particles were precipitated with hexane, washed and suspended in DMF. Particles in DMF were about 37nm in average and were not affected by the dilution indicating good stability (Figure 3.31).

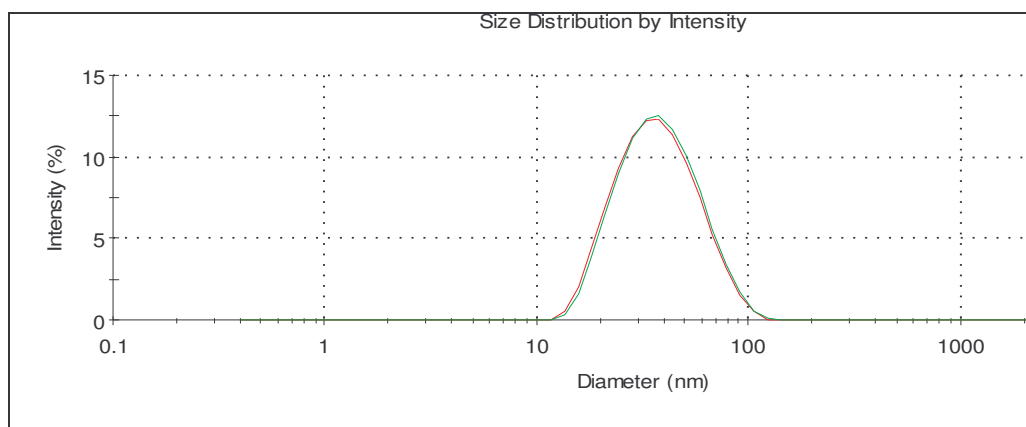


Figure 3.31 Hydrodynamic sizes of CMS coated MNPs in DMF: stock (red), diluted (green)

3.4.2 X-Ray Diffraction

Figure 3.32 shows the XRD analysis of the CMS coated MNPs and LA monolayer MNPs. They are almost the same except the peak at $2\theta = 32.714^\circ$. This peak as said in section 3.1 belongs to LA ammonium salt and it disappears after ligand exchange with CMS. This disappearance shows the particles were well washed after ligand exchange. The crystal sizes of CMS coated MNPs were calculated as 8.95 nm.

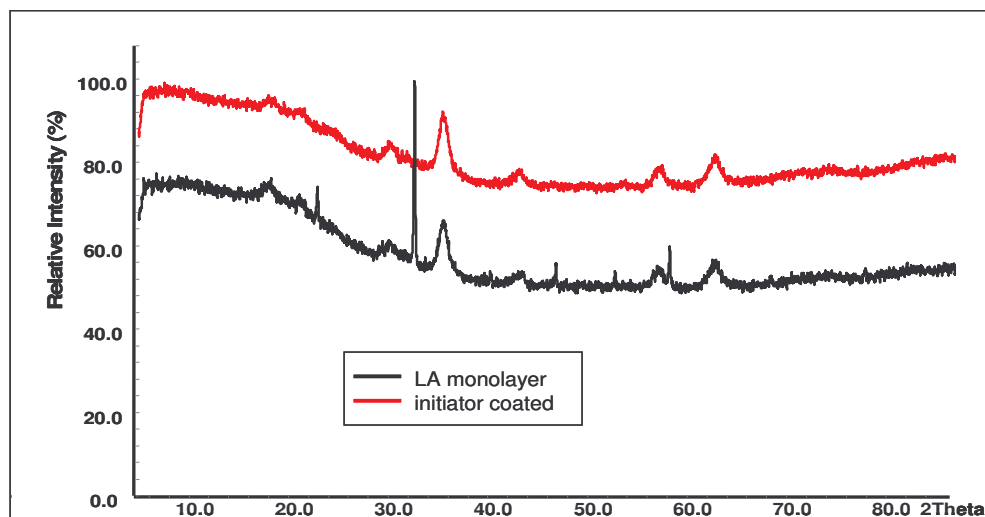


Figure 3.32 XRD diagram of CMS (red) and LA (black) coated MNPs

3.4.3 Infrared Spectroscopy

IR spectrum of CMS initiator and CMS coated particles were investigated to observe if the ligand exchange of CMS with LA is effective on the MNP surface (Figure 3.33). The signals at $639\text{-}590\text{ cm}^{-1}$ are for Fe-O bond of maghemite ($\gamma\text{-Fe}_2\text{O}_3$) and Fe-O-Si bond overlaps with this, therefore invisible [4, 57]. The most important peak was at 700 cm^{-1} indicating the presence of C-Cl. The other peaks that show the adsorption of CMS onto the particle were at $815, 996, 1031$ and 1130 cm^{-1} corresponding to OH vibrations, Si-OH and Si-O-Si groups [57].

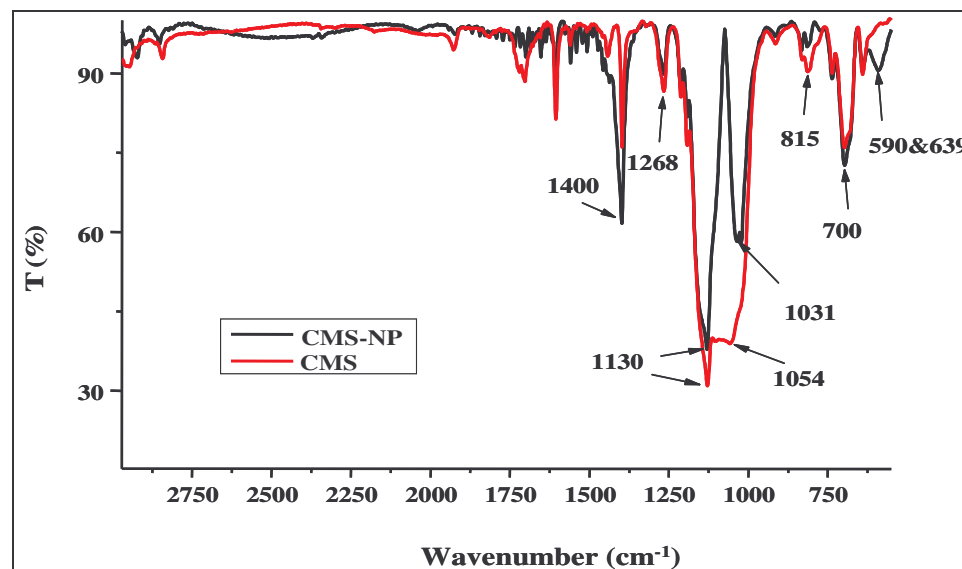


Figure 3.33 FT-IR spectra of CMS (red) and CMS coated MNP (black)

3.4.4 Thermogravimetric Analysis

The amount of CMS adsorbed on the MNP was determined by thermogravimetric analysis (Figure 3.34). The weight loss of 6% at the beginning is for the surface adsorbed water and the weight loss of 12.8% starting at about 220 °C is due to the decomposition of CMS. From the weight loss, the number of molecules per nm² was calculated as 7.45 using equation 1.

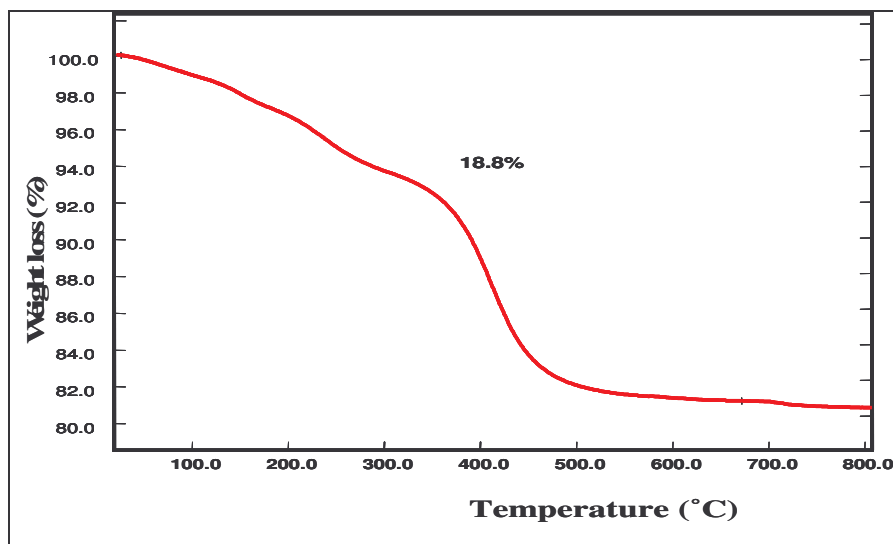


Figure 3.34 TGA data of CMS coated MNPs

Table 3.1 Characterization Table of Different Surfactant Coated MNPs

	Crystal	Crystal Size(nm)	D_h (nm)	Graft density (molecule/nm ²)
LA-MNP	γ -Fe ₂ O ₃	7.25	25 ^a & 120 ^b	25.87
HDMS-MNP	γ -Fe ₂ O ₃	7.3	40 ^c	7.60
PEGSi-MNP	γ -Fe ₂ O ₃	8.1	70 ^d	3.07
CMS-MNP	γ -Fe ₂ O ₃	8.95	37 ^e	5.80

^a in CHCl₃

^b in toluene

^c in toluene

^d in toluene

^e in DMF

Chapter 4

Characterization of Polymer Coated Nanoparticles

To disperse MNPs into the selected domain of a polymer blend or a block copolymer, selected polymer can be grafted from the surface of the nanoparticle as well. If so, there will be no need for another surfactant, which is compatible with the selected domain. The polymer will cause both the stabilization of the particles in a solvent and the selective dispersion in a phase-separated environment. For this reason, PS, PMMA and PMMA-*b*-PS were grown from initiator (CMS) coated MNPs by ATRP (Figure 4.1).

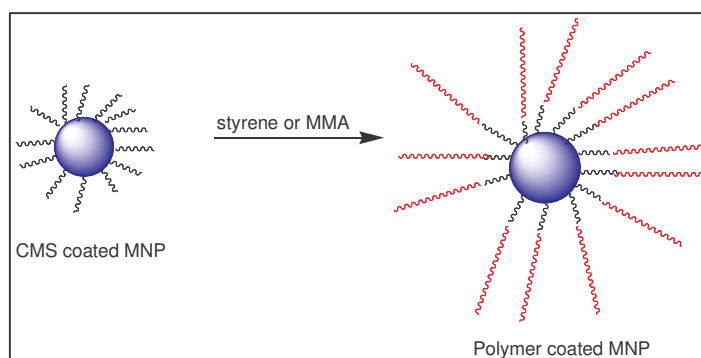


Figure 4.1 Typical scheme of polymerization from CMS coated MNPs

Because ATRP is a controlled polymerization method, polymer molecular weight (MW) can be tailored by the monomer/initiator ratio and the reaction time. Targeted molecular weight for the PS was 300K to match the molecular weight with the PS used for

the blends in this research. This molecular weight provided good phase separation with PEG in the thin films of blends that we have studied. The amount of initiator attached to the particle was calculated from the weight loss of CMS coated MNP recorded on a TGA. Then, the number of moles of monomer needed was calculated from the number of moles of initiator. For example, if there is one mole initiator on the MNP and if 300K MW is targeted, then the number of moles of monomer needed is 3000. However, this is the case for 100 % conversion. We assumed 80% conversion in our experiments. The amount of catalyst and CuBr or CuCl was taken as 1/10 of the monomer. Before conducting the experiments with MNPs, a control experiment was run with the unbound initiator to observe if the polymerization occurs with the CMS as an initiator and successful polymerization was achieved

4.1 PS coated MNPs

PS was grown from the particle surface using CMS coated MNPs. Six different polymerizations were performed by changing the conditions in order to achieve a high molecular weight PS. Initiating MNPs (CMS coated) were used either as suspensions in DMF (OT2St&OT3St) or as dried powder (OT4St&OT5St). All the conditions are given in Table 4.1. We have studied the polymerization in bulk and in xylene and at various temperatures. The resulting PS coated MNPs were compared in terms of hydrodynamic size, colloidal stability, molecular weight, MW distribution, monomer conversion, grafting density of PS and the initiator efficiency.

Table 4.1 Polymerization conditions (ATRP) for PS coated MNPs

Sample ID	Initiator/CuCl/PMDETA/ styrene (mol ratio)	Xylene/styrene (V/V)	Temperature (°C)	Time (h)
OT2St ^a	1/1/100 ^a	1/1	70	2
OT3St ^a	1/1/100 ^a	1/1	80	3,5
OT4St ^b	1/10/10/3000	1/1	110	7,5
OT5St ^b	1/10/10/3000	0	110	4,5
OT6St ^c	1/10/10/3600	2/1	110	72

^a dilute colloidal suspension of CMS coated MNPs used as an initiator & unknown amount of initiator

^b dried powder of CMS coated MNPs used as an initiator

^c concentrated colloidal suspension of CMS coated MNPs used as an initiator

Properties of the polymers are summarized in Table 4.3 at the end of this chapter. Monomer conversion (grams monomer used/ grams of polymer obtained) increases with time (1-50%) except OT4St. Molecular weights were in the range of 35K-120K. Higher conversions were reported in the literature by Chang however they are only for few thousand molecular weights [52]. We achieved the highest monomer conversion as 50% for OT6St, at the end of a 3-day reaction. However, for MMA ATRP, 25% monomer conversion was obtained in 1-day.

4.1.1 Dynamic Light Scattering

Increase in the hydrodynamic size of the nanoparticles was observed for all particles after surface initiated polymerization. The hydrodynamic size of CMS coated MNPs, which were in DMF, is about 40 nm. However, after 2 hr polymerization reaction (OT2St), the

hydrodynamic size in chloroform increases to 220 nm, and after 3.5 hr (OT3St) the size in THF was measured as 295 nm (Figure 4.2). The size increased about five fold after polymerization. This is a larger increase than 2.5-fold increase observed by Chang for lower molecular weight PS grown from iron oxide nanoparticles [51]. Also, it is important to note that these hydrodynamic sizes were measured without separation of any unbound polymer from the MNP suspension. However, we can clearly say that, hydrodynamic size increases with the polymerization time, indicating increasing molecular weight of PS with time.

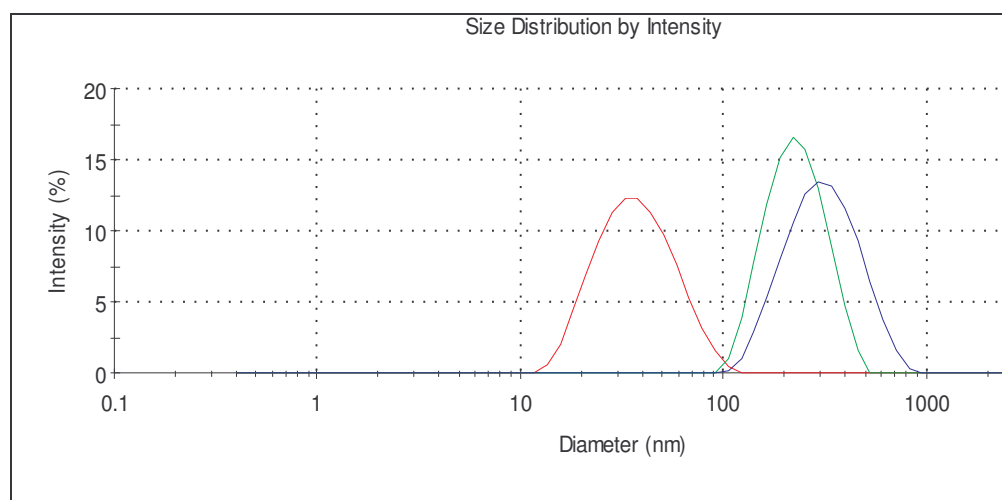


Figure 4.2 Hydrodynamic sizes of CMS coated MNPs in DMF (red); PS coated MNPs after 2 hr (OT2St) (green) and 3.5 hr (OT3St) (blue) polymerization measured in CHCl₃ and THF, respectively

The hydrodynamic sizes of MNPs that was subject to styrene polymerization at 110 °C, OT4St and OT5St, are shown in Figure 4.3. A dramatic increase in the hydrodynamic size after polymerization is seen. These measurements were performed after the unbound polymers were removed from the PS coated MNPs. As explained in section 2.3.4 of

Chapter 2, polymer coated particles were washed with centrifugation to separate unbound polymers produced, if any exist. PS coated MNP after 4.5 (OT5St) and 7.5 hr (OT4St) reaction have comparable sizes but OT5St has a broader size distribution with slightly lower average: 190 nm versus 164 nm. The major difference between these two polymerizations is the reaction solvent. OT5St was done in bulk and OT4St was done in xylene.

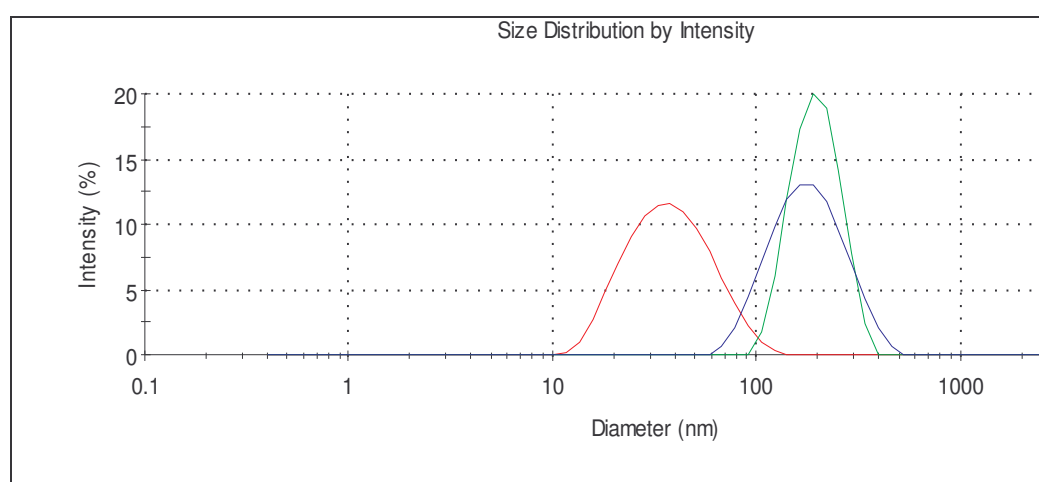


Figure 4.3 Hydrodynamic sizes of CMS coated MNP in DMF (red), 4.5 hr-PS coated MNP (OT5St) (green), 7.5 hr-PS coated MNP (OT4St) (blue)

When these two sets of polymerization reactions are compared in terms of particle size, it is seen that, the presence of solvent and its type are important factors. If the polymerization occurs in a poor solvent for the initiator and polymer or it occurs in bulk, the size & size distribution of the particles (aggregates) will be larger: (i) In bulk reactions, system viscosity increases after a short time giving high molecular weight. High molecular weight corresponds to higher hydrodynamic size. (ii) in addition, if there is another solvent in the system that the polymer is incompatible with, and its amount is as high as the polymerization solvent, both aggregation and system viscosity increases. (iii) Lastly, if the

initiator-coated particles are dried before the polymerizations, especially since they are not dispersed well in styrene or xylene, polymerization will start on aggregated initiators, meaning larger clusters, and it will be difficult to redisperse them in the polymerization medium. Considering these results, xylene was selected as the solvent of the choice and the CMS coated MNPs which were dispersed in DMF were concentrated in order to decrease the DMF/xylene ratio to prevent aggregation of particles. OT6St was performed according to this understanding. The sizes of the particles were not very large compared to the previous ones and no gelation was occurred even after 3 days. In a similar study where PMMA was grown from iron oxide nanoparticles with ATRP method, it was reported that after 4 hours of reaction gelation takes place [47]. Nevertheless, we prevented gelation by concentrating the initiator-coated particles in DMF and increasing the xylene amount. The hydrodynamic size of washed PS coated MNPs (OT6St) were 220 nm in toluene as shown in Figure 4.4.

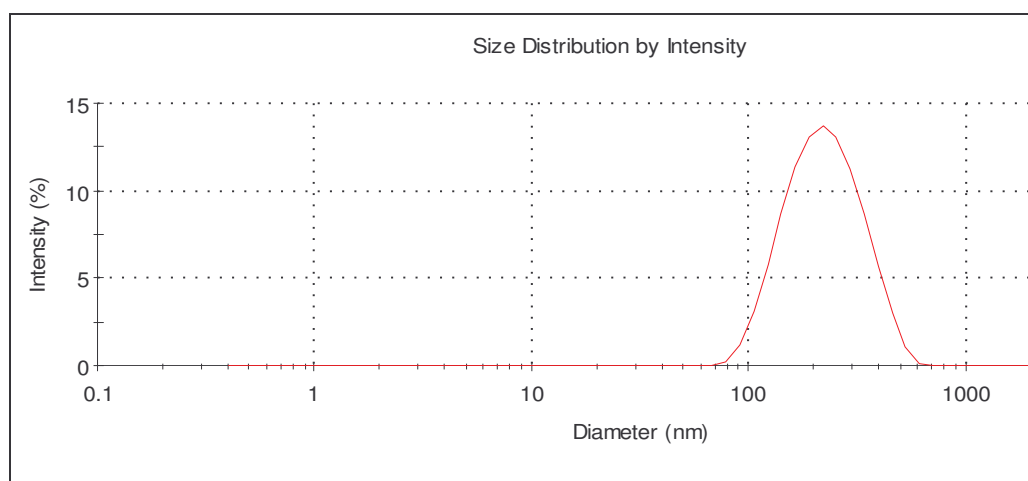


Figure 4.4 Hydrodynamic size of PS coated MNPs after 3-day polymerization: washed and suspended in toluene

4.1.2 Infrared Spectroscopy

Figure 4.5 shows FT-IR spectrum of the CMS initiator and the PS synthesized from the same initiator. Peaks at $3030\text{--}2800\text{ cm}^{-1}$ (C-H), 1600 cm^{-1} , $1400\text{--}1000\text{ cm}^{-1}$ (C=C stretch of aromatic rings) and 700 cm^{-1} are consistent with the PS standard. The peak at about 1120 cm^{-1} , which corresponds to Si-O-Si bond, in the initiator coated MNP spectra was disappeared in PS. FT-IR spectrum of the PS coated MNPs also has the same bands indicating that PS was grafted from MNP surface (Figure 4.6). The Fe-O band at 590 and 639 cm^{-1} in CMS coated MNP spectra shifted to 540 and 622 cm^{-1} in PS coated MNP spectra.

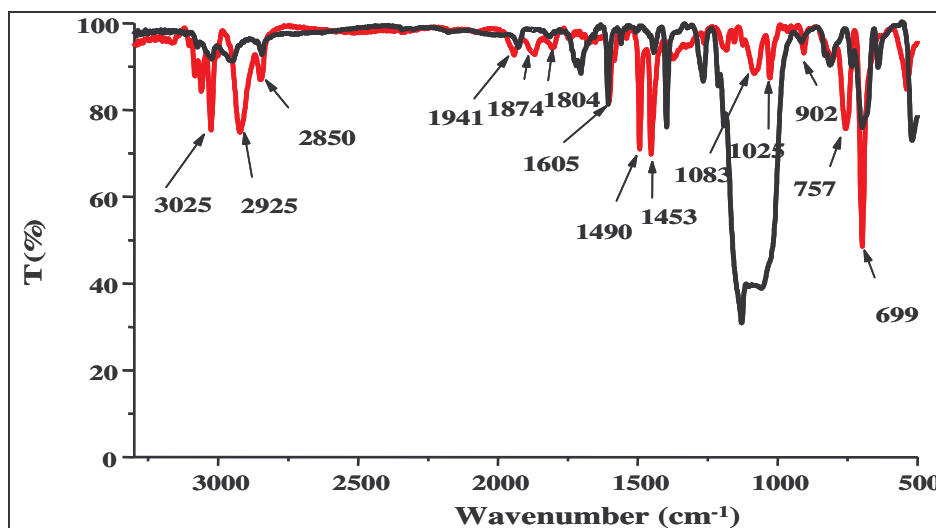


Figure 4.5 FT-IR spectrum of CMS (black) and PS synthesized from CMS (red)

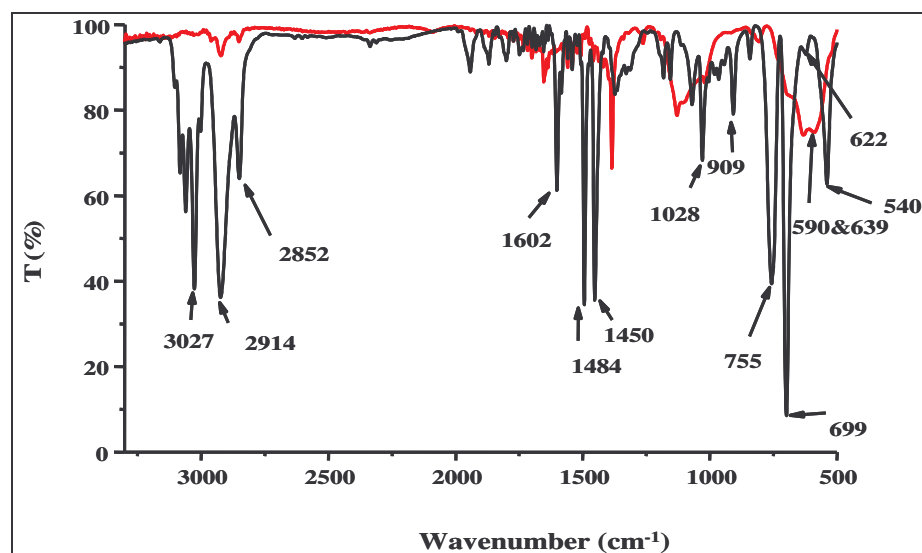


Figure 4.6 FT-IR spectrum of CMS coated (red) and PS coated (black) MNPs

4.1.3 Thermogravimetric Analysis

TGA of polymer-coated nanoparticles was carried out to determine the graft density and graft efficiency for each reaction. Both PS coated MNPs gave identical TGA curves. For some particles, TGA was done for both washed and unwashed PS coated MNPs in order to see if there is any unbound polymer.

In Figure 4.7, it can be seen that as the polymerization time increases, the amount of polymer grafted from the nanoparticle surface increases. The weight loss of unwashed polymers of OT2St is 96.6% after 2 hr reaction and 98.7 % for OT3St after 3.5 hours reaction. In Figure 4.8, TGA curves of unwashed OT4St and unwashed OT5St are shown as well. The weight loss of OT4St and OT5St are 95.9 % and 97 % respectively. These numbers are slightly lower than that of OT2St and OT3St, which indicates that the amount of polymer is higher if the polymerization occurs in a solvent although DMF/xylene ratio is high. The graft densities were calculated as 1.78 and 1.89 molecules/nm² for OT2St and OT3St, respectively by using equation 1 given in chapter 4. These values are much higher

than those reported by Chang (0.38 molecules /nm²) [51]. Initiator efficiencies were calculated by simply dividing the graft density of the polymer by the graft density of the initiator and by multiplying the result with 100. They are 30.6 and 32.6 %, respectively, which are similar to those reported by Takahara et al [59]. Although this is a high value among the literature values, the reason of such low efficiencies might be the limited access of the monomers or complexation of the growing end as the polymer chain grows from one initiator, limiting the approach to the neighboring groups through sterics and chain entanglement.

The graft densities of OT4St and OT5St were calculated as 0.95 and 0.92 molecules /nm², respectively and initiator efficiencies are 16.3 and 15.9 %, respectively. So, use of the initiating MNPs in dry powder form is not as effective as using the DMF suspension as can be reflected with these results. When the particles were dried, it does not disperse in xylene or styrene, causing some aggregation as well, which altogether decreases the available exposed initiator amount.

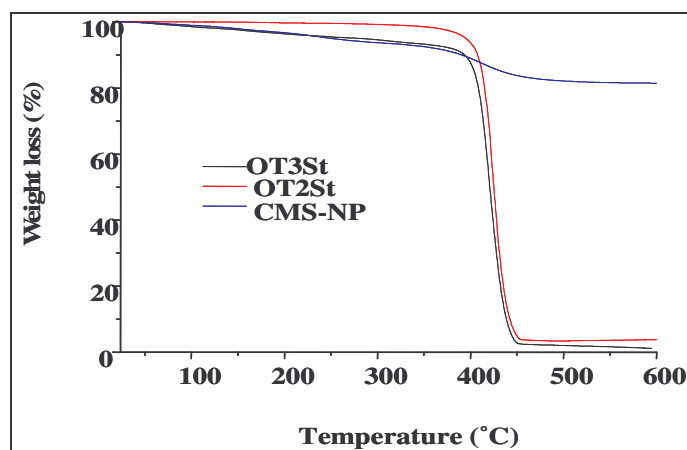


Figure 4.7 TGA of CMS-coated MNP, unwashed OT2St and unwashed OT3St

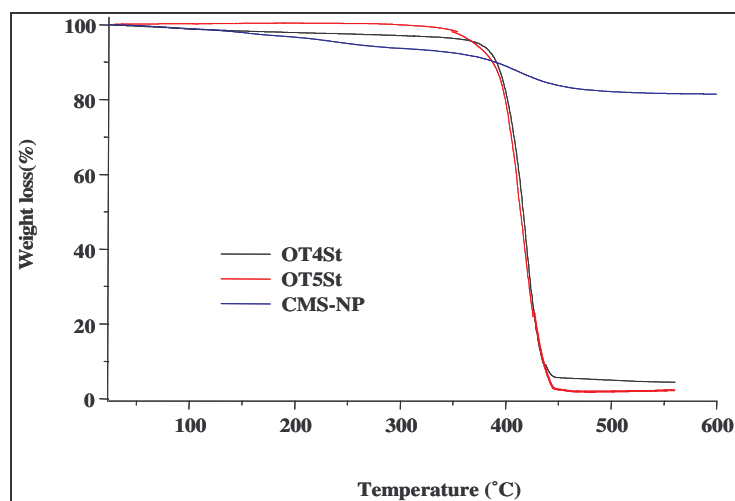


Figure 4.8 TGA of CMS-coated MNP, unwashed OT4St and unwashed OT5St

Weight losses of washed and unwashed PS-coated MNPs are compared in Figure 4.9. There is about 10% unbounded, free polymer after the polymerization. The reasons may be; (i) although CMS-coated MNPs were washed, there can be still free initiator, (ii) as said before CMS coated particles can be dispersed well in only DMF and when they were mixed with xylene at high ratios, if any weakly bound CMS exist it may desorb from the surface. This can be also a reason of low initiator efficiency. As can be expected, any unbound initiator can form free polymer. Although some of the particles were aggregated at the beginning of the reactions, there was no nanoparticle precipitation at the end of the polymerizations in any of the reactions. This indicates that once the polymerization started and few monomers were added to the particle surface, MNPs showed solubility similar to styrene and suspended well in xylene. Complete suspension of the MNPs also indicates that all particles are effectively coated by the PS.

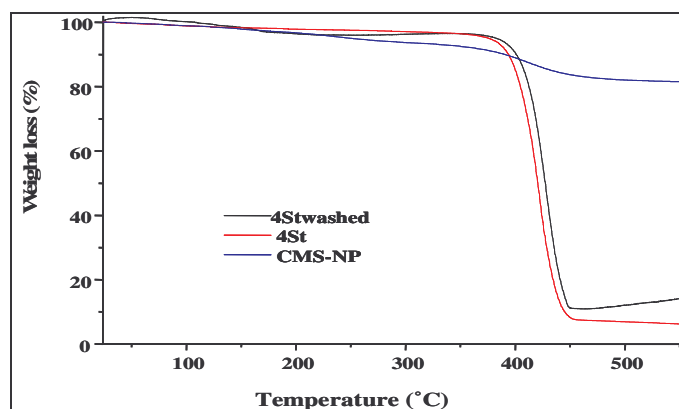


Figure 4.9 TGA curves of CMS-coated (blue), washed (black) and unwashed (red) PS coated MNPs

The least amount of free polymer was observed for OT6St. The weight losses of unwashed and washed OT6St are 97.7% and 94%, respectively (Figure 4.10). Therefore, graft density of polymer is 1.26 molecules/nm² and initiator efficiency is 21.7%.

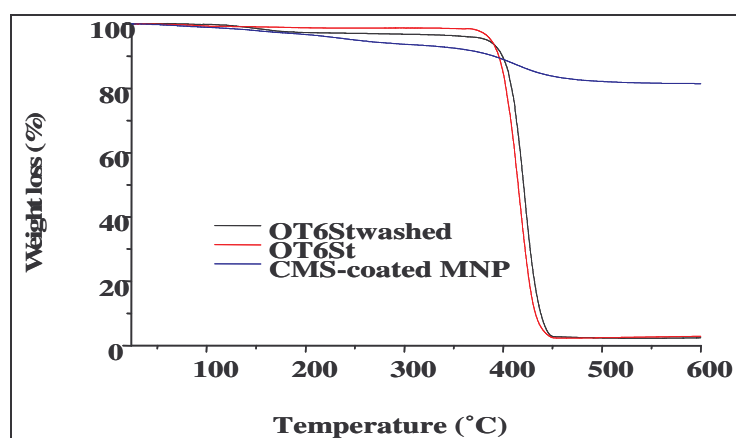


Figure 4.10 TGA curves of CMS coated MNP (blue), OT6St washed (black) and unwashed (red)

5.1.4 Gel Permeation Chromatography

GPC measurements of OT4St, OT5St and OT6St were also performed to identify the molecular weights and MW distributions. It was desired to separate the magnetic nanoparticles completely from any unbound polymer however centrifugation at 50,000 rpm was not sufficient to perform an efficient separation. Use of an ultracentrifuge would aid tremendously. Nevertheless, we managed to separate the PS-coated MNPs to a large extent by adding few drops of methanol, which causes to precipitate the polymers.

In Figure 4.11, GPC traces of washed and free OT4St after cleavage (etching the nanoparticle) and OT4St before cleavage were given. OT4St with no washing or separation showed two peaks with M_n of 330K and 37K. The targeted MW was 300K. When PS coated MNPs were separated by centrifuge and polymer was cleaved, MW determined for this PS was recorded as 55K with a small peak also at 4K. This indicates that polymerization from dried nanoparticles is not controllable although PDI values of each peak are narrow. Free polymer obtained in the polymerization showed a similar GPC trace to unwashed PS coated MNP. Comparison of the three traces further indicates that when dried initiators are used a significant amount of free polymer of high molecular weight is produced.

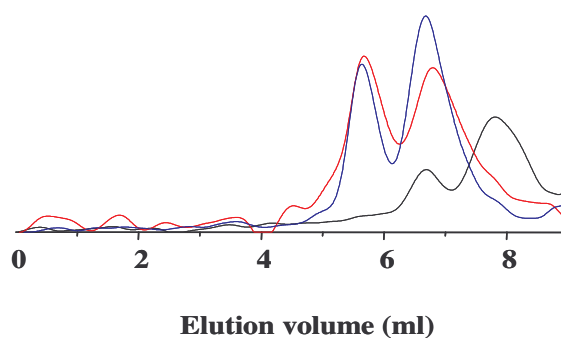


Figure 4.11 GPC traces of unwashed OT4St (blue), cleaved PS from MNPs (black) and free PS (red)

In Figure 4.12, GPC traces of OT5St as prepared and after cleavage are shown. The polymer cleaved from the particle had multiple peaks with the highest molecular weight component at M_n of 63 K with polydispersity of 1.17. However, the free polymer had a M_n of 413K with a PDI of 1.1. Therefore, from these two polymers (OT4St&OT5St), it can be concluded that bulk polymerization gives polymers, which have higher molecular weights, and polymerizations from dried nanoparticles are not controllable.

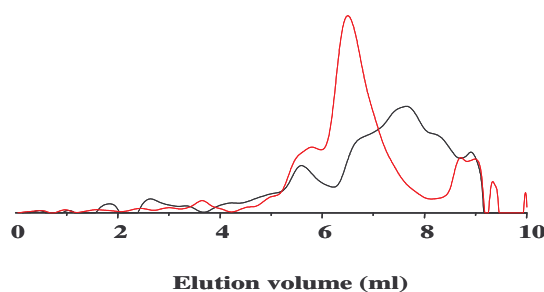


Figure 4.12 GPC traces of OT5St as prepared (red) and PS cleaved from the MNP surface (black)

OT6St showed indication of a controlled polymerization. PS coated MNPs as prepared and PS cleaved from the surface of these nanoparticles gave a single peak and at comparable molecular weight in the GPC analysis: M_n of 100K and PDI of 1.37 for the PS cleaved from the surface and M_n of 105K for the PS-MNP (Figure 4.13). This also indicates no or much less formation of free PS during the polymerization.

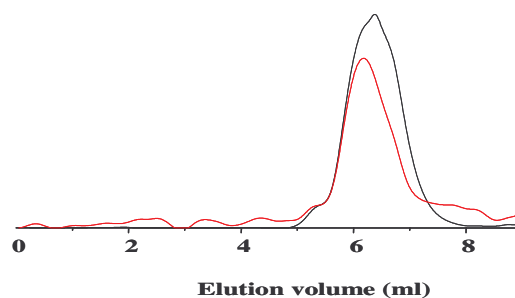


Figure 4.13 GPC traces of cleaved OT6St (black) and OT6St with nanoparticles (red)

4.1.5 Atomic Force Microscopy

A typical AFM image of PS coated MNPs (OT4St) is given in Figure 4.14. The size distribution is not monodisperse because these images belong to unwashed particles which showed also bimodal size distribution in the GPC. There is about 10% excess unbound PS around the particles confirmed by TGA.

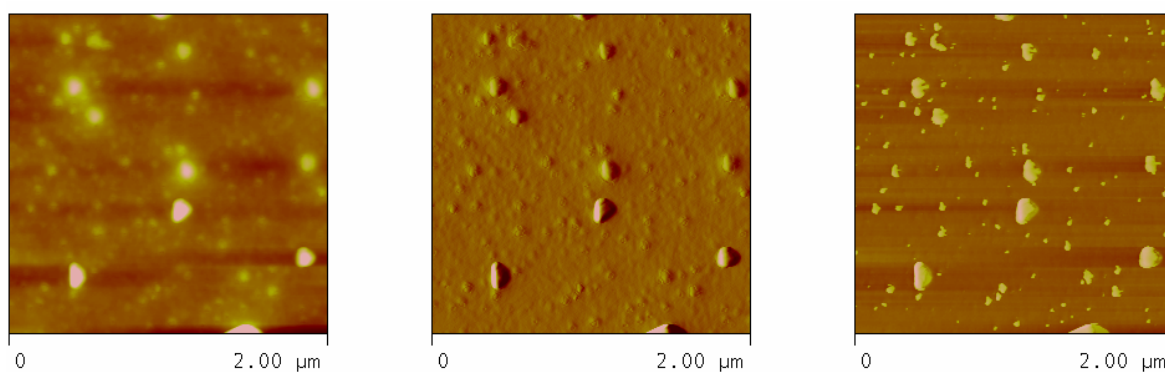


Figure 4.14 AFM (height, amplitude and phase) images of PS coated MNPs

4.2 PMMA coated MNPs

Because it is easier to graft PS onto PMMA for the block copolymer synthesis by ATRP, MNPs were also grafted with PMMA. Two same polymerization was performed for PMMA coated MNPs. The synthesis conditions are given in Table 4.2. The target molecular weight for PMMA was 200K. In MMA polymerization with ATRP, CuBr₂ was also added as a deactivator in order to decrease the rate of polymerization so that high molecular weight polymers and high conversions can be obtained.

Table 4.2 Polymerization conditions (ATRP) for PMMA coated MNPs

Sample ID	Initiator/CuBr/CuBr ₂ PMDETA/MMA	Solvent/MMA (V/V)	Temperature (°C)	Time (h)
OT1PMMA ^a	1/10/0.5/2500	2/1	70	24
OT2PMMA ^a	1/10/0.5/2500	2/1	70	24

^a concentrated colloidal suspension of CMS coated MNPs used as an initiator

4.2.1 Dynamic Light Scattering

Size distribution of PMMA coated particles, which are washed and suspended in toluene (OT1PMMA), is shown in Figure 4.15. Hydrodynamic size in toluene is about 90 nm with size distribution ranging from 30 to 400 nm. The hydrodynamic size of CMS-coated MNPs was about 40nm, therefore there is only 2 fold increase after polymerization.

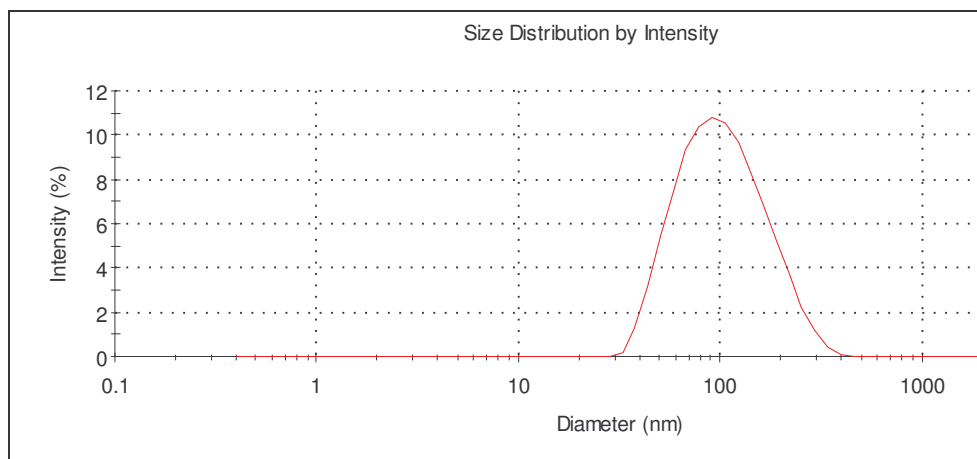


Figure 4.15 Hydrodynamic size of PMMA coated washed MNPs (OT1PMMA) in toluene

4.2.2 Infrared Spectroscopy

The FT-IR spectra of PMMA and CMS coated MNP is shown in Figure 4.16. The sharp intense peak at 1731 cm^{-1} appeared due to the presence of ester carbonyl group stretching vibration.

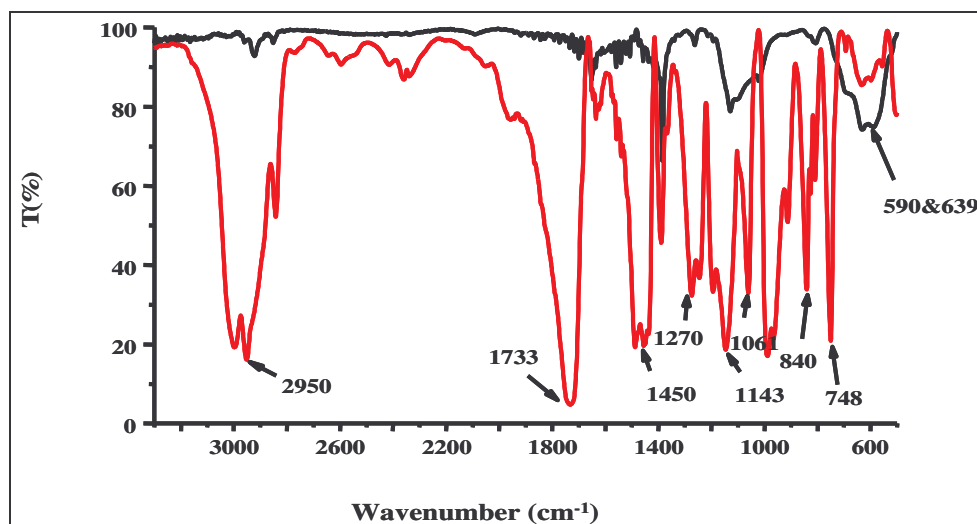


Figure 4.16 FT- IR spectrum of CMS (black) and PMMA (red) coated MNPs

4.2.3 Thermogravimetric Analysis

TGA of washed and unwashed PMMA coated MNPs give idea about the ungrafted polymer (Figure 4.17). As in the PS case, there is about 10%-ungrafted polymer. Weight losses of unwashed and washed particles are 98% and 87%, respectively. The graft density of PMMA on MNPs is 0.60 giving an initiator efficiency of 10.3%.

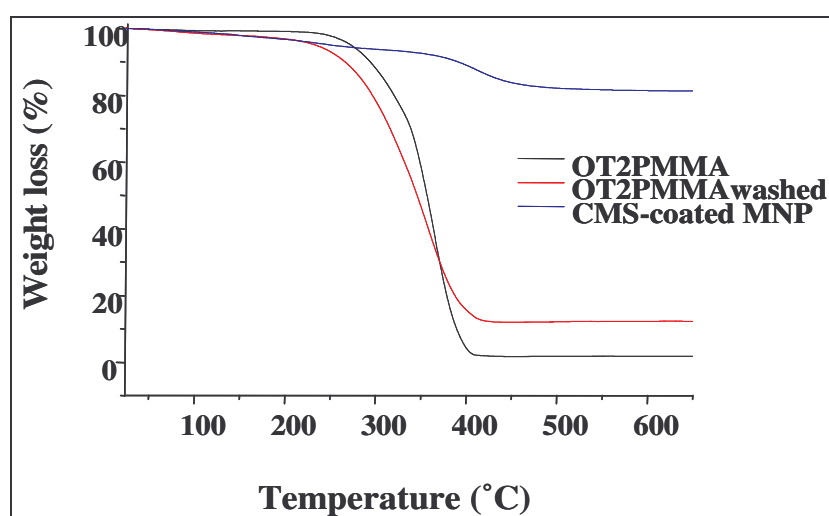


Figure 4.17 TGA of CMS coated (blue), washed (red) and unwashed (black) PMMA coated MNPs (OT2PMMA)

4.2.4 Gel Permeation Chromatography

Cleaved PMMA of PMMA coated MNPs had a M_n of 150K which is closer the targeted M_n (200K) with polydispersity of 1.2 (Figure 4.18). Therefore, MMA polymerization can be judged as a controlled reaction.

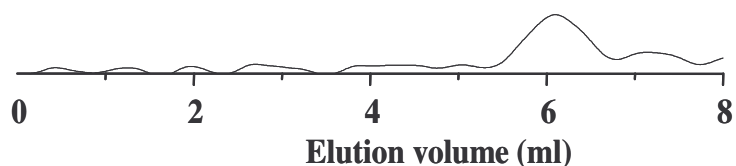


Figure 4.18 GPC trace of cleaved PMMA coated MNPs

4.3 PMMA-*b*-PS coated particles

PMMA-*b*-PS coated MNP was synthesized from PMMA coated MNP macroinitiator (Figure 4.19). If the M_w s of the polymers can be arranged precisely, the block copolymer should form phase-separated morphology. By this way, the particles would be in PMMA phases of block copolymer selectively.

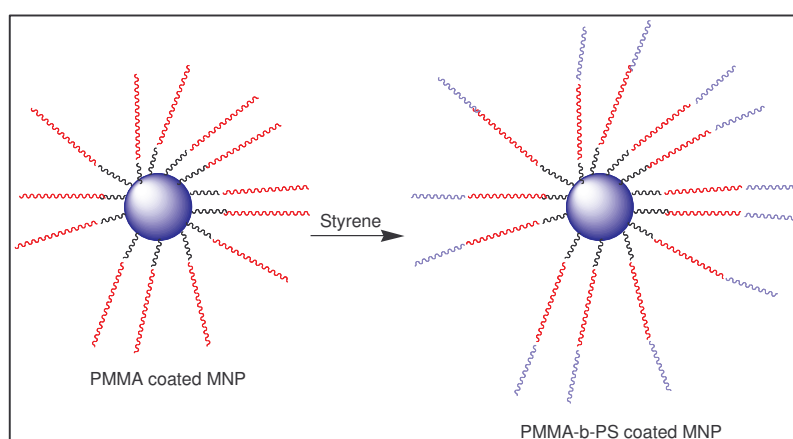


Figure 4.19 Typical scheme of block-copolymerization from PMMA coated MNPs

4.3.1 Dynamic Light Scattering

The hydrodynamic size of PMMA coated MNP was 90 nm. When the PS was grafted from PMMA, the hydrodynamic size in toluene increased to 141 nm as seen in Figure 4.20, as expected.

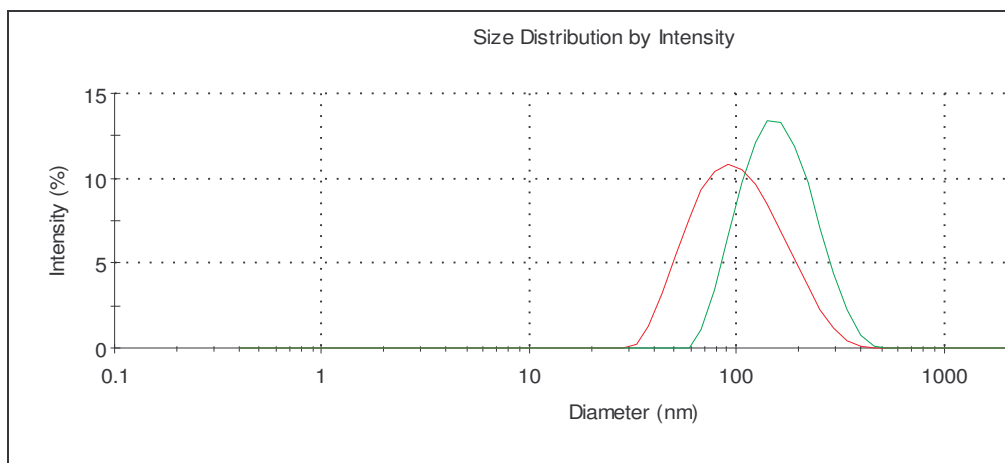


Figure 4.20 Hydrodynamic sizes of washed-PMMA (red) and PMMA-b-PS (green) coated MNPs in toluene

4.3.2 Infrared Spectroscopy

IR spectra of PMMA and PMMA-b-PS coated MNPs are given in Figure 4.21. The band at 1700 cm^{-1} (for ester carbonyl group) for PMMA and 698 cm^{-1} for PS both seen in the FT-IR spectra of PMMA-b-PS coated MNPs.

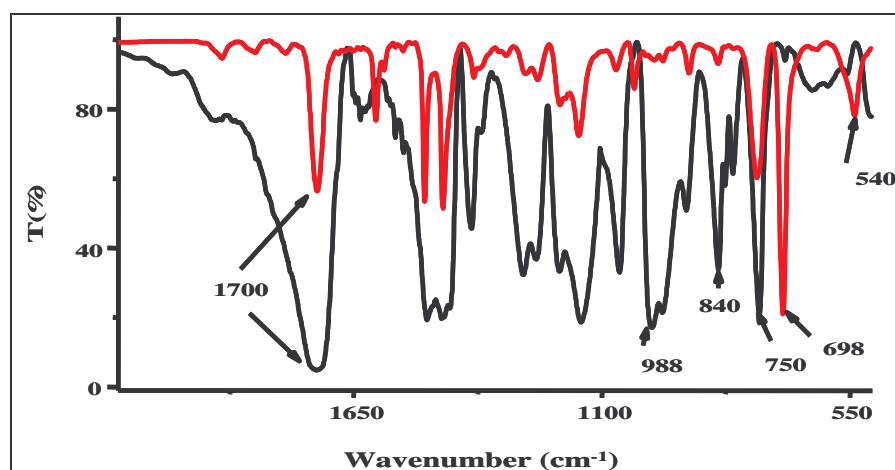


Figure 4.21 FT-IR spectrum of PMMA (black) and PMMA-b-PS (red) coated MNP

4.3.3 Thermogravimetric Analysis

Weight loss of PMMA coated MNPs are 87%, but upon addition of styrene on it, weight loss of PMMA-b-PS coated MNPs increased to 98% (Figure 4.22).

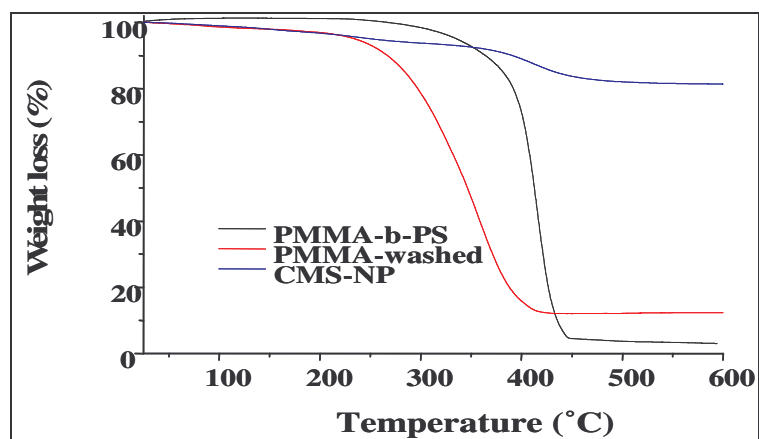


Figure 4.22 TGA of CMS (blue), PMMA (red) and PMMA-b-PS (black) coated MNPs

4.3.4 Gel Permeation Chromatography

Block copolymer had a M_n value of 58K with a PDI of 1.7. The M_n of block copolymer with particles (64K) is higher as expected (Figure 4.23).

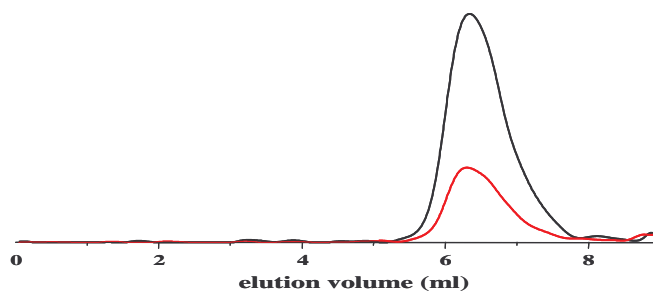


Figure 4.23 GPC traces of cleaved PMMA-b-PS (black) and PMMA-b-PS-MNP (red)

The summary of the characteristics of all polymer coated MNPs are given in Table 4.3.

Table 4.3 Characteristics of Polymer coated MNPs

Sample ID	Time (h)	Conversion (%)	D _h (nm)	M _w	PDI	Graft density ^{**} (G _d) Molecules/nm ²	Initiator efficiency G _d of polymer/G _d of initiator*100
OT2St	2	1	220				
OT3St	3	2	295				
OT4St	7,5	10	190 [*]	60000	1.16&1.09	0.95	16.3
OT5St	4,5	10	164 [*]	70000	1.17&1.1	0.92	15.9
OT6St	72	50	190 [*]	120000	1.5	1.26	21.7
OT1PMMA	24	25	90 [*]	118000	1.32	0.6	10.3
OT1Block	24	50	141	100000			

* washed particles

** graft densities were calculated by using M_w

Chapter 5

Selective Dispersion of Nanoparticles in Polymer Blends

5.1 Films containing surfactant coated MNPs

5.1.1 LA coated MNPs

To investigate the ability of LA coated iron oxide nanoparticles (LA-NP) to disperse selectively in a chemically compatible component of a polymer blend, films were spin coated from solutions containing PS, PEG and NPs in toluene or chloroform. These two solvents are good solvents for both PS and PEG and homogeneously disperse LA-NPs as well. PS has been kept as the minor component in the blends (mass fraction < 0.5) to prevent complete coverage of the top surface of the films by PS which has lower surface energy and has tendency to segregate to the film/air interface. Both components of the blends were clearly seen and identified by the optical microscope and the atomic force microscopy. Films cast from chloroform required annealing for better phase separation. Figure 5.1 shows the phase separation of the PS-PEG homopolymer blend cast from chloroform at PS mass fraction smaller than 0.3 before and after annealing.

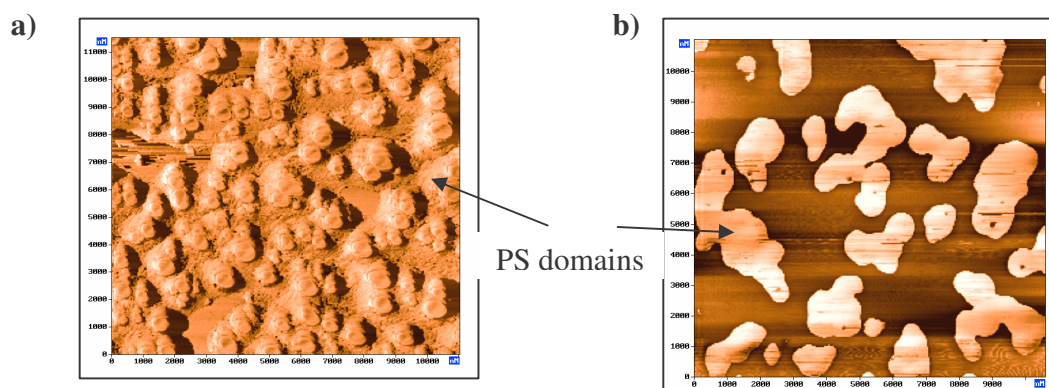


Figure 5.1 AFM phase images of PS/PEG blend (30/70 weight ratio) cast from chloroform
a) not annealed b) annealed

PS forms elongated structures, which has about 2-5 micron width at 0.3 PS mass fraction, and small ca 250 nm sized islands at 0.05 PS mass fraction as seen in Figure 5.2. Smaller domain sizes can be achieved with block copolymers. In case of PB-b-PEO block copolymer the size of micro-phase separated domains were only 10-20 nm as shown in Figure 5.3. We thus obtained polymeric domains whose sizes were controlled from micrometer to nanometer scale by changing the mass fractions of macro-phase separating polymer blends or using micro-phase separating block copolymers.

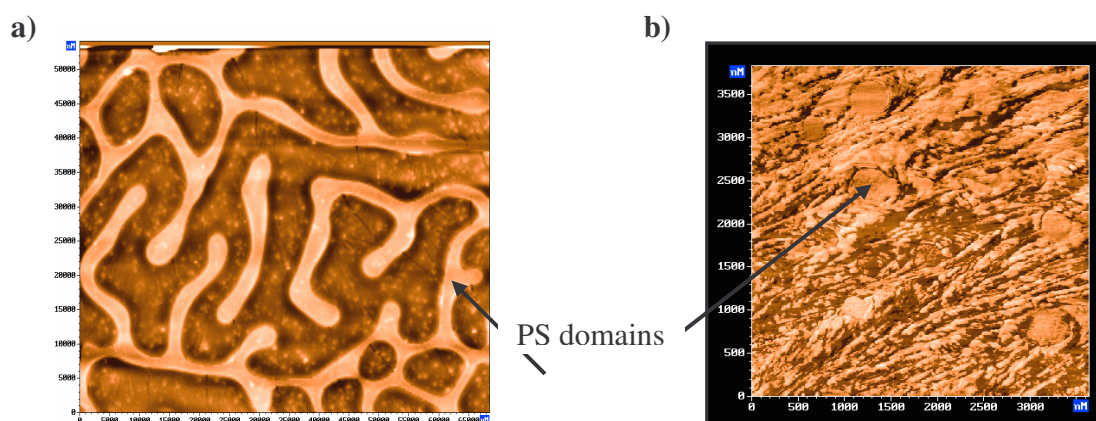


Figure 5.2 AFM images of PS/PEG blends cast from toluene at a) 30/70 (height) b) 5/95 (phase) weight ratio

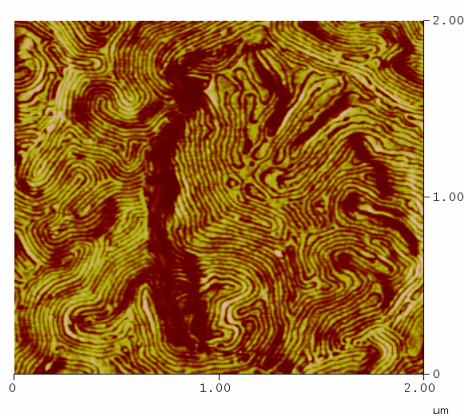


Figure 5.3 AFM height image of PB-b-PEO

As it was mentioned in the first paragraph, films of polymer blends cast from chloroform required annealing to identify each phase clearly. Annealing process was also required for the films of polymer blends with LA- MNPs. Therefore, in order to see the particles one by one and to eliminate the need for annealing, the particles, which were prepared by precipitation method described in chapter 2, were used for the AFM studies since this process provide larger particles that are easier to see by AFM.

Hydrodynamic sizes of these particles were 122 nm. When these particles were diluted to the film concentration of 0.5 mg/mL, a bimodal size distribution centered at 40 nm and 190 nm was observed (Figure 5.4). Better dispersion of smaller clusters with dilution and possibly some aggregation of not well-coated NPs might cause such bimodal size distribution. Yet, considering the size of the iron oxide crystals, these peaks represent NP clusters or aggregates in toluene, which is usual for this type of systems.

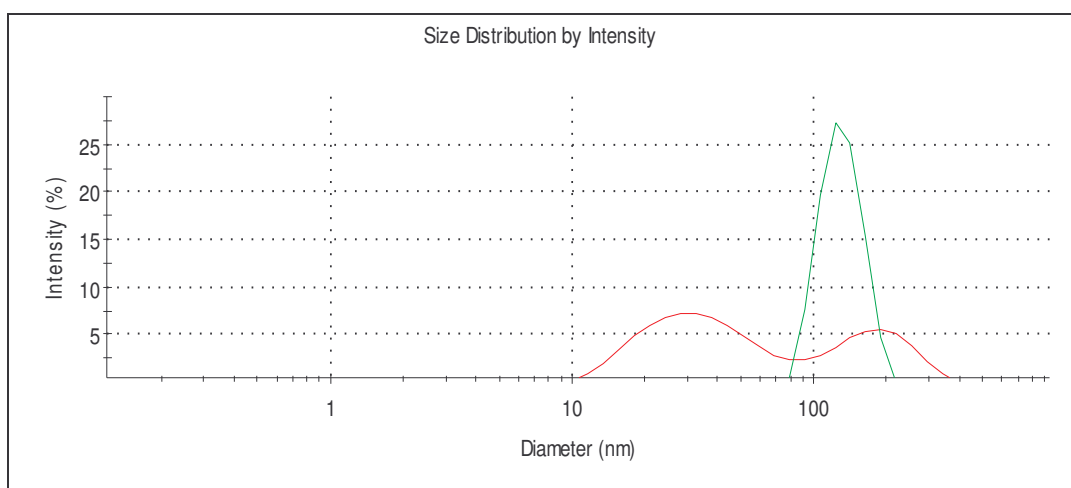


Figure 5.4 Dilution (red) and stock (green) sizes of LA coated MNPs, which were used for the preparation of thin films

When the particles were dispersed in the polymers, the hydrodynamic sizes should be different. It was seen that there are three different size distributions in the PS/LA-MNP solution in toluene (Figure 5.5). The smaller sizes (15 and 50 nm) belong to the PS homopolymer and may be small LA-MNP clusters, the larger one, which is about 400 nm, belongs to the particle aggregates.

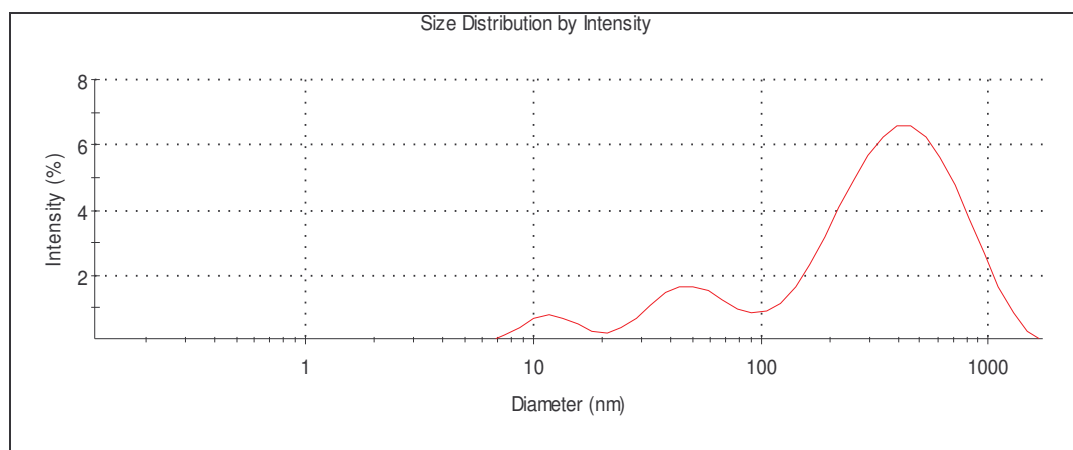


Figure 5.5 Hydrodynamic sizes of the structures formed with the mixture of LA-MNPs and PS homopolymers in toluene

Figure 5.6 shows the dispersion of LA-NPs in the PS homopolymer film. A homogenous distribution of NP clusters was observed on the PS surface. NPs formed small clusters containing few particles with average width of ~ 200-300 nm. Aggregate sizes seen in the AFM images were in agreement with the measured hydrodynamic sizes by DLS. The average height for the aggregates was ca. 10 nm indicating that the NPs were mostly buried in the film. The uniform distribution of NPs in PS homopolymer films without formation of large aggregates indicates the effectiveness of the LA coating in making the NPs chemically compatible with PS. LA binds to the surface of iron oxide crystal through carboxylate and the hydrocarbon tail forms a hydrophobic coating. Uniform distribution of small clusters of hydrophobically modified NPs in PS at small loadings is consistent with the previous observations [60].

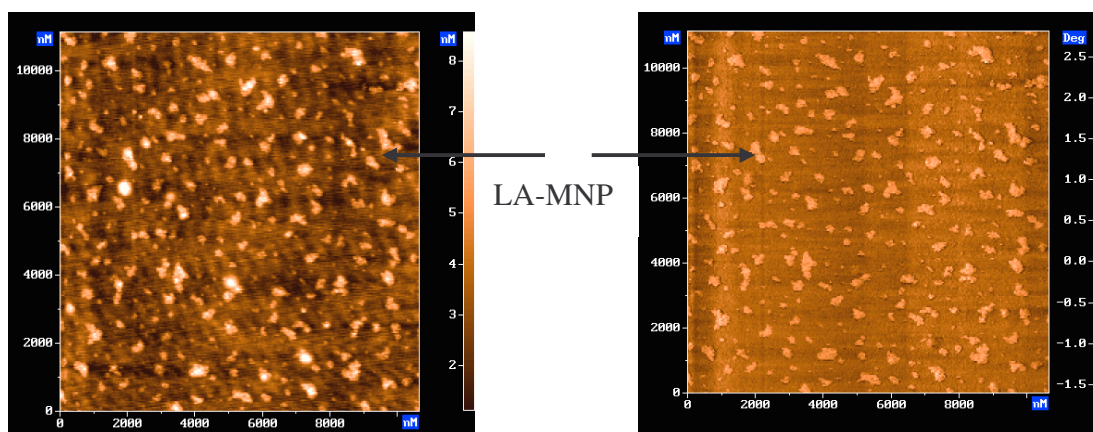


Figure 5.6 AFM height and phase image of LA-MNPs dispersed in PS

Figure 5.7 shows the dispersion of LA-NPs in the homopolymer films of PEG homopolymer. A homogeneous and even better distribution of LA-NPs was also observed in the PEG films. No large aggregates could be observed. Individual NPs were seen clearly in the phase image due to the crystallization-induced roughness on the surface of PEG. The sizes of the particles observed in AFM were ca 50 nm and hydrodynamic sizes of particles in PEG were smaller than LA-NP in PS proving the better distribution of particles in PEG (Figure 5.8).

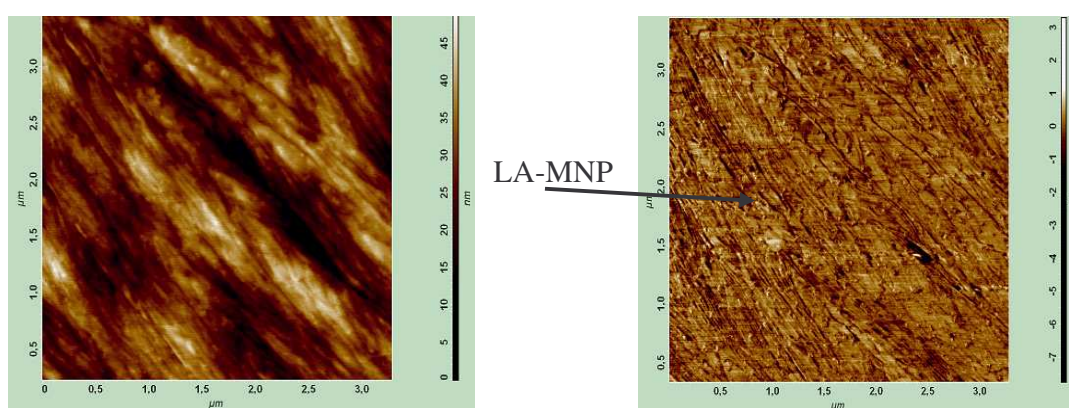


Figure 5.7 AFM height and phase image of LA-MNPs dispersed in PEG

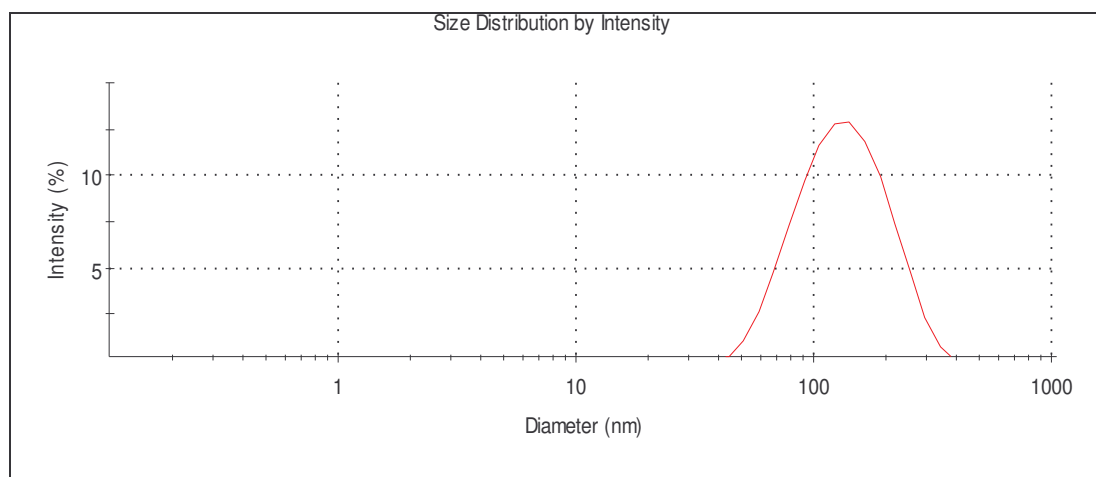


Figure 5.8 Hydrodynamic sizes of the structures formed with the mixture of LA-MNPs and PEG homopolymers in toluene

When the particles were added to PS/PEG blend, LA-NPs were observed to disperse selectively only in the PEG, without any NP visible in the PS domains of the thin films. Preference of hydrophobic LA-NPs towards hydrophilic PEG was quite unexpected. Figure 5.9 shows the AFM pictures of the LA-NPs dispersed in 30/70 and 5/95 PS/PEG blends. The dispersion of the NPs in the PEG phase was homogenous as in the film of PEG homopolymer without formation of any large aggregates. The size of the particle clusters were about 65 nm and the size of PS islands were 250-300 nm which is the corresponding size measured by DLS (Figure 5.10). No LA-NPs were seen in the PS domains. Composition of the blend did not affect the selectivity of the LA-NPs for the compositions tested with PS mass between 5-50 %.

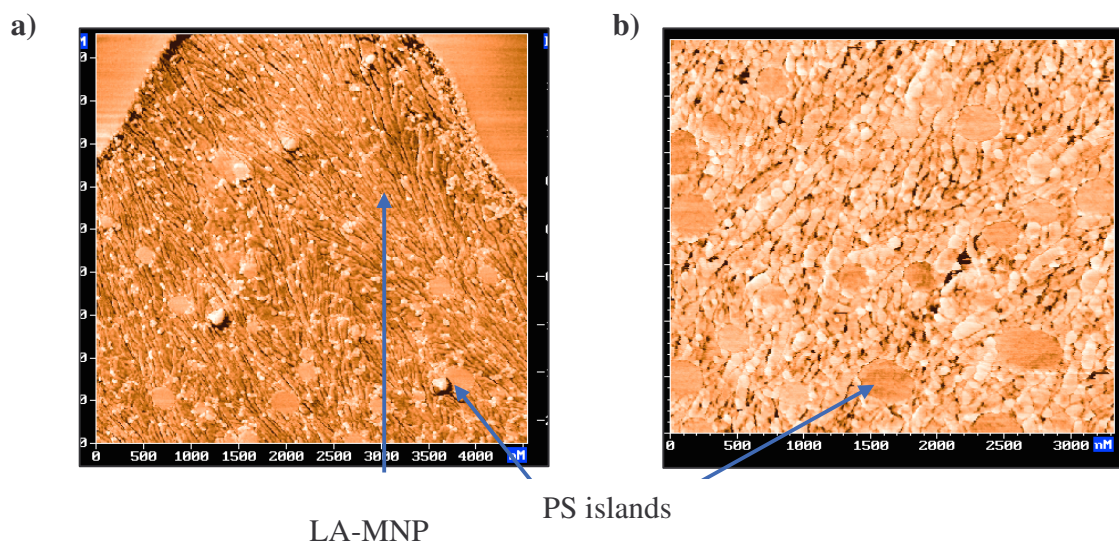


Figure 5.9 AFM phase images of LA MNPs dispersed in blends of a) 30/70 b) 5/95 PS/PEG

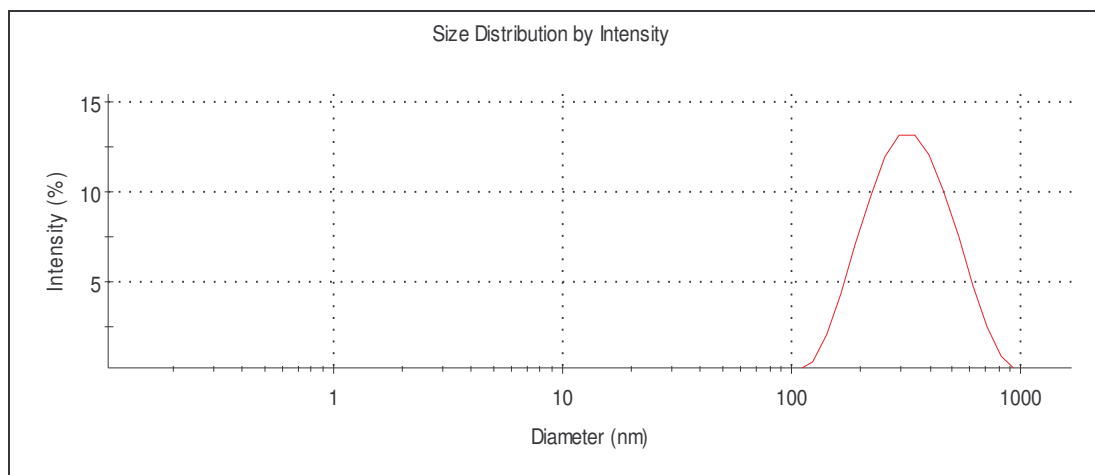


Figure 5.10 Hydrodynamic size of the structures formed with the mixture of LA-MNPs and PS-PEG blend in toluene

Better dispersion of LA-MNPs in the hydrophilic PEG and selectivity towards PEG in the blends can be due to two reasons: i) incomplete surface coverage of LA molecules during NP synthesis may cause penetration of PEG chains onto the NP surface. Large PEG molecules may then dominate over the LA molecules making the NP surfaces hydrophilic. ii) PEG molecules exchange the LA molecules on the NP surface completely. We rule out the first possibility, since LA-NPs disperse well in the toluene and have quite good stability over time. In addition, the weight loss corresponding to the LA adsorbed directly on the crystal surface in LA bilayer and LA monolayer coated MNPs were comparable in TGA indicating no dramatic LA loss from the surface during the monolayer precipitation step (Figure 3.10). To check the second possibility, namely that surface ligand exchange was responsible for the observed behavior, we have done a control experiment of extraction.

A simple ligand exchange experiment was performed in the vials. PEG was dissolved in water and shaken 5 min with the LA-MNPs dispersed in toluene phase, both in concentrations used for the films. All the nanoparticles were extracted into the aqueous phase, as clearly seen with the discoloration of the toluene (Figure 5.11). Dark brown color of the aqueous phase indicates transfer of NPs into the water.

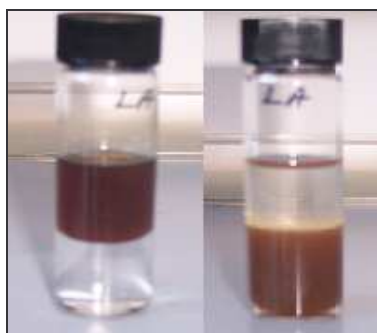


Figure 5.11 Extraction of LA coated particles into PEG phase. On the left, LA- NP s are in toluene at the top of the aqueous phase containing PEG. On the right, all NP s are in the aqueous phase containing PEG.

In order to obtain spectroscopic evidence, LA-MNPs were sonicated with toluene solution of PEG for 15 minutes at the concentrations used for the film formation, centrifuged at 21,000 rpm for 15 min and the clear colorless solution is separated from the dark brown precipitate. In the IR spectra of the dried colorless toluene solution, carbonyl peaks of LA were detected at 1733 and 1712 cm^{-1} but no indication of LA was observed in the brown precipitate where iron oxides should exist. This supports complete exchange of LA with PEG (Figure 5.12).

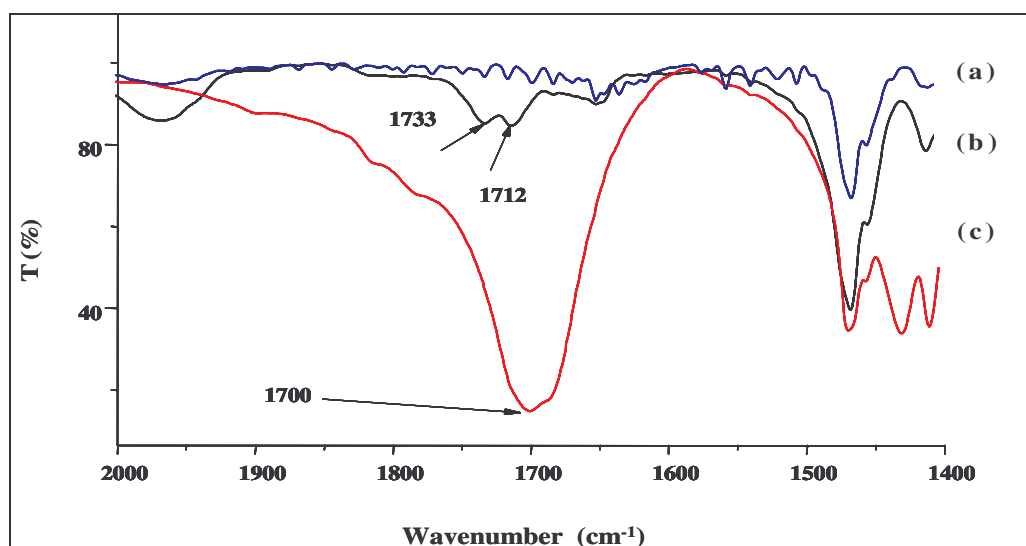


Figure 5.12 FT-IR spectra of the a) precipitated MNPs after ligand exchange b) colorless toluene phase and c) LA

Lauric acid binds to iron oxide surface through chemical adsorption of carboxylate yet the binding is reversible. It is possible to exchange such ligands with a second molecule. [5,61] Alcohols such as decanol or polyvinyl alcohol is known to stabilize iron oxide nanocrystals as well. Similarly, PEG with electron rich oxygens of each ethylene

glycol repeat unit can cause a ligand exchange on the crystal surface. Once polymer chains adsorb on the surface, it may result in better de-aggregation and stabilization through steric stabilization. This could explain better dispersion and smaller cluster size of LA-MNPs in PEG films with respect to those observed in PS (Figure 5.8). In case of blends such ligand exchange would transfer particles into the PEG domains as well.

5.1.2 HDMS coated MNPs

LA was bound on the MNP surface through chemical adsorption. Therefore, when LA coated MNPs were dispersed into the phase-separated blend of PS-PEG, they selected to disperse into the PEG instead of PS by ligand exchange. For that reason, to disperse the MNPs into the PS domain, HDMS was bound onto the MNP surface by Fe-O-Si covalent bond expecting this bond would be strong enough to avoid the ligand exchange. Thus, HDMS coated MNPs were dispersed in PS, PEG and blend of PS-PEG to observe the selectivity (Figure 5.13).

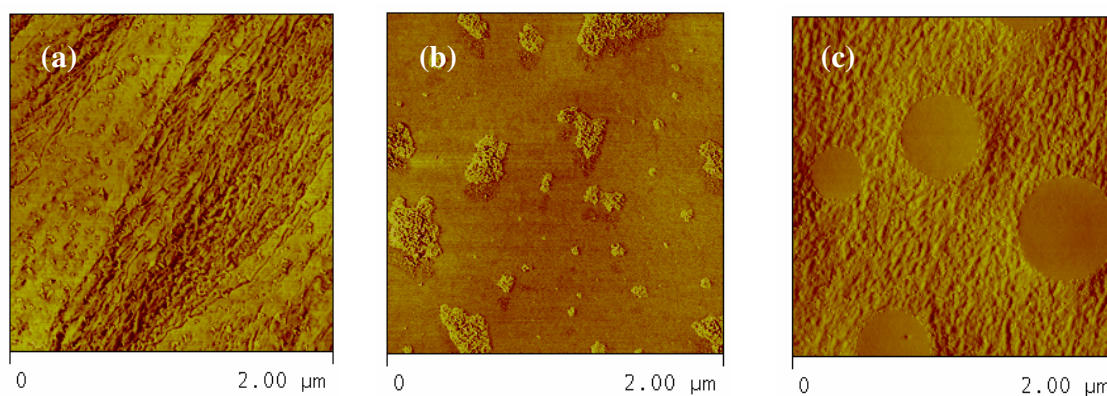


Figure 5.13 AFM phase images of HDMS coated MNPs in a) PEG, b) PS and c) PS-PEG blend

In the PS-PEG blend, there were no particles in PS domain, and unexpectedly the particles disperse in PEG phase. However, the difference from LA coated MNPs was, HDMS coated MNPs were located mainly at the interface of PS-PEG (Figure 5.14).

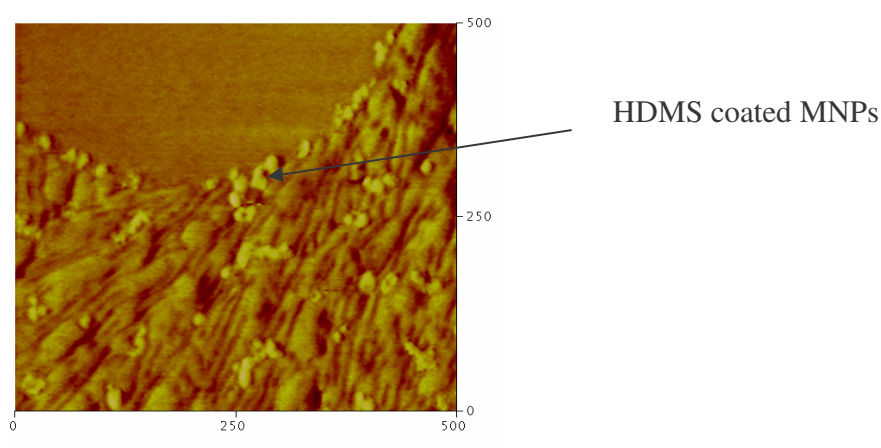


Figure 5.14 AFM phase image of HDMS coated MNPs in PS-PEG blend

In order to understand this unexpected selectivity, the simple extraction experiment done for the LA coated MNPs was also performed for HDMS coated MNPs, but the result was different. Little amount of particles were extracted to the aqueous phase. These extracted particles may be LA coated MNPs which did not exchange their ligands during HDMS exchange, or not well coated particles. So, the particles remained in the toluene phase should be hydrophobic and resistant to ligand exchange. Therefore, these particles were dispersed in the blend as well (Figure 5.15). Particles found in the PEG phase again with no indication of NP in the PS domains. But, they did not disperse very well in the PEG domain as in the case of LA coated MNP but rather formed clusters throughout the film and at the interface of PS-PEG.

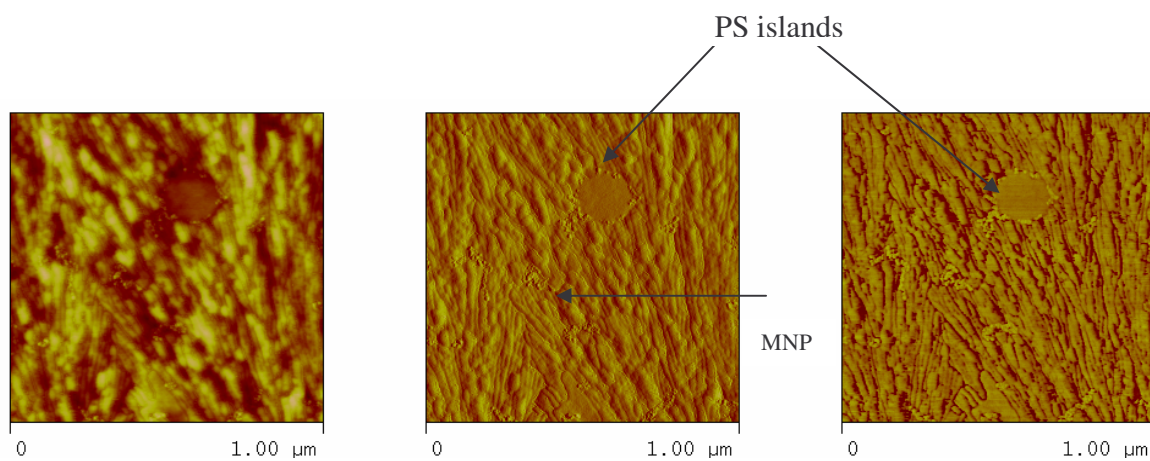


Figure 5.15 AFM height, amplitude and phase images of HDMS coated MNPs (remained after extraction) in PS-PEG blend

5.1.3 PEG-Si coated MNPs

Hydrophilic and covalently bonded PEG-Si coated MNPs were also dispersed in the PS-PEG blends. AFM indicated existence of no MNPs in PS and dispersion in PEG phase selectively. In Figure 5.16, dark PEG crystalline branches seem to have undergone clipping at the sites of MNPs. The brighter dots in these dark areas are PEG-Si coated MNPs.

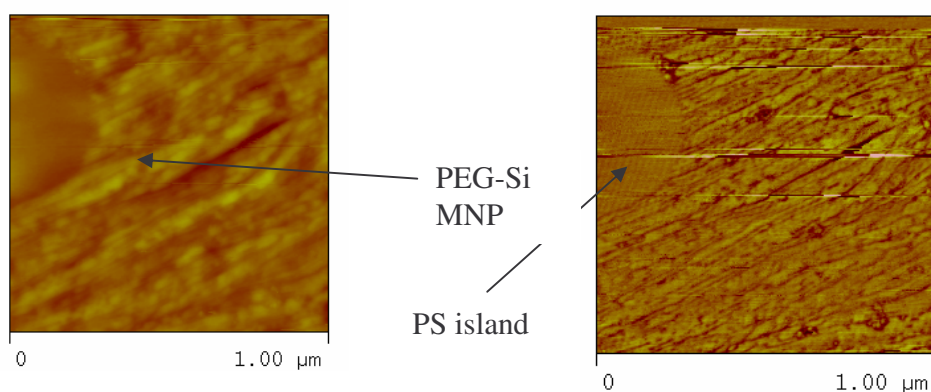


Figure 5.16 AFM height and phase images of PEG-Si coated MNPs dispersed in PS-PEG blend

5.2 Films containing polymer coated MNP

PS, PMMA and PMMA-*b*-PS were grafted from MNP surface to avoid the need of another coating material for selective dispersion of MNPs in phase-separated polymers.

5.2.1 PS coated MNPs in PEG

PS coated MNPs were mixed with PEG in ca 30 wt% PS content. Thin films cast from toluene showed elongated PS domains. However, individual particles could not be seen due to unbound PS chains (Figure 5.17).

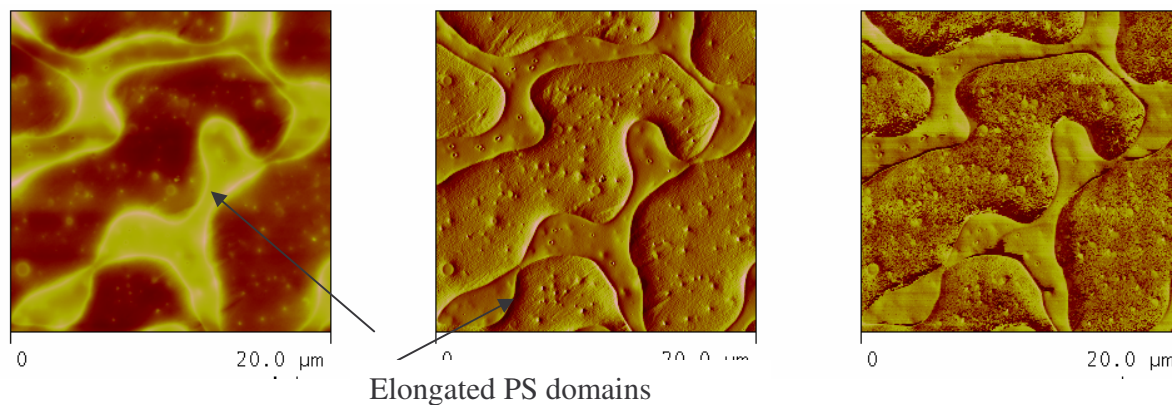


Figure 5.17 AFM height, amplitude and phase images of PS coated unwashed MNP in PEG

Then, the unbound PS was washed and mixed with PEG at 5-weight %. PS formed islands which are about 100-500 nm in PEG domains. The particles cannot be observed one by one in these islands. The brighter AFM phase image of these islands can be attributed to the hardness due to embedded MNPs (Figure 5.18). Hydrodynamic sizes observed for the structures formed by the PS coated MNPs/PEG blend in toluene were about 220 nm, which is consistent with AFM images (Figure 5.19).

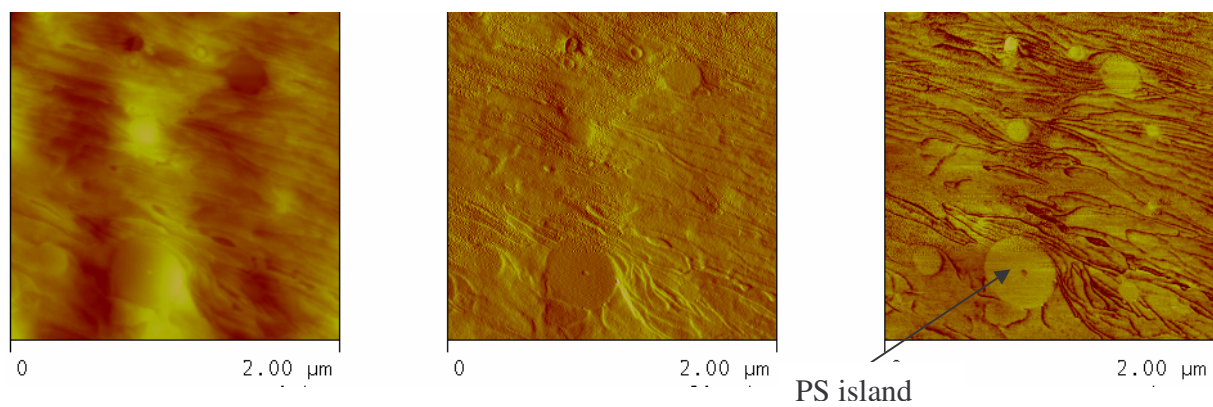


Figure 5.18 AFM height, amplitude and phase images of PS coated washed MNPs in PEG

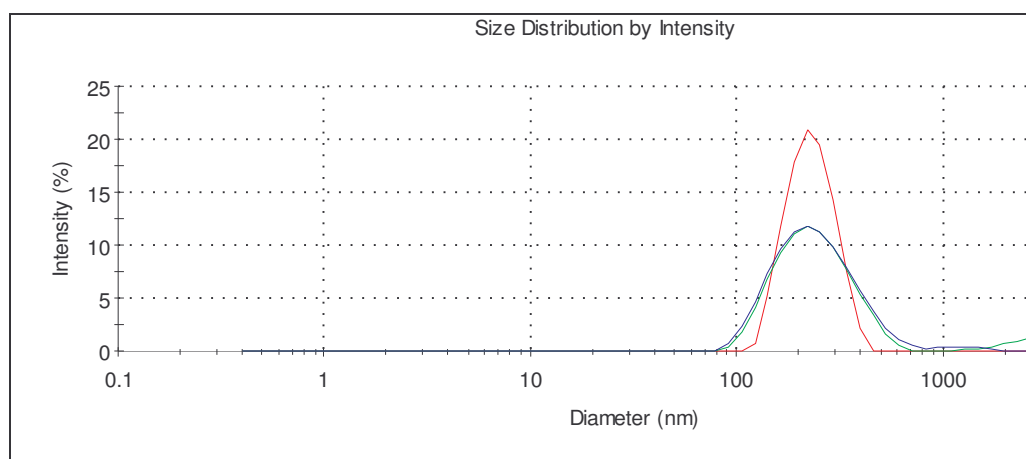


Figure 5.19 Hydrodynamic size of PS coated washed MNPs mixed with PEG in toluene

5.2.2 PS coated MNPs in PMMA

PS coated and washed MNPs were also dispersed into PMMA. They also formed islands of PS at 5-weight % loading of PS. There are iron oxide nanoparticles having 4-5 nm height and 40 nm width in these islands (Figure 5.20).

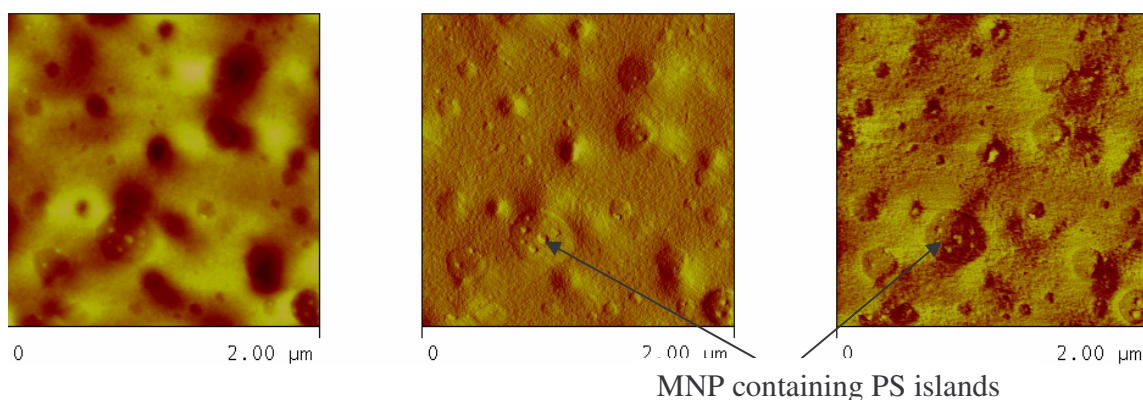


Figure 5.20 AFM height, amplitude and phase images of PS coated washed MNPs in PMMA

5.2.3 PMMA coated MNPs in PS

To prepare PMMA-b-PS, first PMMA was grafted from iron oxide MNPs because it is easier to graft PS onto the PMMA in ATRP. The PMMA coated MNPs were also dispersed in PS homopolymer at 5 weight %. NPs embedded in these PMMA islands can be seen in Figure 5.21. The hydrodynamic sizes of these islands are about 342 nm as shown in Figure 5.22.

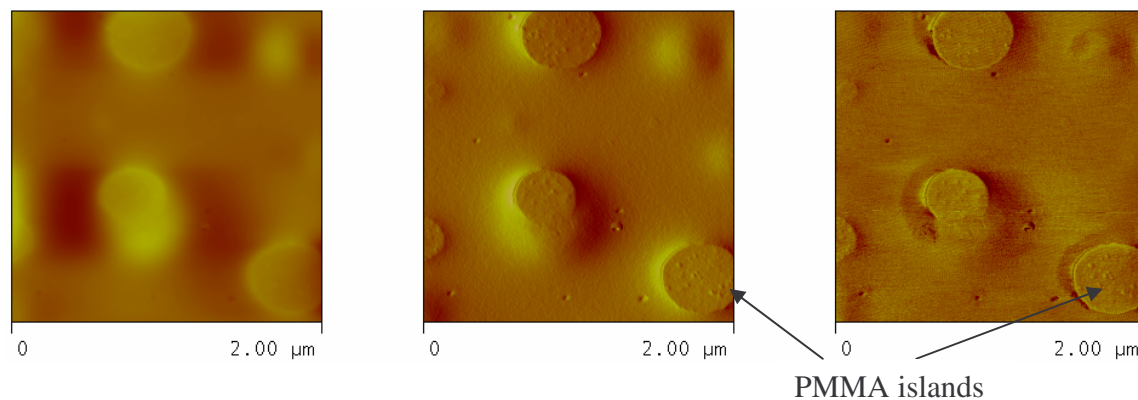


Figure 5.21 AFM height, amplitude and phase images of washed PMMA-MNPs in PS

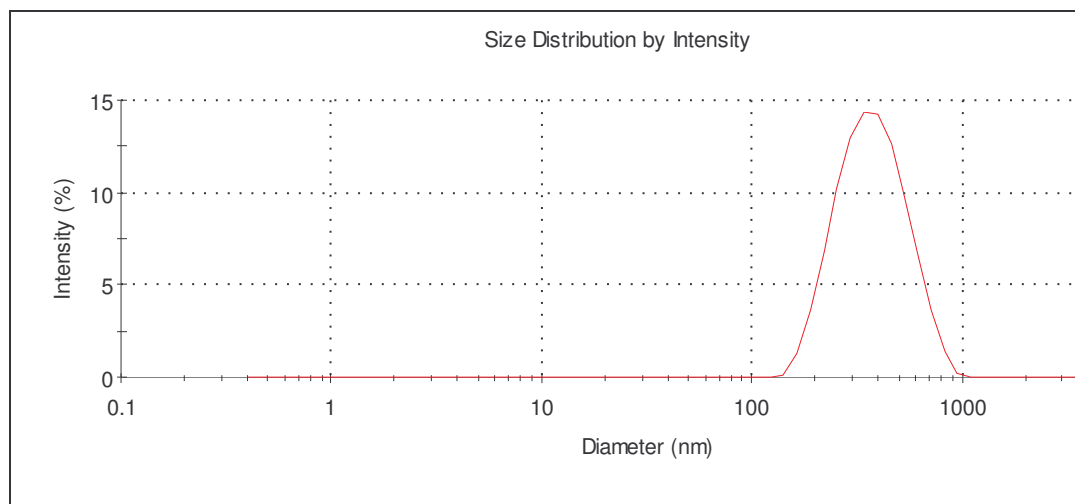


Figure 5.22 Hydrodynamic size of washed PMMA- MNPs mixed with PS in toluene

5.2.4 PMMA-*b*-PS coated MNPs

Block copolymers can micro-phase separate. Therefore, the selective distribution of nanoparticles in block copolymers creates new structures at nanoscale. When the polymer and the nanoparticle were prepared separately, according to the nanoparticle loading, the morphology of the block copolymer might be changed [62].

To achieve better positioning of nanoparticles in block copolymer matrices, the block copolymer was grafted from the MNP surface by ATRP. Films formed from these materials were investigated by AFM (Figure 5.23). There are protrusions on the surface having 200-400 nm width and 30 nm height. These are the regions where the particles aggregated as shown clearly in Fig. 5.23 in magnified view. The matrix corresponds to the unbound PMMA-*b*-PS molecules, the micro-phase separated morphology of which is also apparent in the phase image of Fig. 5.23. The spherical islands were also observed in another study, which is about synthesis of PMMA-*b*-PS coated silica nanoparticles via reverse ATRP [63].

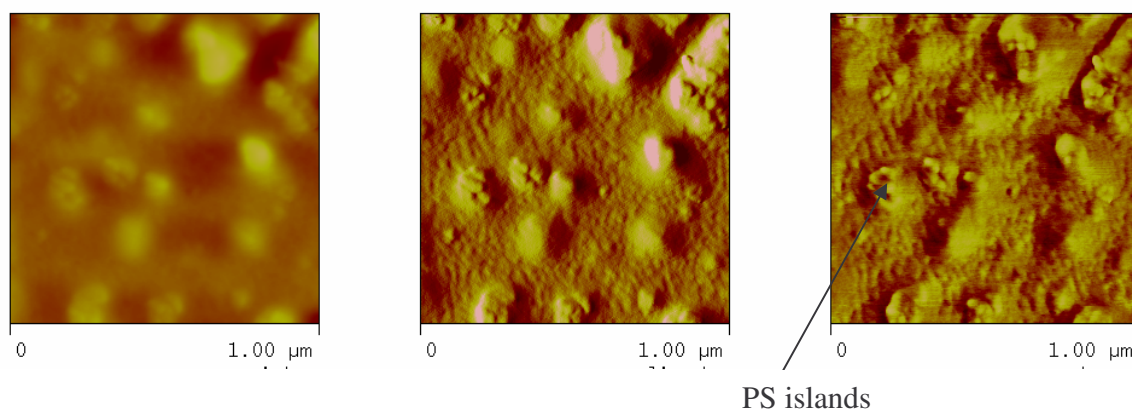


Figure 5.23 AFM height, amplitude and phase images of PMMA-*b*-PS coated MNP

Chapter 6

CONCLUSIONS

In this thesis, selective dispersion of iron oxide nanoparticles with different surface functionalities in phase separated polymer films was studied. Two different approaches were investigated: due to the well known behavior and simplicity polymer blends of widely studied PS/PEG and PS/PMMA were chosen for macro-phase separated systems; due to the ability of micro-phase separation allowing finer structures, again well studied PS-*b*-PMMA block copolymers were studied at different stages of this study. First, SPIO surfaces were functionalized with small molecules, namely, LA, HDMS and PEG-Si providing hydrophobic and hydrophilic particles compatible with the selected polymers. In an alternative approach, polymers (PS, PMMA and PMMA-*b*-PS) were grown/grafted from the surface of SPIOs. Selective dispersion in phase separated films were studied on thin films of functionalized SPIOs/polymer mixtures.

LA and PEG-Si coated iron oxide nanoparticles were synthesized in water using in situ coating approach. LA formed bilayer coating on the surface in water and the particles were made hydrophobic either extracting them to chloroform or precipitating them into alcohols. HDMS was exchanged with LA to form HDMS coated nanoparticles. The crystal structures and crystal sizes were identified by X-Ray Diffraction and FTIR. All of them are determined as γ -Fe₂O₃ of 7-9 nm. The hydrodynamic sizes (D_h) were also measured by DLS. D_h of LA monolayer coated iron oxides depend on the preparation. Chloroform

extraction from aqueous suspension provides 25 nm clusters whereas small aggregates of 120 nm in toluene by precipitation method. HDMS coated particles had 40 nm hydrodynamic sizes in toluene after ligand exchange. The ligand exchange of HDMS was confirmed by FT-IR spectroscopy. PEG-Si coated particles were synthesized in water, but they can also disperse in toluene forming 70 nm clusters. Atomic force microscope (AFM) images helped to observe particle size. Hydrodynamic sizes were also confirmed with AFM images. For all of these particles, drying and then redispersing cause larger hydrodynamic sizes because of irreversible aggregation. When we compare the graft densities calculated from the result of TGA, LA coated MNPs had more coating molecules per nm^2 , which is 25.87, then HDMS coated MNPs (7.60) and PEG-Si (3.07). Silanes cover larger area on the particle surface than carboxylates and steric hindrance of the PEG tail of PEG-Si may limit the number of molecules that can pack on the surface.

As a part in the preparation of LA coated iron oxide nanoparticles, Design of Experiment method is utilized to determine the effective reaction factors in controlling the hydrodynamic size of the LA bilayer coated nanoparticles. Influence of iron concentration, coating/Fe ratio and existence of NaNO_3 on hydrodynamic size and stability of LA bilayer coated iron oxide nanoparticles and magnetization was investigated. Results are in agreement with the prior study carried out by Demirer and Yagci on PAA coated iron oxide nanoparticles: (i) $0.03 \leq [\text{Fe}] \leq 0.265$ and $\text{LA/Fe} \geq 0.1$ is necessary for stability, (ii) most important factor affecting the D_h is LA/Fe ratio but as this ratio increases bimodality can be seen, (iii) no transfer function that can predict the D_h from the variables could be obtained since standard deviation was too large to identify differences between different reactions. If the correlation equation established for PAA is used, experimental results obtained for LA were less than 50 % of the theoretical sizes. This difference is mainly because of the 3-D conformation caused by macromolecular structure of PAA and the chain entanglement when compared with LA.

PS, PMMA or PMMA-b-PS coated iron oxide nanoparticles were also synthesized by using surface initiated ATRP method. For this, CMS was exchanged with LA and used as a surface bound initiator. For styrene polymerization, five different experiments with different conditions were performed to achieve high molecular weight polystyrene having low MW distribution. Based on our results, bulk polymerization does not provide the necessary control and use of dry initiator is not preferable due to its initial insolubility in the medium. The polymerization medium should be compatible with both the polymer and the initiating nanoparticle. Therefore, for high monomer conversion and initiator efficiency, for controlled molecular weight and low size distribution, concentrated colloidal suspension of CMS coated particles in DMF should be used as an initiator and the polymerization should be conducted in xylene at 110°C for several hours. In case of MMA polymerization, lower hydrodynamic size, monomer conversion, graft density and initiator efficiency were obtained. Synthesis of PMMA-b-PS was performed with the same method and the block formation was supported by TGA and DLS.

LA, HDMS and PEG-Si coated MNPs were mixed with PEG and PS separately and with their blends. Thin films cast from these mixtures were analyzed by AFM. Hydrophobic LA-NPs dispersed well in both PS and PEG films homogeneously, yet formed smaller clusters in PEG. These NPs dispersed selectively in PEG domains of the PS-PEG blends. Origin of such selectivity is determined as the exchange of LA from the iron oxide crystal surface with PEG. This is actually quite simple and promising finding to disperse fatty acid coated particles into hydrophilic domains with no additional surface modification of the NPs. The most widely used coatings in the aqueous synthesis of SPIOs are SDS (sodium dodecylsulphate) and OA (oleic acid) and this mechanism should easily work for these coatings as well. Such exchange also provides steric stabilization and coating that is more compatible with PEG domains therefore creating better dispersion of NPs in PEG than PS. Lauric acid binds to iron oxide surface through chemical adsorption of carboxylate

yet the binding is reversible. To prevent this reversible binding, silane coupling agents, which are HDMS and PEG-Si, were used with the thought of formation of stronger covalent Fe-O-Si bond. When HDMS coated MNPs were dispersed in the blend of PS/PEG, expecting to select PS, they were mainly located at the interface of the polymers and they formed large clusters in PEG. Unexpectedly, there were no particles in the PS phase again. However, in the PEG-Si case, the particles were dispersed in the PEG phase of the blend as expected. This approach provided a good model for the studies involving block copolymers but also and most importantly provided a simple and versatile route for preparation of polymer/NP hybrid structures. It would be beneficial to extend this study to non-crystallizing hydrophilic polymers to eliminate the possible impact of PEG crystallization in such distribution of HDMS coated particles.

The nanoparticles coated by PS and PMMA were also mixed with different immiscible polymers to have the selective distribution of nanoparticles in phase separated polymer films. In all cases, PS coated MNP in PEG, PMMA coated MNP in PS and PS coated MNP in PMMA, nanoparticle-containing islands were formed in the continuous phase and their sizes were compatible with the DLS measurements. This approach arrested the particles in one of the phases irreversibly.

A well-ordered micro-phase separation could not be observed for the first trial of PMMA-b-PS coated MNPs but the nanoparticles were observable. Further studies in this area would potentially create unique structures.

Appendix

Statistical Evaluation of LA coated Magnetic Nanoparticles

Lauric acid (LA) stabilized iron oxide nanoparticles were synthesized from the aqueous solution of iron salts with NH_4OH in the presence of excess amount of LA. Lauric acid provides an interdigitated bilayer around the nanocrystal surface, thus dispersing particles in water as shown in Figure A.1. [5,64]

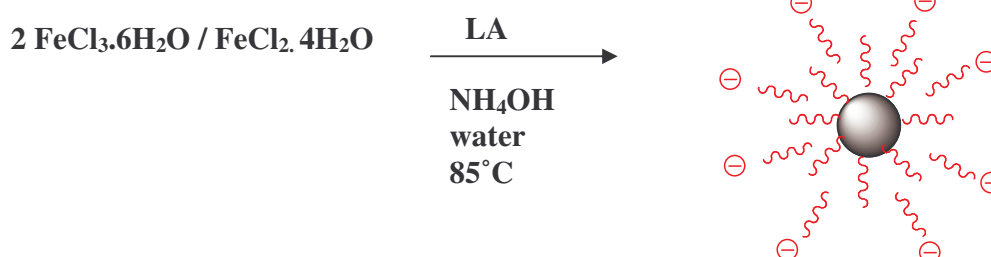


Figure A.1 Typical scheme of bilayer coated iron oxide nanoparticles' synthesis

Sixteen systematic experiments generated by Design Expert and Minitab programs with two center points per block generated by the two-level full factorial design were performed to correlate the reaction variables to hydrodynamic size of the LA coated MNPs. Iron concentration, LA/ iron ratio and presence of NaNO_3 (on/ off factor) were the reaction variables. Intensity and number based size distribution measured by DLS for each experiment are shown in (Table A.1).

All reactions produced magnetic nanoparticles as they have responded to 0.3 T magnet.

TableA.1 Reaction parameters and the results

VARIABLES			PARTICLE SIZE		
[Fe] (M)	LA/Fe (mol/mol)	NaNO ₃	Dh-I(1) ^a (nm)	Dh-I(2) ^b (nm)	Dh-N ^c (nm)
0,03	0,100	NO	ppt*	ppt	Ppt
0,03	1,00	NO	68	712	15
0,265	0,55	NO	32	519	23
0,265	0,55	NO	37	396	21
0,265	0,55	NO	63	-	14
0,265	0,55	NO	78	-	12
0,50	1,00	NO	100	-	23
0,50	0,10	NO	ppt	ppt	Ppt
0,03	0,10	YES	ppt	ppt	Ppt
0,03	1,00	YES	78	615	62
0,265	0,55	YES	32	1000	13
0,265	0,55	YES	35	565	11
0,265	0,55	YES	36	400	15
0,50	0,10	YES	ppt	ppt	Ppt
0,50	1,00	YES	35	295	17
0,265	0,55	YES	58	-	21

^a hydrodynamic size, intensity average , first peak

^b hydrodynamic size, intensity average, second peak

^c hydrodynamic size, number average

* ppt: particles precipitated

Precipitation of nanoparticles was observed at LA/Fe ratio of 0.1 during the reaction indicating insufficient coating to suspend the particles. At high Fe concentrations fast nucleation and growth might cause larger particles and aggregates that eventually sediments. Aqueous colloidal suspensions with long-term stability can be achieved at $[Fe] \leq 0.265$ and $LA/Fe \geq 0.1$ (Figure A.2). This represents a window where a balance was achieved between the LA number per nanoparticle, number of nanoparticles and crystal growth rate.

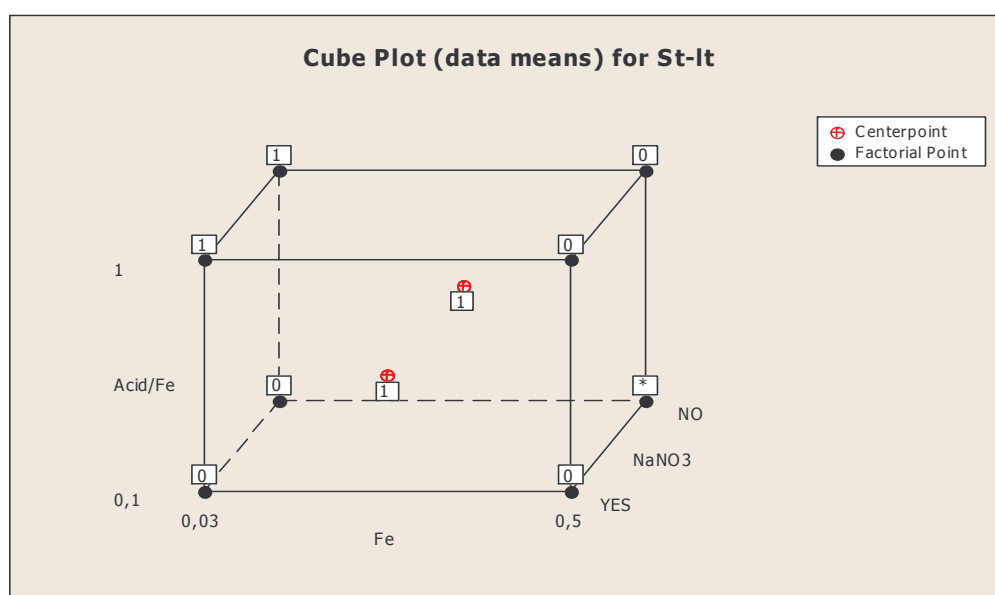


Figure A.2 Cube plot for the stability of nanoparticles (1) suspension, (0) precipitate

Minitab14 Release program was used to evaluate the four factors by using 'Main Effects Plot', which indicates the most influential variables on particle size. Unfortunately, precipitated reactions cause problems when data is statistically evaluated and correlated to the particle size. Therefore, we have used 1000nm as the size of the precipitated particles to be able to analyze the data. With or without a transfer function (log normal) the most

significant factor on the hydrodynamic size of the particles was found as LA/Fe ratio (Figure A.3). LA prevents the crystal growth by adsorbing onto the crystal and causes electrostatic repulsion. Therefore, smaller particles can be obtained with larger LA/Fe ratio meaning less nanoparticles and more coating. In the Main effects Plot, steeper angles indicate stronger impact.

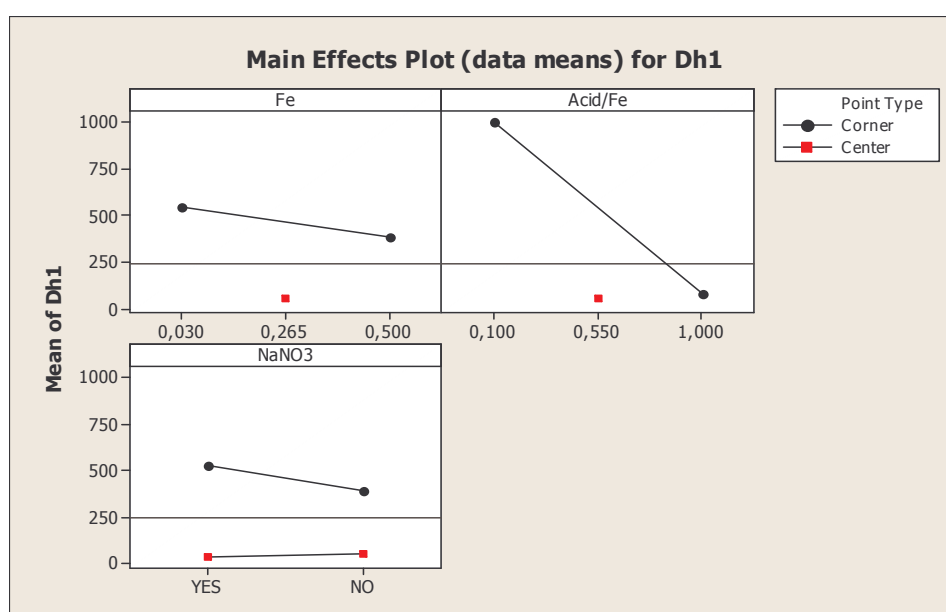


Figure A.3 Main effects chart for hydrodynamic size after synthesis. Large slope means strong effect

There is an important problem in this system. Similar result of different reactions made it difficult to determine the two-way interactions. For example, the standard deviation of the three reactions (7.64 nm) in table A.2 is smaller than the eight reactions (17.5) which are in the middle of the area of all reactions.

Table A.2 Hydrodynamic size based on intensity and number average distribution by DLS

Factors			Size of the nanoparticle *	
Fe (M)	LA/Fe (mole ratio)	NaNO ₃	Dh-I(1) (nm)	Dh-N (nm)
0,03	1,0	NO	68	15
0,265	0,55	NO	63	14
0,265	0,55	NO	78	12
St.dev			7,64	1,53

* Hydrodynamic size

The number average hydrodynamic sizes (Dh-N) of particles were smaller than the intensity average sizes (Table A.2). This is usually the case for particles with relatively broad size distribution. In order to determine the affect of the reaction parameters on Dh-N, a value of 200 nm was given to the precipitated reactions and analyzed by the statistical programs. The Main Effects Plot and Interaction Plot points out Fe concentration, LA/Fe ratio and the interaction of the two as the significant factors for hydrodynamic size (Figure A.4).

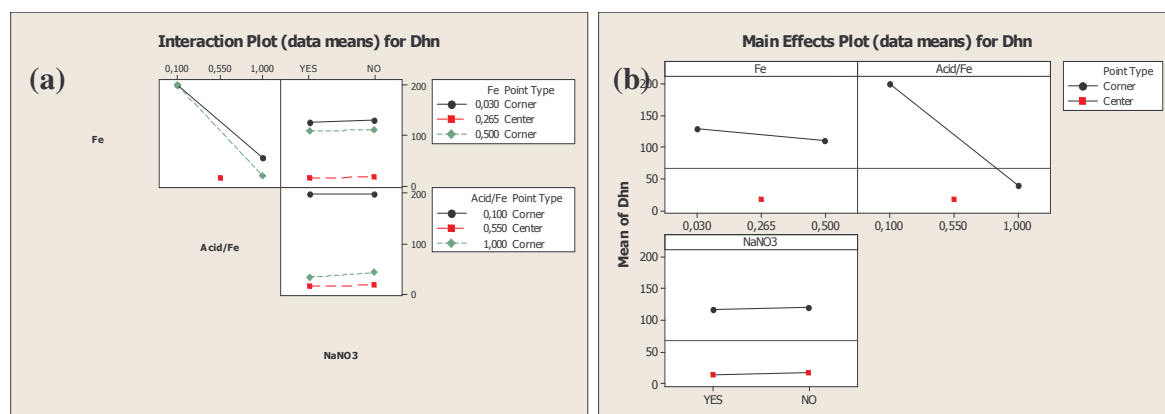


Figure A.4 a) Interaction plot of the variables b) Main effects chart for hydrodynamic size after synthesis

Another important point here is the bimodal size distribution in the intensity based calculations at the high LA/Fe ratios and/or high Fe concentration. This is mainly because of excess LA. It may cause micelle formation.

Results that we have obtained are consistent with the similar study done by Yagci and Demirer using PAA coating on MNPs [65]. As the amount of coating material increase, the growing nanoparticles are coated more rapidly and growth is arrested. Dense coating is provided with increasing coating/Fe ratio. Using concentrated solutions is another problem. Precipitation of particles occurs at high iron concentrations for both coating. Therefore, 0.03-0.3M of iron concentrations is reasonable for both coatings.

Usually, an equation relating the variables to the response, which is the size here, can be created by the statistical programs that we have used. Unfortunately, since the hydrodynamic sizes of the particles obtained from centre points reactions were quite different from each other (standard deviation: 17.5), it was impossible to obtain an equation. In the PAA coated iron oxides study, such equation was created between the

significant factors (iron concentration, LA/Fe ratio, and the interaction between two) and the hydrodynamic size.

$$\ln(D_h) = 4.73927 - 0.11358 \times [\text{Fe}] - 0.63233 \times [\text{Fe} \cdot \text{LA}/\text{Fe}] + 1.8986 \times [\text{Fe}] \times [\text{Fe} \cdot \text{LA}/\text{Fe}] \quad \text{Eq.1}$$

The sizes of LA coated particles were also predicted with this equation but as seen in Table A.3, experimental results are less than 50 % of the theoretical results. This difference is mainly because of the 3-D conformation caused by macromolecular structure of PAA and the chain entanglement.

Table A.3 Comparison between theory and the experimental sizes

Factors			Particle size	
[Fe] (M)	LA/Fe	NaNO ₃	Dh* (nm)	Theoretical** (nm)
0,030	1,00	NO	68	112
0,265	0,55	NO	63	143
0,265	0,55	NO	78	143

* DLS measurement

** Eqn. 1 [65]

BIBLIOGRAPHY

-
- [1] Ajay Kumar Gupta, Mona Gupta, *Biomaterials* 2005,26,3995-4021
- [2] Kim K, *Nanomedicine: Nanotechnology, Biology, and Medicine* 3 (2007) 103–110
- [3] Alivisatos, A.P., *Science* 1996,271, 933
- [4] *The Iron Oxides*, R.M Cornell, U. Schwertmann
- [5] Yagci Acar, H; Garaas, R. S.; Syud, F.; Bonitatebus, P.; Kulkarni, A. M. J. *Magnetism and Magnetic Materials* 2005, 29(1), 1-7.
- [6] S. Mornet, J. Portier, E. Duguet, *J. Magnetism and Magnetic Materials*,2005, 293, 127-134
- [7] Advincula R, *Surface Initiated Polymerization from Nanoparticle Surfaces*, *Chemical Reviews* (2001) 101, 9
- [8] www.wikipedia.org
- [9] <http://www.physics.nyu.edu/pine/research/nanocopoly.html>
- [10] Segalman R.A., *Materials Science and Engineering R* 48 (2005) 191–226
- [11] B. H. Sohn and B. H. Seo, *Chem. Mater.* 2001, 13, 1752-1757
- [12] Walheim S., Ramstein M., Steiner U., *Langmuir* 15 (1999) 4828.
- [13] R. Shenhar, T. Norsten, V.M. Rotello, *Advanced Materials*, 2005,17,657-669
- [14] J W Hamley, *Nanotechnology*,2003, 14, R39-R54
- [15] A. Balazs, T. Emrick, T. Russell, *Science*, 314,1107-1110
- [16] C. Park, J. Yoon, E. L. Thomas, *Polymer*, 2003,44, 6725–6760
- [17] A. Ethirajan, U. Wiedwald, Hans. Boyen, B. Kern, L. Han, A. Klimmer, F. Weigl, G. Kästle, P. Ziemann, K. Fauth, J. Cai, R. J. Behm, A. Romanyuk, P. Oelhafen, P. Walther, J. Biskupek, U. Kaiser, *Advanced Materials*, 2007, 19, 406-410
- [18] H. Yusuf, W. Kim, D.H. Lee, Y. Guo, M.G. Moffitt, *Langmuir* 2007, 23, 868-878

-
- [19] F. Weigl, S. Fricker, H. Boyen, C. Dietrich, B. Koslowski, A. Plettl, O. Pursche, P. Ziemann, P. Walther, C. Hartmann, M. Ott, M. Möller, *Diamond and Related Materials*, 2006, 15, 1689-1694
- [20] Y. Lin, A. Böker, J. He, K. Sill, H. Xiang, C. Abetz, X. Li, J. Wang, T. Emrick, S. Long, Q. Wang, A. Balazs, T. Russell, *Nature*, 2005, 434, 55-59
- [21] Y. Lin, A. Böker, J. He, K. Sill, H. Xiang, C. Abetz, X. Li, J. Wang, T. Emrick, S. Long, Q. Wang, A. Balazs, T. Russell, *Nature*, 2005, 434, 55-59]
- [22] C.C. Weng, K.H. Wei, *Chem. Mater.* 2003, 15, 2936-2941
- [23] M.J. Park, J. Park, T. Hyeon, K. Char, *Journal of Polymer Science: Part B: Polymer Physics*, 2006, 44, 3571-3579
- [24] C. Mineli, I. Geissbuehler, R. Eckert, H. Vogel, H. Heinzelmann, M. Liley *Colloid Polym Sci*, 2004, 282, 1274-1278
- [25] C. Mineli, I. Geissbuehler, R. Eckert, H. Vogel, H. Heinzelmann, M. Liley *Colloid Polym Sci*, 2006, 284, 482-488
- [26] C.W. Wang, M. G. Moffitt, *Chem. Mater.* 2005, 17, 3871-3878
- [27] Chung H, Ohno K, Fukuda T, Composto R, *Nano Letters*, 2005, 5, 10, 1878-1882
- [28] Eric J. Amis, *Macromolecules* 2002, 35, 4852-4854
- [29] Matyjaszewski K, Xia J, *Atom Transfer Radical Polymerization*, *Chem. Rev.* (2001) 101, 2921-2990
- [30] Hawker, C. J.; Bosman, A. W.; Harth, E. *Chem. Rev.* (2001) 101, 3661-3688
- [31] Matyjaszewski K, *Patent T*, *Advanced Materials*, 1998, 10, 12
- [32] Brittain J, W, Boyes S, Granville A, Baum M, Akgun B, *Surface Science*, 570, 2004, 1-12
- [33] Brittain J, W, Treat N, Ayres N, Boyes S, *Macromolecules*, 2006, 39, 26-29
- [34] Li J, Cui Y, *Chem. Mater.* 2007, 19, 412-417
- [35] Patent E. T, Farmer S C, *Chem. Mater.*, 2001, 13, 3920-3926

-
- [36] Zhao B, Li D, Jones L, Dunlap J, Hua F, *langmuir*, 2006, 22, 3344-3351
- [37] Wang J, Zhang K, Ma B, Zhao S, Li Y, Xu Y, Yu W, *Materials Letters* 61, 2007, 949-952
- [38] Matyjaszewski K, Savin D, Pyun J, Patterson G, Kowalewski T, *Journal of Polymer Science: Part B: Polymer Physics*, 2002, 40, 2667-2676
- [39] Boue F, Harrak E, Carrot G, Oberdisse J, Jestin J, *Polymer* 2005, 46, 1095-1104
- [40] Patten T, Werne T, *JACS*, 2001, 123, 7497-7505
- [41] Fukuda T, Ohno K, Morinaga T, Koh K, Tsujii Y, *Macromolecules*, 2005, 38, 2137-2142
- [42] Matyjaszewski K, Pyun J, Jia S, Kowalewski T, Patterson G. D, *Macromolecules*, 2003, 36, 5094-5104
- [43] Neoh G, Fu G.D, Shang Z, Hong L, *Macromolecules* 2005, 38, 7867-7871
- [44] Hult A, Nyström D, Molmström M, Whittaker M, *Macromolecular Rapid Communications*, 2005, 26, 524-528
- [45] Fukuda T, Morinaga T, Ohkura M, Ohno K, Tsuji Y, *Macromolecules*, 2007
- [46] Fukuda T, Ninjbadgar T, Yamamoto S, *Solid State Sciences*, 2004, 6, 879-885
- [47] Modragon I, Garica I, Janke A, Tercjak A, Stamm M, *Journal of Polymer Science: Part A: Polymer Chemistry*, 2007, 45, 925-932
- [48] Schmidt M, Gelbrich T, feyen M, *Macromolecules*, 2006
- [49] Neoh K, Hu F, Cen L, Kang T, *Biomacromolecules*, 2006, 7, 809-816
- [50] Zhang J, Vestal C, *JACS*, 2002, 124, 14312-14313
- [51] Peng Y, Sun Y, Ding X, Zheng Z, Cheng X, Hu X, *European Polymer Journal*, 2006, 42, 2107-2112
- [52] Li Z, Bai Y, Teng B, Cen S, Chang Y, *Macromolecular Rapid Communications*, 2006, 27, 2107-2112

-
- [53] Pyun J, Matyjaszewski K, Kowalewski T, Savin D, Patterson G, Kickelbick G, and Huesing N, Synthesis of Well-Defined Block Copolymers Tethered to Polysilsesquioxane Nanoparticles and Their Nanoscale Morphology on Surfaces, *J. Am. Chem. Soc.* (2001), *123*, 9445-9446
- [54] Shen, L.; Stachowiak, A.; Hatton, T.A.; Laibinis, P.E *Langmuir* 2000, *16*, 9907-9911.
- [55] R. Baigorri, J.mina, G. Gaitano, *Colloids and Surfaces A*,2007, *292*, 212-216
- [56] Liu X, Xing J, Guan Y, Shan G, Liu H, *Colloids and Surfaes A: Physicochem. Eng. Aspects* (2004), *238*, 127-131
- [57] Yamaura M, Camilo R.L, Sapaio L.C, Macedo M.S, Nakamura M, Toma H.E, *Journal of Magnetism and Magnetic Materials* (2004) ,*279*,210-217
- [58] Bourlinos A.B., *Journal Of Materials Science Letters* (2005)
- [59] Takahara A, Kobayashi M, Matsuno R, Otsuka H, *Science and Technology of Advanced Materials*, 2006,*7*,617-628
- [60] M.Y.Yüce, A.L. Demirel, *Langmuir*, 2005
- [61] Lee, S.Y.; Haris, M. T. *Journal of Colloid and Interface Science* 2006, *293*, 401–408
- [62] Yeh S-W, Wei K-H, *Macromolecules* 2005, *38*, 6559-6565
- [63] Wang Y, Pei W, He X, Yuan K, Wan, *European Polymer Journal*, 2005, *41*, 1326-133
- [64] Shen, L.; Stachowiak, A.; Hatton, T.A.; Laibinis, P.E *Langmuir* 2000, *16*, 9907-9911.
- [65] Controlled synthesis of superparamagnetic iron oxide nanoparticles in the presence of poly(acrylic acid), Thesis by Miray Demirer, Koç University, 2006.